IRE Transactions on ANTENNAS and PROPAGATION

Volume AP-6 **APRIL, 1958** **Number 2**

Published Quarterly

TABLE OF CONTENTS

PUBLISHED BY THE

Professional Group on Antennas and Propagation

IRE TRANSACTIONS® PGAP IS A QUARTERLY PUBLICATION DEVOTED TO EXPERIMENTAL AND THEORETICAL PAPERS ON ANTENNAS AND WIRELESS PROPAGATION OF ELECTROMAGNETIC WAVES

MANUSCRIPTS should be submitted to John B. Smyth, Editor, Smyth Research Associates, 3555 Aero Court, San Diego 11, Calif. Manuscripts should be original typewritten copy, double spaced, plus one carbon copy. References should appear as footnotes and include author's name, title, journal, volume, initial and final page numbers, and date. Each paper must have a summary of not more than 200 words. News items concerning PGAP members and group activities should be sent to the News Editor, Mr. Arthur Dorne, Dorne and Margolin, Inc., 30 Sylvester Street, Westbury, L.I., N.Y.

ILLUSTRATIONS should be submitted as follows: All line drawings (graphs, charts, block diagrams, cutaways, etc.) should be inked uniformly and ready for reproduction. If commercially printed grids are used in graph drawings, author should be sure printer's ink is of a color that will reproduce. All halftone illustrations (photographs, wash, airbrush, or pencil renderings, etc.) should be clean and ready to reproduce. Photographs should be glossy prints. Call-outs or labels should be marked on a registered tissue overlay, not on the illustration itself. No illustration should be larger than 8 x 10 inches.

Copies can be purchased from
THE INSTITUTE OF RADIO ENGINEERS
1 East 79 St., New York 21, N.Y.

PRICE PER COPY: members of the Professional Group on Antennas and Propagation, $1.15; members of the IRE, $1.75; nonmembers, $3.45.

ANNUAL SUBSCRIPTION PRICE: PGAP members, included in PGAP fee of $4.00; IRE members, $8.50; Colleges and public libraries, $10.00; nonmembers, $17.00.

IRE TRANSACTIONS ON ANTENNAS AND PROPAGATION

Entered as second-class matter, at the post office at Menasha, Wisconsin, under the act of August 24, 1912. Acceptance for mailing at a special rate of postage is provided for in the act of February 28, 1925, embodied in Paragraph 4, Section 412, P. L. & R., authorized October 26, 1927.

news and views

A Report from the Chairman

I should like to summarize briefly what has occurred recently in the PGAP and what is planned for the immediate future. There has been very little communication between administration and members, so that a "state of the union" report appears opportune.

The big problem in the PGAP since 1956 has been a lack of adequate funds. This state of affairs was created when our Group published the papers of the Electromagnetic Theory Symposium held at the University of Michigan, which wiped out our financial reserves and created a backlog of papers awaiting publication in our TRANSACTIONS. Since then, the administrative committee and officers of the PGAP have spent an inordinate amount of time trying to obtain sufficient funds for proper operation. These efforts resulted in the neglect of some other matters, which I shall mention later as needing action.

Therefore, it is with some pride, and relief, that I am able to report that this backlog of papers was removed by publication in the January issue. The necessary money was raised by the sale of more than $6000 worth of advertising in our TRANSACTIONS. Delmer Ports and Art Dorne are primarily responsible for this work, accomplished despite the arbitrarily high rates established by the IRE Executive Committee. This means that papers accepted by our reviewers can now be published promptly in the following issue of TRANSACTIONS.

I do not wish to convey the idea that our financial troubles are over. A glance at the following financial statement shows that the PGAP was still destitute at the close of 1957.

For the Period from January 1, 1957 to December 31, 1957:

Balance from January 1, 1957		$ 3,448.13
Receipts During Period:		
IRE Matched Funds	$ 2,404.00	
Assessments	9,950.71	
Advertising	2,192.60	
Sale of Publications	1,329.35	
Surplus from Meetings	272.32	
Other Sources	–0–	
Total Receipts		$16,148.98
Total (Original Balance and Receipts)		$19,597.11
Expenses During Period:		
Publications	$19,514.15	
Membership Service Charges	318.12	
Others	–0–	
Total Expenses		$19,832.27
Balance as of December 31, 1957		$ 235.16 Credit

Our credit balance will change to debit as money is received from advertising already sold. However, more advertising needs to be sold in order that a working reserve can be built up. Any member wishing to help should contact Delmer Ports, as described on the back pages of recent issues of the TRANSACTIONS.

A very interesting statistic, and evidence of the vigor of the PGAP, is that we have published 2278 pages in these TRANSACTIONS from 1951 to 1957 inclusive. This is over 700 pages more than any other professional group has published in the same period. This record is even more impressive when one remembers our financial difficulties and realizes that there are eight other professional groups larger than we, two of which are over twice as large.

Membership in the PGAP is increasing rapidly, further proof that our Group is healthy and dynamic. Here are the figures for our growth since 1952.

Paid Membership	*End of Year*
980	1952
1219	1953
1276	1954
1470	1955
1997	1956
2406	1957

In addition, there are about 400 student members.

There are eleven PGAP chapters as follows:

Chapter	*Chairman*
Akron	George H. Welch
Albuquerque-Los Alamos	Dick Moore
Boston	J. T. deBettencourt
Chicago	N. J. Sladek
Denver-Boulder	Herman V. Cottony
Los Angeles	Robert J. Stegen
Orange Belt	Glenn A. Scharp
Philadelphia	E. J. Forbes
San Diego	David Proctor
Syracuse	William T. Whistler
Washington, D. C.	Harry Fine

A chapter is being formed in San Francisco and a joint chapter with the PGMTT is being organized on Long Island. Certainly, the PGAP is an organization which can be recommended to your friends and coworkers.

As in the past, the PGAP has sponsored technical sessions this year at the National Convention in New York, at the joint IRE-URSI Spring Meeting in Washington, and at WESCON in Los Angeles. Another national symposium is planned in October in Washington under the leadership of Harry Fine. The general topic is propagation in the troposphere and ionosphere, and by meteor trials.

There are several current items which require action on the part of the Administrative Committee of the PGAP. At our next meeting I will propose that the scope of our Group be expanded to include officially the field of Radio Astronomy. This is recognition of what we are already doing. Such action will require the approval of the IRE Executive Committee. I will propose also that an award program be initiated within our Group, *e.g.*, awards for best papers in the TRANSACTIONS or at meetings. I will continue to urge a newsletter, a much-needed means of communication among members as to chapter activities, PGAP participation in technical meetings, current actions of the Administrative Committee, and other news items of general interest. Such a publication should aid in obtaining new members. And, of course, the financial question will come in for its share of attention. The present conditions under which advertising in the TRANSACTIONS is sold are unsatisfactory. A change in policy by the Institute is needed whereby the advertising rates are made reasonable and continuity of sales is maintained. Every effort to improve this situation will be made.

In summary, I can say that both the present state and the future of the PGAP appear good; indeed, even better than in the past few years as attested to by the facts submitted earlier. Also, the future of the professional group system appears bright, with the groups assuming more responsibility and leadership in the Institute. To that end, I refer the reader to the article written by the President of the IRE, Donald Fink, in the September, 1957 issue of PROCEEDINGS.

J. I. BOHNERT
Chairman, PGAP

NEWSLETTER

This is the last News and Views column. It will be replaced shortly by a *Newsletter*, and is expected to be much more useful than News and Views has been. The lead time required to get it out will be much shorter. Additionally, it will appear more frequently: every other month.

I will continue as PGAP News Editor. Accordingly, please send news items to me, Arthur Dorne, 29 New York Avenue, Westbury, Long Island, N. Y.

contributions

The Role of Turbulent Mixing in Scatter Propagation*

RALPH BOLGIANO, JR.†

Summary—**The Villars-Weisskopf-Wheelon theory describing turbulent mixing of an established gradient is shown to contain a contradiction which necessitates its being discarded. To fill the gap thus created, the theory of isotropic mixing is extended to account for the presence of a gradient. The results indicate that "mixing-in-gradient" cannot be employed to explain the wavelength dependence characteristic of much of the radio data. On the other hand, it is shown that experimentally determined spectra of refractive index fluctuations lend strong support to the mixing theory herein set forth. Hence, the conclusion is reached that scatter theory, as it is currently based on atmospheric turbulence, can provide, at best, an incomplete description of transhorizon propagation.**

I. Introduction

SEVERAL years ago Batchelor,[1] on the one hand, and Villars and Weisskopf,[2] on the other, came to the conclusion quite independently that turbulent mixing of established mean gradients of refractive index must play a major role in the generation of the index fluctuations which are believed to account[3] for a significant, if not the principal, portion of signal propagated well beyond the horizon. In their same paper Villars and Weisskopf proposed a theoretical description of such a turbulent mixing process which leads to a fluctuation-size dependence for the scattering coefficient σ of L_σ^5. ($L_\sigma \equiv \lambda/[2 \sin \theta/2]$, the scattering eddy-size.) For the troposphere this yields σ proportional to λ. Wheelon[4,5] subsequently was led to the same result by independent reasoning, basically dimensional in character. Since there is a large and growing body of data[6–9] which, when considered within the framework of scatter

* Manuscript received by the PGAP, September, 14, 1957. Portions of this paper were presented at the URSI-IRE meeting in Washington, D. C., May 25, 1957, under the title "The spectrum of turbulent mixing and its application to scatter propagation." This research was supported by the Wright Air Development Center under contract AF 33(616)-3236.

† School of Elec. Eng., Cornell University, Ithaca, N. Y.

[1] G. K. Batchelor, "The Scattering of Radio Waves in the Atmosphere by Turbulent Fluctuations in Refractive Index," School of Elec. Eng., Cornell University, Res. Rep. EE 262; September 15, 1955.

[2] F. Villars and V. F. Weisskopf, "On the scattering of radio waves by turbulent fluctuations of the atmosphere," PROC. IRE, vol. 43, pp. 1232–1239; October, 1955.

[3] See for example: H. G. Booker and W. E. Gordon, "A theory of radio scattering in the troposphere," PROC. IRE, vol. 38, pp. 401–412; April, 1950.

[4] A. D. Wheelon, "Radio frequency and scattering angle dependence of ionospheric scatter propagation at vhf," *J. Geophys. Res.*, vol. 62, pp. 93–112; March, 1957.

[5] A. D. Wheelon, "Spectrum of turbulent fluctuations produced by convective mixing of gradients," *Phys. Rev.*, vol. 105, pp. 1706–1710; March 15, 1957.

[6] L. G. Trolese, "Characteristics of tropospheric scattered fields," PROC. IRE, vol. 43, pp. 1300–1305; October, 1955.

[7] J. H. Chisholm, *et al.*, "Investigations of angular scattering and multipath properties of tropospheric propagation of short radio waves beyond the horizon," PROC. IRE, vol. 43, pp. 1317–1335; October, 1955.

[8] K. Bullington, *et al.*, "Results of propagation tests at 505 mc and 4,090 mc on beyond-horizon paths," PROC. IRE, vol. 43, 1306–1316; October, 1955.

[9] J. H. Chisholm, *et al.*, "Experimental investigations of the angular scattering and multipath delays for transmissions beyond the horizon," presented before Combined Technical Session, URSI, Washington, D. C., May 23–25, 1957.

phenomena, has been interpreted[10] as being in agreement with such a λ dependence, many investigators have recently been inclined to accept scatter propagation theory, based on "mixing-in-gradient," as rather well established.

Unfortunately, Wheelon's analysis contains a contradiction which, as it is fully appreciated, casts grave doubt upon the entire L^5 law. It is the intent of this paper, first, to set forth clearly this inconsistency. Secondly, by extending Batchelor's isotropic theory to the case of turbulent mixing in the presence of a gradient, it will be shown that the $L^{11/3}$ form, previously predicted by both Batchelor and Silverman,[11] is still appropriate for a large range of fluctuation sizes. Further, it will be brought out that, if the presence of a gradient of mean refractive index has any effect, it must be to weaken (make the exponent smaller) this dependence at large scales, not strengthen it. Thirdly, by analyzing refractometer data directly, support will be introduced for the contention that the refractive index fluctuations themselves have a mean square spectral density which is in consort with the $L^{11/3}$ law. Finally, three methods of calculating values of σ will be discussed.

II. Inconsistency of the L^5 Law

In Section 4 of his paper[4] Wheelon assumes *a priori* that, in the inertial subrange, the spectrum of mean square fluctuations is independent of the molecular diffusivity D, the wave number $k(\equiv 2\pi/L)$ being taken to be much smaller than k_s, the viscosity cutoff. By purely dimensional arguments he then arrives at his L^5 law. However, this implies the spectrum of molecular "dissipation," $2Dk^2E_n(k)$, is proportional to k^{-1}. ($E_n(k)$ is the spectral density per unit volume of mean square fluctuations of refractive index and is directly related to the comparable spectrum of, say, moisture vapor density or electron density fluctuations. $E_n(k)$ is synonymous with Wheelon's $B(k)$.) Thus, the distribution of molecular effects has its maximum at a wavenumber much smaller than the range of values he is considering. Therefore, molecular diffusion cannot be neglected in this range, in contradiction with is *a priori* assumption.

It is immediately evident the difficulty is not confined to Wheelon's analysis. An L^5 form implies a k^{-3} mean square fluctuation spectrum in the corresponding wavenumber range, regardless of the method by which it was derived. It then follows, as above, that molecular diffusion is a prominent agent in this range, which is contrary to the premise (Villars and Weisskopf[2]) that this is the inertial subrange. Consequently, the L^5 law must be abandoned as a theoretical description of mixing-in-gradient.

[10] See for example: K. A. Norton, *et al.*, "The use of angular distance in estimating transmission loss and fading range for propagation through a turbulent atmosphere over irregular terrain," Proc. IRE, vol. 43, pp. 1488–1526; October, 1955.

[11] R. A. Silverman, "Turbulent mixing theory applied to radio scattering," *J. Appl. Phys.*, vol. 27, pp. 699–705; July, 1956.

III. Turbulent Mixing of Gradients

In order to pave the way for the theoretical treatment which follows, first consider the problem of turbulent mixing of a mean gradient of refractive index in a heuristic manner. The arguments to be presented here must not be accepted in lieu of the more precise ones of the next section but only as aids in visualizing the entire process.

A. Qualitative Description of Mixing

At all scales present in the velocity field the eddies do, on the average, *mix-in* fluctuations from the mean gradient proportional to their respective sizes. But the local, instantaneous gradient on which the smaller eddies operate is, on the average, more intense than the mean gradient as a result of the stretching of fluid lines and surfaces by the turbulence, thereby bringing equivalue surfaces closer together. Hence, the smaller eddies mix-in progressively more and more than their share figured on a mean gradient basis. This is a manifestation of the "internal mixing" or inertial transfer mechanism, the conversion of fluctuations of one size to others of smaller scales. This transfer across the spectrum (see Fig. 1) continues until the local gradients become so

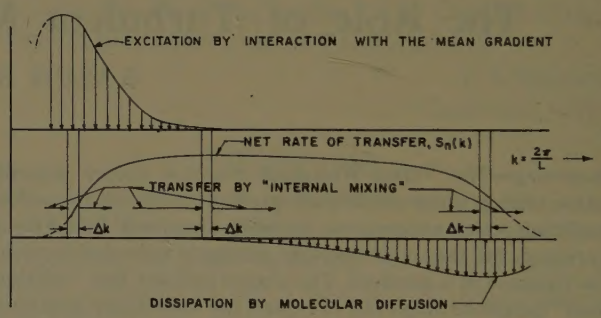

Fig. 1—Conceptual model of the mixing, transfer, and diffusion processes in turbulent mixing.

intense that molecular diffusion acts to dissipate them. In the intermediate range, in which inertial transfer is the principal process at work, a statistical steady-state is reached. Then one has a simple relation between the spectral density, $E_n(k)$, the net rate of transfer of mean square fluctuations across k, $S_n(k)$, and the "lifetime" of a given size eddy, τ_L,

$$E_n(k) \sim \frac{S_n(k)\tau_L}{k} \sim LS_n(k)\tau_L. \tag{1}$$

The universal equilibrium theory of turbulence[12] leads, in this inertial subrange, to

$$\tau_L \propto L^{2/3}.$$

[12] See, for example, G. K. Batchelor, "The Theory of Homogeneous Turbulence," Cambridge University Press, Cambridge, Eng., p. 114 ff.; 1953.

Thus, in the region where $S_n(k)$ is approximately constant, the mean square fluctuation spectrum is proportional to $L^{5/3}$; and at larger scales, where the effects of mixing-in-gradient should be more pronounced, the rate of transfer, S_n, increases with k (decreases with L) so that the spectral density will depend upon L according to

$$E_n(k) \propto L^{\nu}, \qquad \nu \leqq 5/3. \tag{2}$$

These arguments have much appeal. Nevertheless, there are fundamental questions which frequently arise; the following two are important examples. What evidence is there that the local gradients are, in fact, more intense than the average gradient and that, at the smaller scales, the inertial transfer mechanism therefore dominates the mixing-in process? Is there basis for the assumption, on which the above reasoning squarely stands, that it is mean square fluctuations which are conserved in this inertial transfer?

B. Analytical Development

In order to find answers to these questions and to place the whole development on a more substantial foundation, consider explicitly the interaction of the velocity field with a property of the atmosphere principally responsible for variations of the index of refraction, say, moisture vapor density in the lower troposphere, or electron density in the ionosphere. Let the symbol ψ, a scalar point function of position and time, represent such a density. Then, from the conservation of matter (assuming the fluid is dynamically incompressible) it is known that ψ satisfies

$$\frac{\partial \psi}{\partial t} = - u_i \frac{\partial \psi}{\partial x_i} + D_\psi \frac{\partial^2 \psi}{\partial x_r \partial x_r}. \tag{3}$$

Here $u_i (\equiv u)$ is the vector velocity, D_ψ is the molecular diffusivity, and standard tensor notation has been employed—a repeated index means summation over all the vector components. This equation shows that the time rate of change of ψ is determined by the net effect of convection and molecular diffusion, neglecting such factors as evaporation and condensation since we are later going to consider only steady-state conditions. Writing ψ as the linear sum of its average value and a fluctuation component $\delta\psi$,

$$\psi(x, t) \equiv \bar{\psi}(x) + \delta\psi(x, t),$$

the overbar indicating time, and/or ensemble, average, and similarly

$$u_i(x, t) \equiv \overline{u_i}(x) + \delta u_i(x, t),$$

and then subtracting the average of (3) from (3) itself yields a conservation equation for the fluctuation component,

$$\frac{\partial \delta\psi}{\partial t} = - \delta u_i \frac{\partial \bar{\psi}}{\partial x_i} - (\overline{u_i} + \delta u_i) \frac{\partial \delta\psi}{\partial x_i} + \overline{\delta u_i \frac{\partial \delta\psi}{\partial x_i}} + D_\psi \frac{\partial^2 \delta\psi}{\partial x_r \partial x_r}. \tag{4}$$

On the reasonable assumption that mean values of the fluctuation components are nearly independent of position the term $\overline{\delta u_i (\partial \delta\psi / \partial x_i)}$ in (4) is of smaller order of magnitude than the other terms and may be neglected. This may be said generally of spacial derivatives of mean values of the varying components and is tantamount to making the usually satisfactory assumption of local homogeneity.

1) *The Relative Intensity of Local Gradients:* Multiplying each of the remaining terms in (4) by $2\delta\psi$ and again taking averages leads to a statement of the conservation of mean square fluctuations in which the significant terms are

$$\frac{\partial \overline{\delta\psi^2}}{\partial t} = - \overline{2\delta\psi \delta u_i} \frac{\partial \bar{\psi}}{\partial x_i} - 2D_\psi \overline{\left(\frac{\partial \delta\psi}{\partial x_i}\right)^2}$$

$$= 2K_\psi (\text{grad } \bar{\psi})^2 - 2D_\psi \overline{(\text{grad } \delta\psi)^2}, \tag{5}$$

where $-\overline{\delta\psi \delta u_i}$ has been expressed in terms of the eddy diffusivity, K_ψ, and the mean gradient. The first term on the right represents the average generation of ψ-fluctuations by interaction of the turbulent velocities with the mean gradient, while the last term describes the dissipation of these fluctuations by molecular action. Under steady-state conditions such that the time derivative is zero, it becomes apparent that the magnitude of the gradient of the fluctuation component far exceeds that of the mean value since it is well known empirically that the eddy diffusivity is several orders of magnitude greater than the molecular diffusivity. This then is the evidence sought in answer to the first question in Section III-A above.

2) *The Conservation of Mean Square Fluctuations:* Restricting the consideration to a finite volume V and substituting for ψ and u_i in (4) in terms of their transforms in three-dimensional Fourier space, $\overline{A_\psi}(k) + \delta A_\psi(k, t)$ and $\overline{A_i}(k) + \delta A_i(k, t)$, respectively, it may be shown, assuming $\partial \bar{\psi} / \partial x_i$ to be constant in V, (see Appendix I).

$$\overline{\frac{\partial \left| \delta A_\psi(k, t) \right|^2}{\partial t}} = - 2\mathcal{R}\left\{ \overline{\delta A_i(k, t) \delta A_\psi^*(k, t)} \right\} \frac{\partial \bar{\psi}}{\partial x_i}$$

$$+ \int_{k\text{-space}} Q_\psi(k, k') dk' - 2D_\psi k^2 \overline{\left| \delta A_\psi(k, t) \right|^2}. \tag{6}$$

Here $\mathcal{R}\{\ \}$ stands for the real part of the quantity within the brackets, * indicates the complex conjugate, $dk \equiv dk_1 dk_2 dk_3$, and $Q_\psi(k, k')$ is the spectral density of the rate of transfer of mean square ψ-fluctuations to the Fourier component of wavenumber k from that of wavenumber k'. Again in this form the first and last

terms on the right describe the excitation and dissipation, respectively. The extra, integral term represents the internal mixing, between all other Fourier components in the spectrum and that particular component being considered, of wavenumber k. On close inspection it is found that the function Q_ψ is antisymmetric in its two arguments (see Appendix I); i.e.,

$$Q_\psi(k, k') = -Q_\psi(k', k).$$

Thus the exchange term contributes nothing to the overall fluctuations since its integral over all k-space will be zero. In turn this implies the conservation of mean square fluctuations in the inertial transfer process and provides the answer to the second question in Section III-A.

3) *The Transfer Function and the Fluctuation Spectrum:* Integrating (6) over all directions of the vector wavenumber k and suitably normalizing with respect to the volume V over which the Fourier transforms were defined, yields, in the steady-state, (see Appendix I) the relation

$$I_{i\psi}(k)\frac{\partial\bar{\psi}}{\partial x_i} + \int_0^\infty P_\psi(k, k')dk' = 2D_\psi k^2 E_\psi(k), \qquad (7)$$

where

$$E_\psi(k) \equiv \frac{k^2}{8\pi^3 V}\int_{4\pi}\overline{|\delta A_\psi(k, t)|^2}d\Omega(k),$$

the spectral density of mean square ψ-fluctuations per unit volume (m.s. $\delta\psi$/vol.). $d\Omega(k) \equiv$ elemental solid angle in k-space. Once more the first term on the left is the excitation, the second is the exchange, and the term on the right is the molecular dissipation. Now, integrating (7) from a given value of wavenumber to infinity one has, taking account of the antisymmetry which P_ψ inherits from Q_ψ.

$$2D_\psi\int_k^\infty k''^2E_\psi(k'')dk'' - \frac{\partial\bar{\psi}}{\partial x_i}\int_k^\infty I_{i\psi}(k'')dk''$$

$$= \int_k^\infty dk''\int_0^k P_\psi(k'', k')dk' \equiv S_\psi(k). \qquad (8)$$

Thus $S_\psi(k)$ is the net rate of transfer of m.s. $\delta\psi$/vol. across wavenumber k. This transfer function is analogous to the corresponding kinetic energy transfer, $S(k)$, which many authors[13] have considered in the case of turbulent flow, except that there decaying turbulence is treated rather than the steady-state situation postulated here.

[13] *Ibid.*, pp. 126 ff.

The following properties of $S_\psi(k)$ should be noted.

a) If there is a large k-range over which

$$\int_0^k k''^2E_\psi(k'')dk'' \langle\langle\langle \int_k^\infty k''^2E_\psi(k'')dk'' \qquad (9a)$$

and

$$\int_0^k I_{i\psi}(k'')dk'' \rangle\rangle\rangle \int_k^\infty I_{i\psi}(k'')dk'', \qquad (9b)$$

$S_\psi(k)$ is sensibly constant in this range. This corresponds to the inertial subrange in the universal equilibrium theory.

b) If, for the eddy sizes of interest, molecular diffusion is of secondary importance; *i.e.*, $L\delta u_L/D_\psi \gg 1$, where δu_L is the rms turbulent velocity characteristic of L-size eddies, (9a) above is satisfied for the corresponding k range. Then, over the range of interest, $S_\psi(k)$ *is either constant, or as a result of the gradient of* $\bar{\psi}$, *an increasing function of* k.

c) Over that range of k such that, in any small wavenumber interval, the total of mean square ψ-fluctuations produced by the excitation and removed by the dissipation is of a smaller order of magnitude than that exchanged among the various Fourier components by the inertial transfer process—the cumulative nature of the excitation and dissipation insures this condition is satisfied well beyond the inertial subrange in both directions—$E_\psi(k)$ depends only upon $S_\psi(k)$, $S(k)$, and k. Under these circumstances, on dimensional grounds alone, $E_\psi(k)$ and $S_\psi(k)$ are related in general magnitude by

$$E_\psi(k) \sim S_\psi(k)[S(k)]^{-1/3}k^{-5/3}. \qquad (10)$$

Combining (b) and (c) it is apparent that the result (2) reached in Section III-A by heuristic reasoning must in fact be true. Fig. 2 depicts the relations among the various spectra and the transfer function $S_\psi(k)$.

4) *The Scattering Coefficient:* It has been shown[1,2] that the scattering coefficient

$$\sigma \equiv \frac{\text{angular density of scattered power per unit volume of scatterer}}{\text{power density of the wave front incident upon the scatterer}}$$

is related to $\overline{|\delta A_n(k, t)|^2}$ by

$$\sigma = \frac{4\pi^2\sin^2\chi}{\lambda^4}\frac{\overline{|\delta A_n(k_\sigma, t)|^2}}{V}. \qquad (11)$$

$\delta A_n(k, t)$ is the analysis, in 3-dimensional Fourier space, of the index of refraction variations within the volume V, χ is the angle between the incident electric field at V and the ray to the receiver, and k_σ is defined in Fig. 3. If $\overline{|\delta A_n(k, t)|^2}$ is isotropic at k_σ,

$$\sigma = \frac{8\pi^4\sin^2\chi}{\lambda^4}\frac{E_n(k_\sigma)}{k_\sigma^2}. \qquad (12)$$

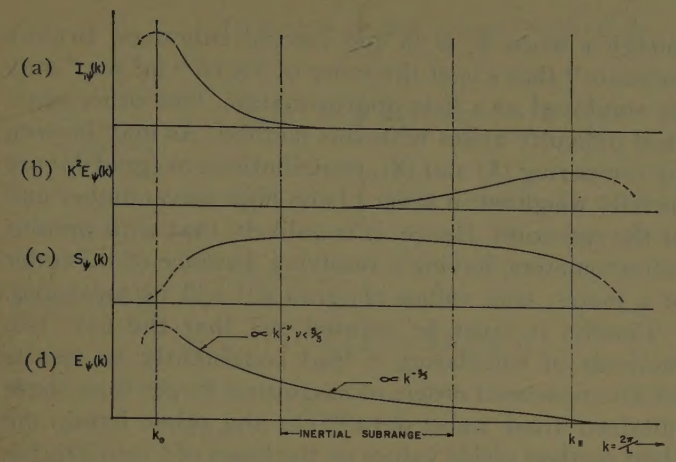

Fig. 2—Relative shapes of the spectral and transfer functions which play a role in turbulent mixing. (a) Excitation, (b) dissipation, (c) internal transfer, (d) spectral density.

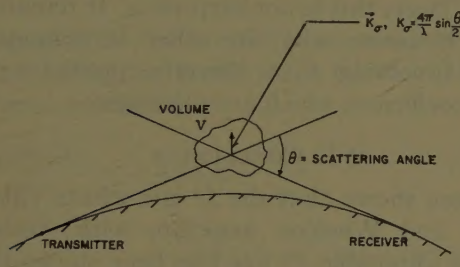

Fig. 3—Geometry of the scatter problem.

Fluctuations of the refractive index are, in general, attributable to fluctuations of one or several properties of the atmosphere (electron density in the ionosphere, moisture vapor concentration and temperature in the troposphere) each of which is conserved according to (3).[14] Consequently, $E_n(k)$ will take the form of (10) and (12) becomes

$$\sigma \sim \frac{8\pi^4 \sin^2 \chi B_\psi}{\lambda^4} S_\psi(k_\sigma)[S(k_\sigma)]^{-1/3} k_\sigma^{-11/3}, \qquad (13)$$

where B_ψ is the conversion factor from m.s. $\delta\psi$ to m.s. δn. Thus, as long as $k_\sigma \ll k_s$, so that molecular diffusion is of little importance, σ obeys an $L_\sigma^{11/3}$, or weaker, law. *The presence of a gradient of $\bar{\psi}$, if it has any effect, can only cause $S_\psi(k)$ to increase with k (decrease with increasing L) and therefore weaken the dependence.*

IV. Measured Refractive Index Spectra

There is now some direct evidence regarding the spectrum $E_n(k)$. Within the last several years Crain,[15] and others, have used the airborne refractometer to gather data on the microvariations of refractive index. Many of these data have been translated into mean square fluctuation spectra. True, they are one-dimensional spectra, $\Phi_n{}^1(k_1)$, derived from data along a line, whereas $E_n(k)$ is representative of the index variations throughout a volume. Nevertheless, assuming isotropy, which is strongly supported both theoretically and experimentally so long as the scale considered is small compared to the largest eddies, it may be shown (see Appendix II) that these two types of spectra are related by

$$E_n(k) = -k\frac{d\Theta_n(k)}{dk} = -k\frac{d\Phi_n{}^1(k)}{dk}. \qquad (14)^{16}$$

Thus, if they are power functions of k, they are identical except for a multiplicative constant. Consequently, it is of some interest to study log-log plots of such spectra to determine what k dependence is indicated. Each curve in Fig. 4 is the mean of several individual spectra derived from data collected in a given region at a particular altitude and time.[17] This tends to smooth out the random character of the individual samples. Note that the value of the slope is very close to $-5/3$, in excellent agreement with that predicted by (10) for the inertial subrange.

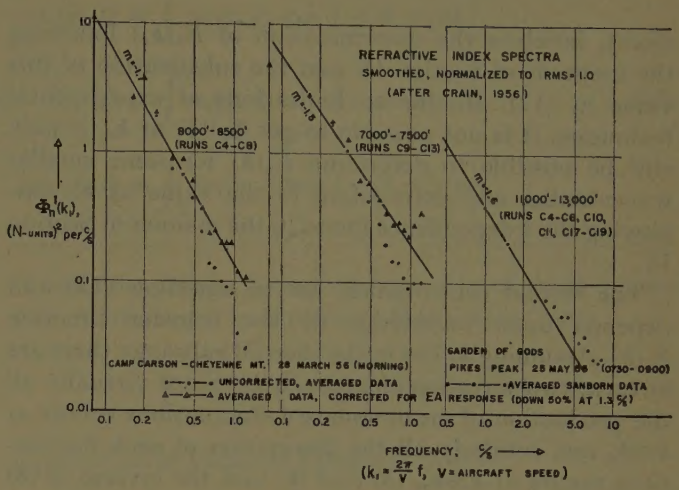

Fig. 4—Experimental verification of the $k^{-5/3}$ form for the spectrum produced by turbulent mixing. Each curve is the mean of the normalized spectra derived from the data of individual runs as indicated.

V. Evaluation of σ

There are two routes by which the value of the scattering coefficient may be calculated. The first, and more

[14] Temperature itself is not a conservable property; heat content is, however. Under the assumption of small Mach number, temperature, being a good measure of heat, obeys (3) to a close approximation. For a more complete discussion of this matter see reference 20.

[15] C. M. Crain, "Survey of airborne microwave refractometer measurements," Proc. IRE, vol. 43, pp. 1405–1411; October, 1955.

[16] The first half of this relation has been given previously by L. S. G. Kovasznay, M. S. Uberoi, and S. Corrsin, "The transformation between one- and three-dimensional power spectra for an isotropic scalar fluctuation field," *Phys. Rev.*, vol. 76, pp. 1263–1264; October 15, 1949. However, they did not discuss the second half, which is essential to the present argument.

[17] C. M. Crain, "Index of Refraction Fluctuations and 1046 MC Phase Difference Measurements Along an 18,000 Foot Elevated Path," University of Texas, Austin, Texas, Elec. Eng. Res. Lab., Rep. No. 6–15; June 1, 1956.

direct, involves the determination of $E_n(k_\sigma)$ following the methods of Section IV and the substitution of this value in (12). If, due to limitations of experimental technique, it is not possible to get $\Phi_n{}^1(k)$ at k_σ, it may still be possible to determine $E_n(k)$ for some smaller wavenumber and extrapolate to the value at k_σ, employing the k dependence found in the manner of Section IV.

The second route makes use of equation (13) and depends upon knowledge of the transfer function $S_\psi(k)$. Assuming k_σ lies in the inertial subrange there are in turn, two ways to calculate $S_\psi(k)$. Since virtually all the production of mean square ψ-fluctuations occurs at $k \ll k_\sigma$ and similarly all the dissipation of such fluctuations occurs at $k \gg k_\sigma$, (5) and (8) and the inverse of (8) (*i.e.*, the integral of (7) from zero to k) may be combined to yield

$$2K_\psi(\text{grad } \bar{\psi})^2 = S_\psi(k_\sigma) = 2D_\psi\overline{(\text{grad } \delta\psi)^2}. \tag{15}$$

The eddy diffusivity K_ψ may be approximated by the product of the scale l and the rms turbulent velocity δu of the turbulent field

$$K_\psi \sim l\delta u \sim l^{4/3}[S(1/l)]^{1/3}. \tag{16}$$

The inertial subrange relations, though not strictly appropriate, have been employed in the final conversion. Assuming further that $S(1/l)$ is approximately equal to $S(k_\sigma)$, substitution in (13) gives

$$\sigma \sim \frac{16\pi^4 \sin^2 \chi B_\psi}{\lambda^4} l^{4/3}(\text{grad } \bar{\psi})^2 k_\sigma{}^{-11/3}. \tag{17}$$

In this formulation it must be noted that, because of the density stratification of the atmosphere, it is not the absolute gradient of $\bar{\psi}$ but rather the deviation from an adiabatic profile[18] which is required. That is, for (grad $\bar{\psi}$) in (17) one must substitute (grad $\bar{\psi}+\Gamma_\psi$), where Γ_ψ, the adiabatic lapse rate of ψ, is given by

$$\Gamma_\psi = \frac{g}{\gamma}\frac{\rho\psi}{p}. \tag{18}$$

g is the acceleration due to gravity, ρ is the density of the composite fluid, p is the pressure, and $\gamma = 1.4$.

If $\overline{(\text{grad } \psi)^2}$, can be determined, since it has been shown in Section III-B, 1) that $\overline{(\text{grad } \delta\psi)^2} \rangle\rangle \overline{(\text{grad } \bar{\psi})^2}$, and it therefore follows that $\overline{(\text{grad } \delta\psi)^2}$ is approximately equal to $\overline{(\text{grad } \psi)^2}$, the right side of (15) may be used to evaluate $S_\psi(k_\sigma)$. The calculation of σ is then straight forward except that a value must be assumed for $S(k_\sigma)$, which corresponds to the rate of dissipation of turbulent energy ϵ when k_σ is in the inertial subrange. Brunt's estimate[19] that ϵ is of the order of 5×10^{-4} m^2 sec^{-3} may be employed as a first approximation. One other practical difficulty arises with this method. As may be seen by comparing (5) and (8), contributions to $\overline{(\text{grad } \psi)^2}$ are heavily weighted in favor of the high wavenumber end of the spectrum. Hence, it is unlikely that with present refractometers, having a resolving distance of the order of a meter, true values of $\overline{(\text{grad } \psi)^2}$ will be measured.

Finally, it must be pointed out that the first two methods of calculating σ lead consistently to results which are several orders of magnitude larger than those obtained from radio data.[20] On the other hand, the third method yields values on the bases of Crain's measurement[21] of $\overline{(\text{grad } n)^2}$ which are too low. In view of the closing comments in the previous paragraph, together with the possibility that Brunt's estimate of ϵ may be too large, this is not surprising. It remains to be explained, however, why the other techniques, especially that involving $E_n(k)$ directly, predict values of scattering coefficient which are too large.

VI. Conclusion

It has been shown that the L^5 law which Villars and Weisskopf and Wheelon associate with "mixing-in-gradient" is untenable. It has also been shown that the $L^{11/3}$ law given by Batchelor and Silverman for isotropic mixing is equally appropriate for a large range of scales when mixing of an established gradient takes place and that, if the presence of a gradient has an effect, it must be to reduce the exponent, not increase it. This implies that the scattering coefficient should be proportional to $\lambda^{-1/3}$ and leaves unexplained the λ dependence which many of the radio data appear to indicate. That empirical spectra of refractive index fluctuations themselves agree with the $L^{11/3}$ law has been demonstrated. The fact that the calculation of σ in accordance with the $L^{11/3}$ law leads to values which are in excess of those measured by radio means is also unexplained. All of these results, taken together, seem to indicate that scatter theory, as it is currently based on atmospheric turbulence, can provide at best an imcomplete description of trans horizon propagation.

Appendix I

Derivation of the Time Rate of Change of the Spectrum of Mean Square ψ Fluctuations

Defining the three-dimensional Fourier transforms of ψ, $\bar{\psi}$, and $\delta\psi$ and u_i, $\bar{u}_i$, and δu_i within the finite volume V by

[18] That is, a vertical distribution of ψ such that a sample of the fluid which is transported vertically through the gravity-induced pressure gradient and which undergoes the corresponding expansion or compression adiabatically will always have a value of ψ equal to the ψ of its surroundings.

[19] D. Brunt, "Physical and Dynamical Meteorology," Cambridge University Press, p. 286; 1941.

[20] R. Bolgiano, Jr., "Turbulent Mixing and Its Role in Radio Scattering," Cornell University, School of Elec. Eng. Res. Rep. EE 334; April 30, 1957.

[21] Private communication.

$$A_\psi(k,t) = \int_V \psi(\mathbf{x},t)\exp\{-jk\cdot\mathbf{x}\}d\mathbf{x} \qquad A_i(k,t) \equiv \int_V u_i(\mathbf{x},t)\exp\{-jk\cdot\mathbf{x}\}d\mathbf{x}$$

$$\overline{A}_\psi(k) \equiv \int_V \bar{\psi}(\mathbf{x})\exp\{-jk\cdot\mathbf{x}\}d\mathbf{x} \quad \text{and} \quad \overline{A}_i(k) \equiv \int_V \bar{u}_i(\mathbf{x},t)\exp\{-jk\cdot\mathbf{x}\}d\mathbf{x} \tag{19}$$

$$\delta A_\psi(k,t) \equiv \int_V \delta\psi(\mathbf{x},t)\exp\{-jk\cdot\mathbf{x}\}d\mathbf{x} \qquad \delta A_i(k,t) \equiv \int_V \delta u_i(\mathbf{x},t)\exp\{-jk\cdot\mathbf{x}\}d\mathbf{x}$$

respectively,

$$A_\psi(k,t) = \overline{A}_\psi(k) + \delta A_\psi(k,t)$$

and

$$A_i(k,t) = \overline{A}_i(k) + \delta A_i(k,t).$$

Now, if $\delta\psi$ satisfies the conservation equation

$$\frac{\partial\delta\psi}{\partial t} = -\delta u_i\frac{\partial\bar{\psi}}{\partial x_i} - u_i\frac{\partial\delta\psi}{\partial x_i} + D_\psi\frac{\partial^2\delta\psi}{\partial x_r\partial x_r} \tag{20}$$

and if grad $\bar{\psi}$ may be treated as constant throughout V, by substituting for ψ and u_i in terms of their Fourier transforms one is led to

$$\frac{\partial[\delta A_\psi(k,t)]}{\partial t} = -\delta A_i(k,t)\frac{\partial\bar{\psi}}{\partial x_i} - \frac{j}{8\pi^3}\int_{k-\text{space}} k_i' A_i(k-k',t)\delta A_\psi(k',t)dk' - D_\psi k^2\delta A_\psi(k,t). \tag{21}$$

Then, expanding

$$\frac{\partial[|\,\delta A_\psi(k,t)\,|^2]}{\partial t}$$

and making use of the assumed dynamic incompressibility of the air,

$$\frac{\partial[|\,\delta A_\psi(k,t)\,|^2]}{\partial t} = -2\mathcal{R}\{\delta A_i(k,t)\delta A_\psi^*(k,t)\}\frac{\partial\bar{\psi}}{\partial x_i} - j\frac{k_i}{8\pi^3}\int_{k-\text{space}}\{\delta A_\psi^*(k,t)A_i(k-k',t)\delta A_\psi(k',t) - \delta A_\psi(k,t)A_i^*(k-k',t)\delta A_\psi^*(k',t)\}dk' - 2D_\psi k^2|\,\delta A_\psi(k,t)\,|^2. \tag{22}$$

Taking averages throughout,

$$\frac{\partial[\overline{|\,\delta A_\psi(k,t)\,|^2}]}{\partial t} = -2\mathcal{R}\{\overline{\delta A_i(k,t)\delta A_\psi^*(k,t)}\}\frac{\partial\bar{\psi}}{\partial x_i} + \int_{k-\text{space}} Q_\psi(k,k')dk' - 2D_\psi k^2\overline{|\,\delta A_\psi(k,t)\,|^2}, \tag{23}$$

where

$$Q_\psi(k,k') \equiv -j\frac{k_i}{8\pi^3}\{\overline{\delta A_\psi^*(k,t)A_i(k-k',t)\delta A_\psi(k',t)} - \overline{\delta A_\psi(k,t)A_i^*(k-k',t)\delta A_\psi^*(k',t)}\}.$$

If one now defines the spectral density of mean square ψ-fluctuations per unit volume, $E_\psi(k)$, such that

$$\int_0^\infty E_\psi(k)dk = \frac{1}{V}\int_V \overline{|\,\delta\psi(\mathbf{x},t)\,|^2}d\mathbf{x}, \tag{24}$$

application of Parseval's theorem yields

$$E_\psi(k) = \frac{k^2}{8\pi^3 V}\int_{4\pi}\overline{|\,\delta A_\psi(k,t)\,|^2}d\Omega(k). \tag{25}$$

On integrating (23) over all directions of the vector wavenumber k and dividing both sides by $8\pi^3 V$, one has

$$\frac{\partial E_\psi(k)}{dt} = I_{i\psi}(k)\frac{\partial\bar{\psi}}{\partial x_i} + \int_0^\infty P_\psi(k,k')dk' - 2D_\psi k^2 E_\psi(k), \tag{26}$$

where

$$I_{i\psi}(k) = -\frac{k^2}{8\pi^3 V}\int_{4\pi}\mathcal{R}\{\overline{\delta A_i(k,t)\delta A_\psi^*(k,t)}\}d\Omega(k)$$

and

$$P_\psi(k,k') = \frac{k^2k'^2}{8\pi^3 V}\int_{4\pi}\int_{4\pi} Q_\psi(k,k')d\Omega(k')d\Omega(k).$$

Appendix II

The Relation Between the One- and Three-Dimensional Spectra of Scalar Point Functions

Let $\delta n(\mathbf{x})$ be a scalar point function defined in a finite volume V and $\delta A_n(k)$ be its Fourier transform, such that

$$\delta n(\mathbf{x}) = \frac{1}{8\pi^3}\int_{k-\text{space}}\delta A_n(k)\exp\{jk\cdot\mathbf{x}\}dk,$$

$$\delta A_n(k) = \int_V \delta n(\mathbf{x})\exp\{-jk\cdot\mathbf{x}\}d\mathbf{x}. \tag{27}$$

Define the covariance of δn, $\phi_{nn}(\xi)$, as

$$\phi_{nn}(\xi) = \frac{1}{V}\int_V \delta n(\mathbf{x})\delta n(\mathbf{x}+\xi)d\mathbf{x} = \frac{1}{8\pi^3 V}\int_{k-\text{space}}|\,\delta A_n(k)\,|^2\exp\{jk\cdot\xi\}dk. \tag{28}$$

Writing

$$\frac{|\,\delta A_n(k)\,|^2}{8\pi^3 V} \equiv \Phi_n(k),$$

one has

$$\Phi_n(k) = \frac{1}{8\pi^3}\int_{\xi-\text{space}} \phi_{nn}(\xi)\exp\{-jk\cdot\xi\}d\xi, \quad (29)$$

since $\phi_{nn}(\xi)\to 0$ rapidly as $|\xi|\to\infty$. Then

$$\phi_{nn}(0) = \frac{1}{V}\int_V |\delta n(x)|^2 dx = \int_0^\infty E_n(k)dk$$

and

$$E_n(k) = k^2\int_{4\pi}\Phi_n(k)d\Omega(k). \quad (30)$$

Now, along any diameter of V, of length M, define

$$\delta n^1(x_1) \equiv \delta n(x_1, 0, 0) = \frac{1}{8\pi^3}\int_{k-\text{space}} \delta A_n(k)\exp\{jk_1x_1\}dk$$

$$= \frac{1}{2\pi}\int_{-\infty}^{\infty}\delta A_n{}^1(k_1)\exp\{jk_1x_1\}dk_1, \quad (31)$$

where

$$\delta A_n{}^1(k_1) \equiv \frac{1}{4\pi^2}\int_{-\infty}^{\infty}\int_{-\infty}^{\infty}\delta A_n(k)dk_2dk_3$$

$$= \int_{-M/2}^{M/2}\delta n^1(x_1)\exp\{-jk_1x_1\}dx_1$$

Then the covariance of $\delta_n{}^1$, $\phi_{nn}{}^1(\xi_1)$, is

$$\phi_{nn}{}^1(\xi_1) \equiv \frac{1}{M}\int_{-M/2}^{M/2}\delta n(x_1, 0, 0)\delta n(x_1+\xi_1, 0, 0)dx_1$$

$$= \frac{1}{2\pi M}\int_{-\infty}^{\infty}|\delta A_n{}^1(k_1)|^2\exp\{jk_1\xi_1\}dk_1 \quad (32)$$

Writing

$$\frac{|\delta A_n{}^1(k_1)|^2}{2\pi M} \equiv \Phi_n{}^1(k_1),$$

one has

$$\Phi_n{}^1(k_1) = \frac{2}{\pi}\int_0^\infty \phi_{nn}{}^1(\xi_1)\cos\{k_1\xi_1\}d\xi_1, \quad (33)$$

since $\phi_{nn}{}^1(\xi_1)\to 0$ rapidly as $\xi_1\to\infty$. Now, either $\phi_{nn}{}^1(\xi_1) = \phi_{nn}(\xi_1, 0, 0)$, or they converge stochastically.

But

$$\phi_{nn}(\xi_1, 0,0) = \int_{k-\text{space}}\Phi_n(k)\exp\{jk_1\xi_1\}dk$$

$$= \int_0^\infty \Theta_n(k_1)\cos\{k_1\xi_1\}dk_1, \quad (34)$$

where

$$\Theta_n(k_1) \equiv 2\int_{-\infty}^{\infty}\int_{-\infty}^{\infty}\Phi_n(k)dk_2dk_3$$

$$= \frac{2}{\pi}\int_0^\infty \phi_{nn}(\xi_1, 0, 0)\cos\{k_1\xi_1\}d\xi_1.$$

Thus, $\Phi_n{}^1(k_1)$, the spectrum of data along a straight line, is equal to $\Theta_n(k_1)$, the one-dimensional contraction of the three-dimensional spectrum $\Phi_n(k)$, or at least they also converge stochastically.

Finally, therefore, if $\delta n(x)$ is isotropic, so that $E_n(k) = 4\pi k^2\Phi_n(k)$ or $\Phi_n(k) = E_n(k)/[4\pi k^2]$,

$$\Phi_n{}^1(k_1) = \Theta_n(k_1) = 2\int_{-\infty}^{\infty}\int_{-\infty}^{\infty}\frac{E_n(k)}{4\pi k^2}dk_2dk_3$$

$$= \int_{|k_1|}^\infty \frac{E_n(k)}{2\pi k^2}2\pi k dk = \int_{|k_1|}^\infty \frac{E_n(k)}{k}dk \quad (35)$$

and

$$\frac{d\Phi_n{}^1(k_1)}{dk_1} = \frac{d\Theta_n(k_1)}{dk_1} = -\frac{E_n(|k_1|)}{|k_1|}$$

or

$$E_n(k) = -k\frac{d\Theta_n(k)}{dk} = -k\frac{d\Phi_n{}^1(k)}{dk}. \quad (36)$$

Acknowledgement

The author is deeply indebted to Dr. G. K. Batchelor, whose lectures and suggestions formed the basis for much of the analytical development contained in this paper. He also wished to express his sincere gratitude to Dr. W. E. Gordon for his invaluable guidance and encouragement, and to K. Naito for many hours given in helpful discussion.

The Influence of Moisture in the Ground, Temperature and Terrain on Ground Wave Propagation in the VHF-Band*

B. JOSEPHSON† AND Å. BLOMQUIST†

Summary—**Results are given from a general investigation regarding the different factors that govern vhf ground wave propagation at low heights and short distances, *i.e.*, mainly in the Sommerfeld region. In this work the influence on field strength from ground moisture and temperature, snow, topography, and vegetation, and also field strength variations along mixed land-water paths have been studied. The measurements refer to terrain typical for middle Sweden.**

Suitable formulas for field strength calculations over smooth ground are developed. The moisture in the ground is found to play a principal role and a method is shown for calculation of changes in the path attenuation caused by known or predicted changes in the water content of ground. The influence of temperature is found to be small, even when the ground freezes, but a covering of snow may be of greater consequence. Characteristics of local variations and exponential attenuation of the field in a forest is demonstrated, the fluctuations being very large and the average exponential attenuation factor mostly very small. Measurements along a mixed land to fresh-water path verifies Millington's recovery effect. The field over a hill is found to have a maximum value a certain distance below the top towards the transmitter.

Theory

FOR a smooth ground, the influence of the ground constants on field strength is determined by the complex dielectric constant (relative value) $\epsilon_k = \epsilon - j60\sigma\lambda = \epsilon(1 - j \text{ tg } \delta)$. By introducing a "ground function" $\zeta = \zeta_0 \cdot e^{jb}$ differently defined for horizontal and for vertical polarization,

$$\zeta_v = \frac{\epsilon_k^2}{\epsilon_k - 1}, \tag{1a}$$

$$\zeta_h = \frac{1}{\epsilon_k - 1}; \tag{1b}$$

general formulas for both kind of polarizations can be developed. The reflection coefficient at small grazing angles will be

$$K = -(1 - 2\psi\sqrt{\zeta}), \tag{2}$$

if

$$\psi\sqrt{\zeta} \ll 1,$$

and the space wave E_{sp} (vector sum of the direct and the ground reflected waves)

$$E_{sp} = \frac{E_0}{R} \left| 2\psi\sqrt{\zeta} + j\varphi \right|, \tag{3}$$

where

$$\varphi = \frac{4\pi H_1 H_2}{\lambda R} \ll 1.$$

H_1 and H_2 are antenna heights, R = distance, $E_0 = \sqrt{30PD}$, P = transmitted power, D = directivity of transmitting antenna.

The surface wave is

$$E_{su} = \frac{2E_0}{Rp}, \qquad p \leq 10, \tag{4}$$

where the numerical distance p is given by

$$p = \pi R/(\lambda\zeta_0). \tag{5}$$

The height-gain function at small heights will be

$$\phi(H) = 1 + j\frac{2\pi H}{\lambda\sqrt{\zeta}}. \tag{6}$$

At vhf, over land and fresh water, $tg\ \delta$ is negligible and the above formulas then give:

Horizontal polarization:

$$E_{sp} = E_h\sqrt{1 + \frac{1}{\epsilon - 1}\cdot G}. \tag{7a}$$

Vertical polarization:

$$E_{sp} = E_h\sqrt{1 + \frac{\epsilon^2}{\epsilon - 1}\cdot G}, \tag{7b}$$

where

$$E_h = E_0\frac{4\pi H_1 H_2}{\lambda R^2}, \tag{8}$$

$$G = \left(\frac{\lambda}{2\pi H_1} + \frac{\lambda}{2\pi H_2}\right)^2. \tag{9}$$

At horizontal polarization the surface wave can be neglected, (7a) thus giving the total field strength.

At vertical polarization it is suitable to calculate the total field strength from the surface wave and the height-gain functions,

$$E_{tot} = E_{su}\cdot\phi(H_1)\phi(H_2), \tag{10}$$

$$E_{su} = \frac{E_0}{R^2}\cdot\frac{\lambda}{\pi}\cdot\frac{\epsilon^2}{\epsilon - 1}, \tag{11}$$

$$\phi(H) = \sqrt{1 + \frac{\epsilon - 1}{\epsilon^2}\left(\frac{2\pi H}{\lambda}\right)^2}, \tag{12}$$

* Manuscript received by the PGAP, July 5, 1957.
† Res. Inst. Natl. Def., Stockholm, Sweden.

if

$$3\lambda\epsilon < R < 12000\cdot\lambda^{1/3} \quad (\lambda \text{ and } R \text{ in } m). \tag{13}$$

From (7)–(13) it can be seen that the field strength at low heights in the Sommerfeld zone at vhf obeys an inverse distance squared law.

Therefore the influence of a change in ϵ is equivalent in this case to a change of the antenna efficiencies; this indicates that only the properties of the ground near the antennas affect the received signal.

With this in mind, and in view of the law of reciprocity, the dielectric constant at both ends of the transmission path should have the same influence on the field strength. For the surface wave at vertical polarization over homogenous ground this influence is, according to (11), represented by the factor $\epsilon/\sqrt{\epsilon-1}$ at each end. If the dielectric constant has the value ϵ_1 at one end and ϵ_2 at the other end of the path the surface wave therefore will be

$$E_{su}(\epsilon_1, \epsilon_2) = \frac{E_0}{R^2}\cdot\frac{\lambda}{\pi}\cdot\frac{\epsilon_1\epsilon_2}{\sqrt{(\epsilon_1-1)(\epsilon_2-1)}}. \tag{14}$$

This has been shown more rigorously by Millington.

The Influence of Moisture in the Ground

Vhf field strength recordings at vertical polarization over smooth ground have shown variations up to 14 db over the same paths at different seasons. The measured field strengths correspond to ϵ-values from about 3 to 30, as calculated from (10)–(12).

Investigations have shown that the value of the effective dielectric constant is determined mainly by the water content of the ground and is relatively independent of the type of ground.

Very dry earth has effective ϵ-values between 2.5 and 3, and for wet earth ϵ is approximately proportional to the percentage water content, w per cent. Therefore, in vhf field strength calculations the empirical relation

$$\epsilon = 0.78\cdot w + 2.5 \tag{15}$$

may be used.

In most parts of Sweden the ground humidity has an average annual variation with maxima in the fall and in the spring and a low minimum in the summer. The range of vhf communication sets with low antennas varies correspondingly up to a ratio of more than 2:1. In military applications it is often important to know the range to be expected in a particular case. It is, however, difficult to determine the value of w in (15), which would enable the calculation of the range. Therefore, an apparatus has been developed for measurement of the effective ϵ, based on measuring the slope of the E vector from an adjacent test transmitter with vertically polarized antenna.

In some cases it is only required to know how the propagation conditions within a certain area have changed from one time to another. In solving this problem the following expression has been found to yield a useful measure of the variations in the water content of the ground,

$$w = C + \sum (p - e), \tag{16}$$

where

p is the precipitation (mm),
e is the evaporation (mm),
C is the water content at the start of observation.

The quantities p and e are relatively easy to determine. A linear relation between ϵ and w, as expressed by (15), is assumed and from measurements at different times the ϵ-w-curve can be drawn. The use of this relation is explained with reference to Fig. 1, showing a sketch of a nomogram between w, ϵ, λ, distance R between transmitting and receiving antennas and the field strength E at the receiver relative to the free space level at the same distance. At a certain time the field strength E_1 is measured, which gives the values ϵ_1 and w_1. If thereafter the water content would decrease with Δw mm a field strength E_2 may be predicted at the receiver.

This method has proved to give good results in time intervals of a few months.

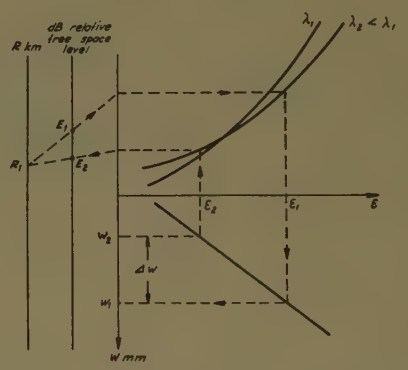

Fig. 1—Sketch of a nomogram for field strength calculations.

The Influence of Temperature and Snow

The temperature coefficient of the dielectric constant of ground is very small, of the order of -0.005 per °C, so no direct influence of temperature on vhf propagation may be expected. To check this, an analysis has been made of field strength measurements from different seasons, and no correlation with ground or air temperature was found.

However, an indirect influence may exist in so far as the ground moisture content and thus ϵ might decrease during an extended warm period.

When the ground becomes frozen or covered with snow, the dielectric constant will change with an amount which depends on the original ϵ-value. The higher this is, the greater will be the change even in relative measure. From propagation measurements at 50 mc over ground with $\epsilon = 15$ originally, the curves in Fig. 2 have

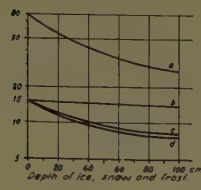

Fig. 2—Influence of ice, snow and frost in the ground on the effective dielectric constant, measured at 50 mc. Curve a = Ice on a lake, Curve b = Frost without snow, Curve c = Snow without frost, and Curve d = Snow and frost.

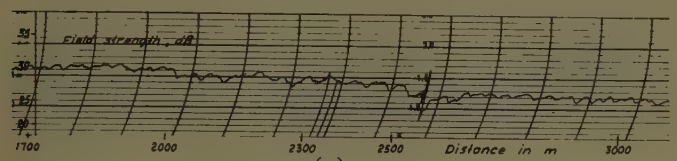

(a)

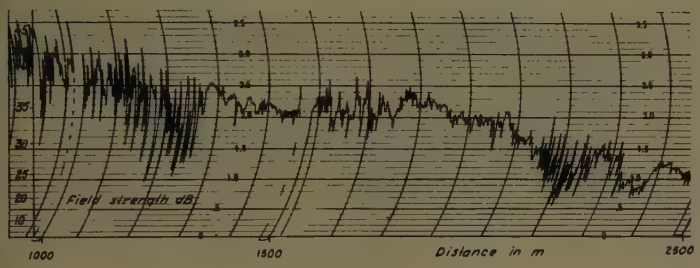

(b)

Fig. 3—Field strength variations, (a) at an open field, (b) in a forest. Frequency 44 mc.

been calculated. It is seen that a covering of snow causes a much greater decrease in ϵ and the field strength than does the freezing of ground.

Field Strength Variations at Open Fields and in Woods

A great number of field strength recordings over different types of terrain have been made within the vhf range both at vertical and horizontal polarization. In carrying out these tests the receiving and recording apparatus were placed at a fixed position while the transmitter was moved at a constant speed. The marked difference between open fields and woods can be seen from Figs. 3(a) and 3(b) respectively, which show typical recordings at 44 mc and vertical polarization. An analysis of such curves measured over approximately plain ground has shown that the field strength median over a 100 m distance obeys an inverse distance squared law, as expected.

The amplitude of the local variations depends on the vegetation, the frequency and the polarization.

The 10 per cent and 90 per cent levels referred to ± 50 m distance from a fixed point have been determined. Fig. 4 shows the difference in db between these two levels in a wood and at a field as a function of frequency. It is seen that at higher frequencies even horizontally polarized waves are much affected by the trees.

A relief picture of the field around a tree is shown in Fig. 5, which refers to 35 mc and vertical polarization.

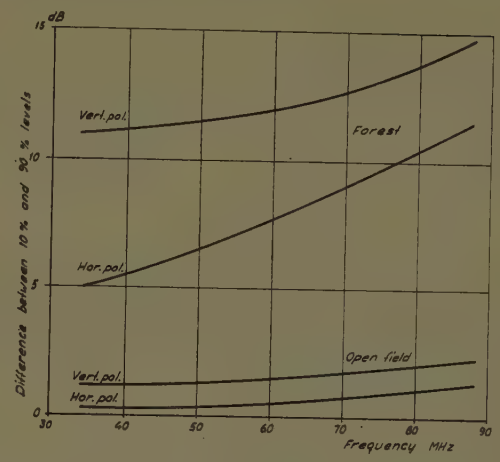

Fig. 4—Frequency dependence of local field variations within a distance of 100 m in a forest and at an open field.

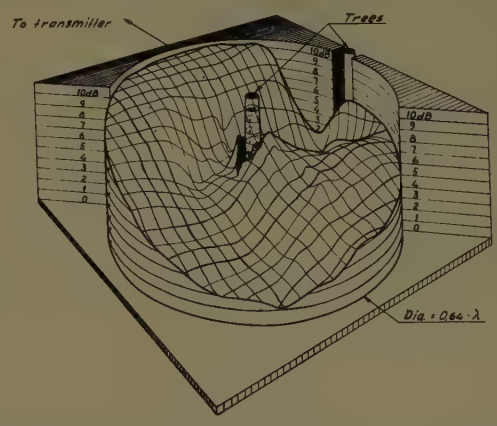

Fig. 5—The field around a tree, 35 mc; vertical polarization.

A variation of 11 db occurs within a distance of 1/3 wavelength from the tree.

These measurements were made in a pine-forest of a height up to about 20 m.

Attenuation in a Forest

In certain cases an exponential distance variation of field strength has been observed over short paths in a forest, *i.e.*, E proportional to $d^{-2} \cdot e^{-\alpha R}$.

For frequencies below 100 mc the exponential factor is insignificant in high pine-forest with little underwood. In a forest with dense leafy underwood attenuation factors at vertical polarization as high as 0.02 db/m at 30 mc and 0.04 db/m at 100 mc have been measured at small heights and over short paths. For longer paths (but in the Sommerfeld region) the attenuation factor α decreases. It is thus evident, that only the trees within a certain distance from the antennas affect the field strength appreciably at the receiving antenna. This is similar to the influence of the dielectric constant of ground.

Field Strength Variation Near a Shore

Fig. 6 shows a measured field strength curve a at a frequency of 44 mc along a mixed land to fresh-water

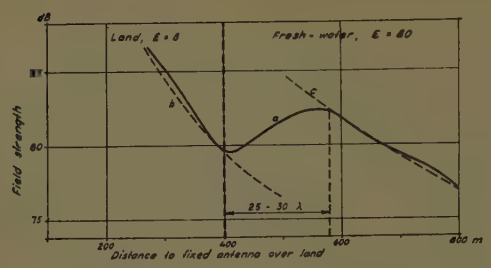

Fig. 6—Curve a = Measured field strength curve for a mixed land-water path, Curve b = Calculated curve for $\epsilon = 8$, and Curve c = Calculated curve for mixed path, $\epsilon_1 = 8$, $\epsilon_2 = 80$. Antenna heights 1.5 m (fixed antenna) and 4.5 m (movable antenna). Frequency 44 mc; vertical polarization.

path. The receiving antenna was located over land 400 m from the shore at a height $H_1 = 1.5$ m. The transmitting antenna was moved at a constant height $H_2 = 4.5$ m.

The dashed curve b is calculated from (10)–(12):

$$E_1 = E_{su}(\epsilon_1)\phi(H_1, \epsilon_1)\phi(H_2, \epsilon_1) \tag{17}$$

This curve corresponds to $\epsilon_1 = 8$ over land. The dashed curve c is calculated from (10), (12), and (14):

$$E_2 = E_{su}(\epsilon_1, \epsilon_2)\phi(H_1, \epsilon_1)\phi(H_2, \epsilon_2) \tag{18}$$

where $\epsilon_2 = 80$.

The transition between the two curves occurs over a distance ΔR, which measured in wavelengths closely corresponds to the quantity

$$\frac{\Delta R}{\lambda} = \frac{\epsilon_1\epsilon_2}{\sqrt{(\epsilon_1 - 1)(\epsilon_2 - 1)}}, \tag{19}$$

i.e., the proportionality factor of the surface wave over the mixed path according to (14).

The measured increase in field strength between the minimum and maximum points of the curve (Millington's "recovery effect") is 3 db which well agrees with calculations from the above formulas.

If the antenna over land were at greater distance from the shore (*i.e.*, $R \gg \Delta R$) the field strength gain when passing from land to water at a low height (*i.e.*, if $\phi(H_2) = 1$) according to (17) and (18) would be

$$\frac{\epsilon_2}{\epsilon_1}\sqrt{\frac{\epsilon_1 - 1}{\epsilon_2 + 1}}$$

which amounts to 9.5 db for $\epsilon_1 = 8$, $\epsilon_2 = 80$.

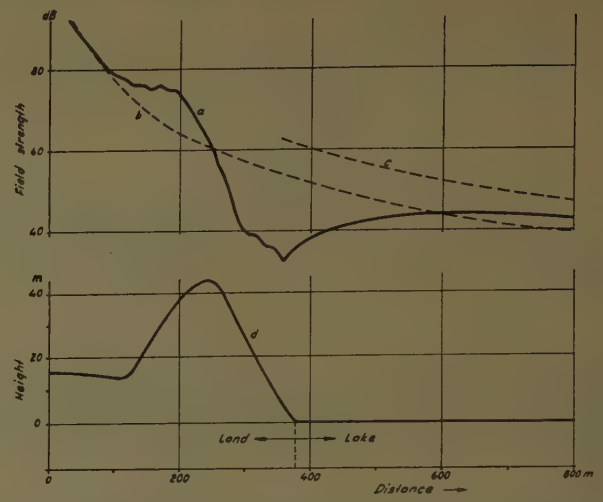

Fig. 7—Curve a = Measured field strength curve over a hill, 35 mc; vertical polarization, Curve b and Curve c = Calculated curves for smooth ground, uniform and mixed respectively, and Curve d = Path profile.

Variation of Field Strength Over a Hill

In Fig. 7 measured field strength curve a is shown over a hill adjoining a lake. The dashed curves a and b are calculated as the corresponding curves in Fig. 6.

The maximum increase in field strength above the inverse distance squared value occurs a short distance (about 5 to 6 wavelengths) before the top of the hill is reached. In the region behind the hill the field strength is determined by a combination of diffraction and the recovery effect over the water surface.

Distance Dependence, Fading Characteristics and Pulse Distortion of 3000-MC Trans-Horizon Signals*

B. JOSEPHSON† AND G. CARLSON†

Summary—Statistical analysis of signal recordings at 10 cm wavelength has given the following results.

The distance dependence of the half-hour signal median F_m over a sea path corresponds to a scattering parameter which is approximately inversely proportional to the height. Between F_m and the surface value of M a correlation coefficient of 0.62 is found, and between F_m and the dew point 0.55. A unit increase of M seems to be followed by a signal increase between the limits 0.3 and 0.8 db. The fading range, as defined between the 10 per cent and 90 per cent of time levels, is 12–14 db, and the fading frequency mostly about 2 c/s for a 300 km path.

Over a 260 km land path the pulse broadening was normally 0.1–0.2 μs which corresponds to a scattering parameter varying inversely as the first to second power of the height. A severe pulse distortion caused by selective fading is found to be very common.

Some other propagation characteristics are also discussed.

I. General

CONTINUOUS recordings of field strengths at 10 cm wavelength have been made during periods of several weeks at different seasons of the year. Paths from 200 to 300 km lengths, both over land and over sea, have been used. The measurements were carried out with pulsed signals, and apart from the study of field strength variations, the shape of received pulses has been observed. Vertical polarization was used throughout.

Geographically the investigation refers to middle and south Sweden including the east and west coast waters.

II. Test Equipment

For the sending end, two radar transmitters have been used, one with 200 kw and the other with 120 kw pulse power. At the earlier tests the pulse width was 2 μs, later 0.8 μs. The bigger transmitter had a rectangular shaped antenna with a directivity of 37 db. The other transmitter was equipped with a centerfed paraboloid reflector of 300 cm diameter having a directivity of 37 db.

At the receiving end the last mentioned antenna type and also a 130 cm paraboloid (29 db directivity) were used.

In the first experiments the receiver had a noise factor of 12 db and in the later 8 db. This was achieved by using cascodes according to Wallman and balanced mixers. The amplitude range was about 50 db. The received signals have been recorded on an Esterline Angus recorder for median values and during short intervals on a Brush recorder for rapid fading analysis. Pulse distortion has been studied on a Tektronix type 514 AD and oscilloscope.

* Manuscript received by the PGAP, July 5, 1957; revised manuscript received, November 19, 1957.

† Res. Inst. Natl. Def., Stockholm, Sweden.

Statistical analysis of the recordings was carried out by the aid of a semiautomatic curve-analyzer, which has been specially developed for propagation studies.

III. Results

In the analysis of the measured data, the propagation factor F is introduced, by which the received power P_r is referred to the calculated free space power level P_{fs} given by

$$P_{fs} = P_t \cdot \frac{G_t A_r}{4\pi d^2}, \tag{1}$$

where

P_t = transmitted power,
G_t = directivity of transmitting antenna,
A_r = absorption cross section of receiving antenna (m^2),
d = path distance (m).

The propagation factor F is then defined by

$$P_r = F^2 \cdot P_{fs}. \tag{2}$$

A. Medians of the Propagation Factor

From the recordings median values of F during half-hour intervals have been determined. In Fig. 1 the distribution of such medians, called F_m, are shown for four different cases. Curves A and B refer to measurements over sea (south Sweden) at distances of 190 km and 290 km respectively along same line from the transmitter, carried out continuously during 5 weeks in the months of October and November. Curves C and D refer to a 260 km path over land (middle Sweden) and represent continuous recordings during December and January respectively. Curve B shows signs of two different distributions.

It is not possible to decide from these measurements to which extent the difference between the curve B and the curves C and D is due to a characteristic difference between sea and land paths. The test paths in both cases are almost of the same length, but obstacles at the two terminals on the land path will give about 4 db extra propagation loss. Furthermore the surface reflection on the sea path may give some interference gain. Weather conditions were quite different, such that the air mass in the scattering region was colder and had lower relative humidity in the C- and D-cases than in the B-case.

In Fig. 2 the distance dependence of the F_m-factor over the two sea paths is elucidated. A distance power law $F_m^2 \sim d^{-n}$ is assumed, and the curve shows the time

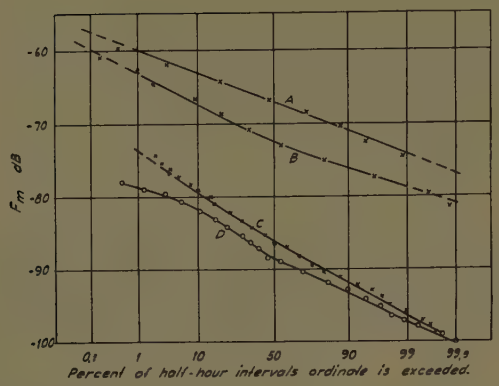

South Sweden

Curve A = 190 km sea path October–November, 1954
Curve B = 290 km sea path October–November, 1954

Middle Sweden

Curve C = 260 km land path December, 1956
Curve D = 260 km land path January, 1957

Fig. 1—Distribution of 3000 mc half-hour median propagation factor (log-normal-distribution).

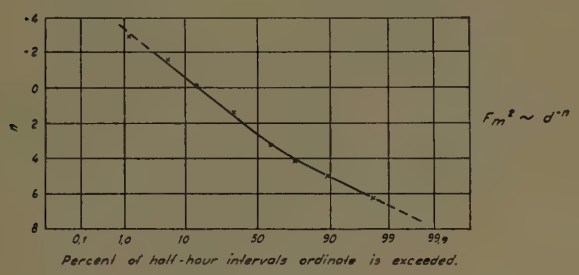

Fig. 2—Distribution of 3000 mc half-hour median distance dependence (log-normal-distribution).

distribution of n. It is seen from this curve, that for shorter periods (approximately 10 per cent of total time) the F_m-factor for the remote receiver has been larger than that for the nearer receiver. An inversion layer at a height and a location suitable for the longer path is a possible explanation.

B. Fading Characteristics

Statistical analysis of short time intervals of the scattered signal shows a Rayleigh distribution of the rapid fading (Fig. 3, lower curve). For longer intervals the distribution changes to normal (upper curve). The fading range, as defined between the 10 per cent and 90 per cent levels, amounts to 12–14 db, and is relatively independent of the momentary signal median, provided this does not exceed the long time median too much.

The fading frequency (number of times per second the median is passed in one direction) is normally about 2 c/s at a 300 km path and is approximately proportional to the path length.

It is interesting to know how often the signal has stayed below a given level for a given time. This has been evaluated for a number of cases, an example of which is shown in Fig. 4. Such analysis is conveniently carried out on the above-mentioned curve analyzer.

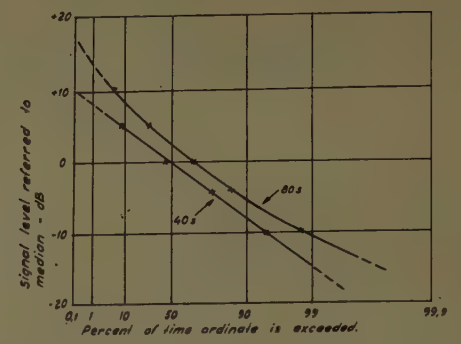

Fig. 3—Distribution of instantaneous 3000 mc signal level (log-Rayleigh-distribution).

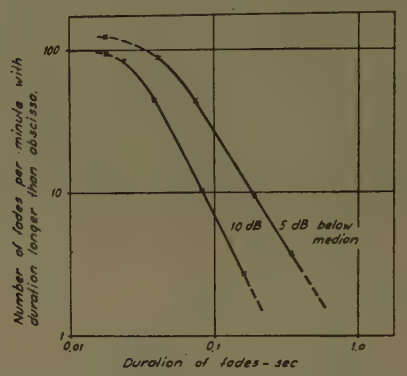

Fig. 4—Number vs duration of fast fades at 3000 mc on a 290 km path.

C. Pulse Distortion

Pulse distortion has been studied over the 260 km land path. The shape of the transmitted pulse is shown in Fig. 5(a), pulse length being 0.8 μs at midheight. The received pulses were photographed with 1/25 sec exposure time, thus giving the average shape of 20 pulses. Normally a pulse broadening of 0.1 to 0.2 μs was observed, as in Fig. 5(b). Also Figs. 5(c) and 5(d) show about 0.2 μs broadening, however in combination with a severe distortion caused by selective fading. This type of distortion is very frequent, and in general the shape of the received pulse is continuously changing within about 0.2 μs increased total width.

Not so often a much more pronounced pulse broadening, up to 0.8 μs, has been observed. Fig. 5(e) shows a pulse of 1.2 μs width, *i.e.*, 0.4 μs broadening.

D. Signal Dependence on Meteorological Factors

From meteorological observations near ground at both ends of the 290 km sea path the dew point t_D °C and the modified refractive index M were calculated. Mean values of t_D and ΔM ($M = 320 + \Delta M$) for both ends of the path at the times 7 AM and 7 PM each day are shown for a 15 days period in Fig. 6. In the same diagram half-hour medians of the propagation factor at times 7 AM and 7 PM are plotted.

From these curves it is evident that a correlation exists between the propagation factor median and both the M value and the dew point (or the partial water

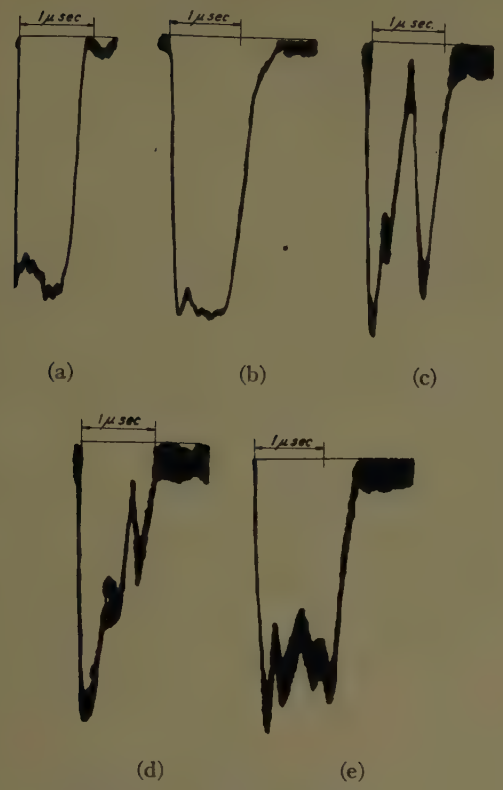

Fig. 5—Pulse distortion over 260 km land path. (a) Transmitted path, (b)–(e) Received pulses.

vapor pressure $e = 6.1 \cdot \exp(0.072 t_D)$mb). The correlation coefficient has been calculated to 0.62 between F_m and ΔM, and 0.55 between F_m and t_D. The correlation analysis for F_m and M gives the two regression lines a slope of 0.3 db and 0.8 db per unit change of M.

It is recognized that these figures are very uncertain in view of the short period analyzed.

The measurements over the 260 km land path which now have been extended over a much longer period will be statistically analyzed in the same way. This will indicate to which extent the deviations between the curves C and D for the land path and curves A and B for the sea paths in Fig. 1 may be correlated with average deviations in refractive index or dew point near ground.

E. Various Observations and Calculations

As mentioned in Section III-A relatively high signals over the longer sea path are sometimes associated with low signals over the shorter path. At such instances the fading frequency over the longer path is much lower than normal, often by a factor of 10, while at the same time a severe pulse distortion occurs of a type indicating multipath propagation.

An opposite situation is also frequently observed, where a high signal level, up to the free space value over

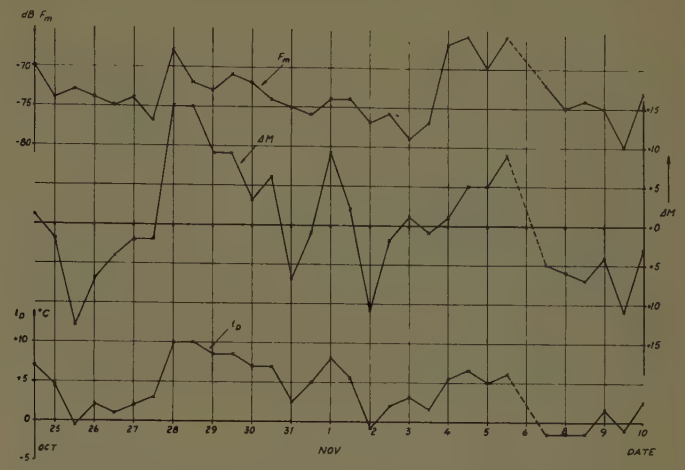

Fig. 6—Propagation factor and simultaneous surface values of modified refractive index and dew point. (290 km sea path, 3000 mc.)

the shorter sea path is concurring with a very low signal at the remote receiver. This is associated with duct propagation over the shorter path. A narrow peninsula of about 70 m height on which the receiver for the 190 km path is situated, prevents the formation of a continuous surface duct along the longer path. The high attenuation over this path may be explained by the change of shape of the lowest lobe caused by the duct. It is also possible that the intensity of the turbulence is smaller at these weather conditions.

The signal received by the scattering mechanism is calculated from the quantity (scattering coefficient)

$$\sigma = S(h) \cdot f(\theta), \tag{3}$$

where θ is the scattering angle and $S(h) = \overline{(\Delta\epsilon/\epsilon)^2}/s$ is the scattering parameter (s = scale of turbulence). The scattering parameter as a function of the height h may be assumed to obey a power law,

$$S = \text{const} \cdot h^{-p}. \tag{4}$$

Different p values give different distance dependence of the signal and different pulse widening.

Fig. 2 shows that the half-hour median of the propagation factor squared during 50 per cent of time has been inversely proportional to approximately the third power of distance. This corresponds to a p value in (4) of slightly more than 1.

As mentioned in Section III-C, a pulse broadening of 0.1 to 0.2 μs was normally observed over the 260 km land path. This corresponds to p values from 2 to 1.

For the type of distortion shown in Fig. 5(e), the pulse widening may be estimated to 0.4 μs, indicating a height difference between the propagation paths of about 3000 m. An inversion or a turbulent layer at a height of about 4500 m would therefore be a possible explanation of this distortion.

Some Microwave Propagation Experiences from a "Just-Below-Horizon" Path*

B. JOSEPHSON† AND F. EKLUND†

Summary—**Based on comparisons between field strength records at 2300 mc and simultaneously measured M curves it is concluded that the most important propagation disturbances on the test path are caused by reflections from discontinuities in the refractive index profile. The occurrence probability for such discontinuities is shown to have a marked seasonal and diurnal period with a maximum in the summer and around sunrise.**

I. Test Path and Measurements

THE path profile is shown in Fig. 1 for a modified earth radius $a_e = 4a/3$. The line between transmitter and receiver is broken mainly by two ridges covered with wood.

Field strength recordings over this path have been made almost continuously since the spring of 1955 at a frequency of 2300 mc. During some periods, meteorological soundings with the aid of thermistor sonds carried by a captive balloon were made at a point on the path up to a height of about 300 m. These measurements were made mostly when the prevailing weather situation was favorable for air stratification at low height.

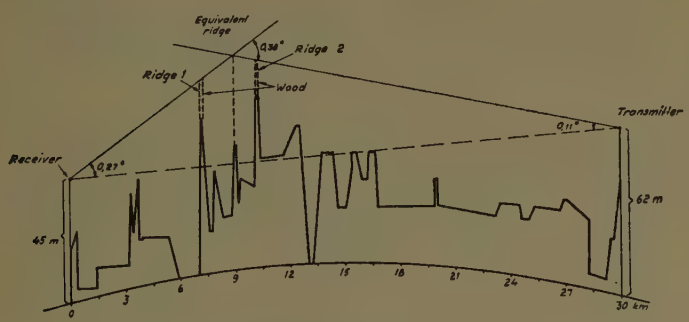

Fig. 1—Path profile. Earth radius 4/3·6370 km.

II. Theoretical Considerations

A. Diffraction

The propagation factor F (the ratio between actual and calculated free space field strengths at receiver) corresponding to diffraction signals has been calculated by two methods: 1) Diffraction over an equivalent sharp edge (calculation carried out by aid of Cornu's spiral). This gives F equal to -18.5 db. As seen later this value is far too high. 2) Diffraction over four spherical surfaces determined by the antenna heights over surrounding terrain and the height and position of the two ridges.[1] The result is F equal to -35 db.

B. Scattering

The propagation factor corresponding to the scattered signal median has been calculated according to the Booker and Gordon theory. The scattering parameter was assumed to be independent of height, which is justified over this short path. An F value of about -50 db was found.

Thus the scattered signal is negligible compared with the diffraction signal.

C. Tropospheric Reflections

A plane horizontal discontinuity in the atmosphere is assumed where the refractive index changes from n to $n(1-\Delta n)$. At nearly grazing angles ψ the reflection coefficients for vertically and horizontally polarized waves will be

$$K_{\text{vert}} = \frac{1 - 2\Delta n - \sqrt{1 - 2\Delta n/\psi^2}}{1 - 2\Delta n + \sqrt{1 - 2\Delta n/\psi^2}} \approx \frac{1 - \sqrt{1 - 2\Delta n/\psi^2}}{1 + \sqrt{1 - 2\Delta n/\psi^2}} = K_{\text{hor.}} \qquad (1)$$

This gives for both kinds of polarizations the relation

$$\Delta M = \psi^2 \cdot \frac{2K}{(1+K)^2}, \qquad (2)$$

where ψ is measured in milliradians and $\Delta M = \Delta n \cdot 10^6$.

In view of the fact that no sharp discontinuities exist in the atmosphere the above formulas may yield too high values of the reflection coefficient. From a rigorous treatment of this problem by Millington[2] it may be concluded, that (1) be fairly accurate if the change ΔM take place in a height Δh fulfilling the inequality

$$\Delta h \leq \lambda/\psi. \qquad (3)$$

When the field at the receiver is composed of diffracted and reflected waves of about the same magnitude this will be observed as interference fading and an about 3 db increase of signal median over the normal diffraction level. This case would occur if the reflection coefficient is equal to the diffraction propagation factor as defined in Section II-A. Thus a diffracted signal of case 2 in Section II-A corresponds to $K = 10^{-1.75} = 0.018$.

The necessary values of ΔM, calculated from (2) to give this value of K over the test path (Fig. 1) are:

Height of discontinuity	150	200	400	900 m
ΔM	1.5	3.2	19	120

* Manuscript received by the PGAP, July 5, 1957.

† Res. Inst. Natl. Def., Stockholm, Sweden.

[1] K. A. Norton, P. L. Rice, and L. E. Vogler, "The use of angular distance in estimating transmission loss and fading range for propagation through a turbulent atmosphere over irregular terrain," Proc. IRE, vol. 43, pp. 1488–1526; October, 1955.

[2] G. Millington, "The reflection coefficient of a linearly graded layer," *Marconi Rev.*, pp. 140–151; October–December, 1949.

D. Refraction

From the path profile it may be calculated that a direct ray can reach the receiver by refraction if the M curve has a gradient

$$dM/dh \leq -0.13\ m^{-1}$$

up to a height of about 150 m. With M gradients in between the normal atmosphere value $+0.118\ m^{-1}$ and the above figure, the diffracted signal will be between its normal value and approximately the free space level.

III. Comparison Between Measured and Calculated Data

The measurements of field strength and refractive index have been analyzed with a view of distinguishing the influence of the different propagation mechanisms just discussed and to show the probability of their occurrence during different parts of the year and of the day.

A. Normal Atmosphere

When the meteorological soundings have shown a normal M curve, the received signal has always been very stable. The propagation factor was then -37 db in good agreement with the calculated diffraction level over spherical surfaces according to case 2 in Section II-A.

B. Low Level Stratification

Many soundings have shown fairly sharp low level discontinuities in the M curve as demonstrated in Fig. 2 together with the simultaneously taken field strength records.

Fig. 2(a) shows a rather small discontinuity. The signal median is somewhat higher than the normal diffraction level. The fading is rapid and has an amplitude of about 10 db. If the assumption is made that the fluctuations depend on varying reflected signal interfering with a steady diffraction signal, the corresponding reflection coefficient of the layer at 120 m height will be approximately 0.02 as calculated from the record. When calculated from (1) and the M curve, K is approximately 0.05.

In Fig. 2(b) a record is shown from an occasion, at which the signal during several hours has exceeded the free space level (*i.e.*, $F>1$). Extremely deep fading is also noticed. Calculations from the M curve shown in Fig. 2 and other M curves measured during the same period given reflection coefficients varying between 0.2 and about 1, mainly because of changes in the height of the layer. The condition (3) is not quite met in this case, but the error will be small. The concave shape of the reflecting surface may possibly further enhance the reflected wave.

Thus it seems probable that the high signals observed in this case and the fading in the first case have been caused by reflections. In fact, at every occasion when

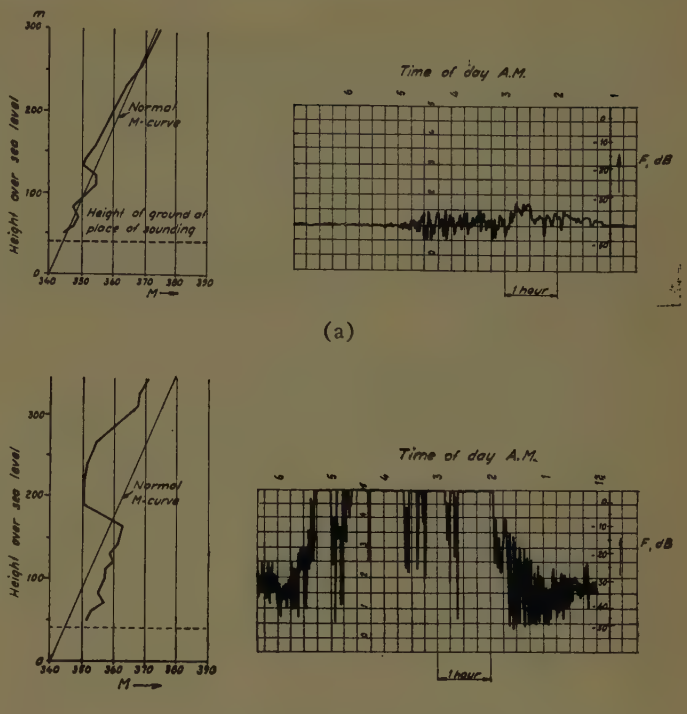

Fig. 2—M curves and signal records. Path as Fig. 1 2300 mc.

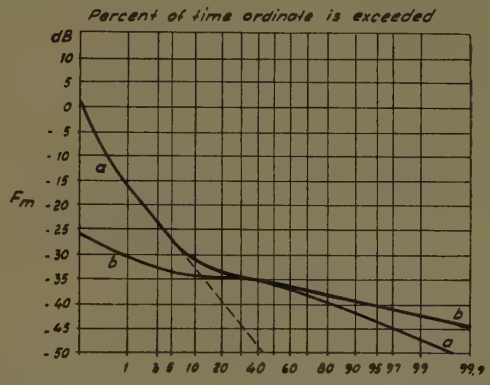

Fig. 3—Distribution curves for half-hour medians. Curve a = month of July, Curve b = month of December.

simultaneous meteorological measurements and signal recordings are available over this path, and the signal has exceeded the normal diffraction level more than about 5 db, this could be explained as caused by low level tropospheric reflections on the same indications as is exemplified above. On the other hand, a refractive index gradient such that a direct wave would be refracted from transmitter to receiver has never been observed.

IV. Statistical Analysis

A. Distribution of Signal Medians

Characteristic distribution curves for half-hour medians of the propagation factor, F_m, are shown in Fig. 3 for one summer and one winter period. One finds that the winter offers much more stable propagation conditions than does the summer.

The curve for the summer period seems to be composed of two different distributions, one connected to diffraction propagation with a median of −37 db, and the other influenced by low level tropospheric reflections. The transition between the two parts takes place at a level around 5 db over the median. The left part of the curve would by extrapolation give a median between −50 and −60 db, and it is interesting to compare this value with the value −50 db calculated for scattering mechanism.

B. Occurrence of M-curve Discontinuities

A minimum signal increase of 5 db over the median value is chosen as a criterion on existence of a reflecting tropospheric layer over the test path. Based hereupon the signal recordings during 18 months have been analyzed to give seasonal variations of the occurrence probability for such discontinuities and the result is shown in Fig. 4. During this summer the layers exist about 10 per cent of the time, during winter only 1 or 2 per cent of time.

Fig. 5 demonstrates the diurnal dependence of the probability during a summer period (months of July and August, 1955), which is seen to be very marked. Reflecting discontinuities have never been found around noon.

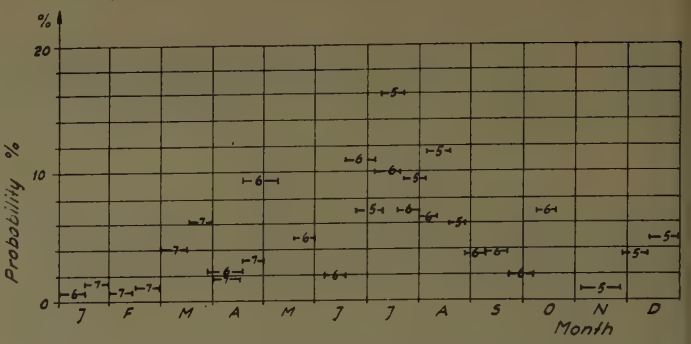

Fig. 4—Occurrence probability of low level reflecting discontinuities. 5—Measurements 1955, 6—Measurements 1956, 7—Measurements 1957.

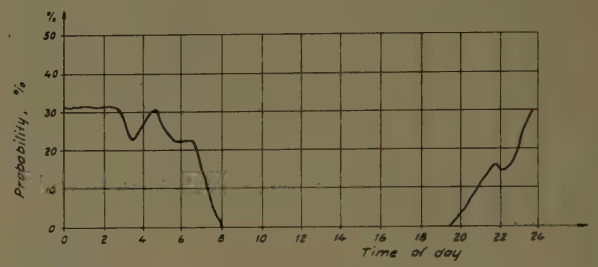

Fig. 5—Diurnal variation of occurrence probability of reflecting discontinuities, July–August, 1955.

Transients in Conducting Media*

PAUL I. RICHARDS†

***Summary*—The exact fields generated by transient electric and magnetic dipoles in an infinite conducting medium are derived. Specialization to brief, approximately triangular pulses then brings out the salient practical features of such signals. The peak signals are attenuated as r^{-3} or r^{-4} rather than exponentially, and, in a practical sense, they travel very slowly (mean effective velocity about equal to sonic speed for a range of 1 km in sea water).**

Introduction

THE electric field excited by a pulsed magnetic dipole, or current loop, in an infinite conducting medium has been obtained in explicit form by Wait.[1] The purpose of the present paper is twofold: 1) to extend Wait's results by deriving explicit formulas for the magnetic field and for the fields excited by an electric dipole; 2) to discuss these solutions and point out some practical aspects of transient electromagnetic signals in sea water.

These practical features are, first, that even the peak values of wide-band signals are not exponentially attenuated but are attenuated according to an inverse power of distance. This, of course, is in sharp contrast to the attenuation of sinewave signals and the distinction can be of great importance when considering the weak fields at "large" distances (100 meters or more in sea water). Secondly, the effective signal velocity is very slow and decreases with range to values as low as sonic velocities at distances of the order of 1 km in sea water.

Methods and Notation

For our purposes, it is expedient to write Maxwell's equations for a *homogeneous* medium in the special form (mks units)

$$2vT\nabla \times B = (1/v)\left[2 + 2T\frac{\partial}{\partial t}\right]E$$

$$2vT\nabla \times E = -2T\frac{\partial B}{\partial t}v$$

* Manuscript received by the PGAP, July 6, 1957; revised manuscript received November 8, 1957. This study was supported by the Office of Naval Research.

† Technical Operations, Inc., Burlington, Mass.

[1] J. R. Wait, "A transient magnetic dipole source in a dissipative medium." *J. Appl. Phys.*, vol. 24, pp. 341–343; March, 1953.

where

$$T = \epsilon/\sigma, \qquad v = 1/\sqrt{\epsilon\mu} \tag{1}$$

are the characteristic time constant and characteristic velocity of the medium. Thus if we introduce normalized space and time variables defined by

$$a = r/2vT, \qquad \tau = t/2T \tag{2}$$

then

$$\nabla_a \times \boldsymbol{B} = (1/v)\left[2 + \frac{\partial}{\partial\tau}\right]\boldsymbol{E}$$

$$\nabla_a \times \boldsymbol{E} = -v\partial\boldsymbol{B}/\partial\tau.$$

Assume that all fields vanish ("almost everywhere") when $t=0$ and take Laplace transforms with respect to the variable τ. This merely replaces $\partial/\partial\tau$ with p and the resulting equations may be solved by taking any solution of

$$\nabla_a \times \nabla_a \times \boldsymbol{Z} + p(p+2)\boldsymbol{Z} = 0 \tag{3}$$

and setting either

$$\boldsymbol{E} = -pv\boldsymbol{Z}, \qquad \boldsymbol{B} = \nabla_a \times \boldsymbol{Z} \tag{4}$$

or

$$\boldsymbol{B} = \frac{p+2}{v}\boldsymbol{Z}, \qquad \boldsymbol{E} = \nabla_a \times \boldsymbol{Z}. \tag{5}$$

Magnetic Dipole Source

If the source is a distribution of currents confined to a very small region of space, its magnetic dipole moment is defined by

$$\boldsymbol{M}(t) = \frac{1}{2}\int\int\int \boldsymbol{r} \times \boldsymbol{J}dV. \tag{6}$$

To determine the fields generated by such a source, it is simplest to observe that the vector potential for a static magnetic dipole[2] is $\boldsymbol{A} = (\mu/4\pi)\boldsymbol{M}\times\nabla(1/r)$ and the magnetic field (in the midplane) is thus proportional to $\mu M/4\pi r^3$. The solution of (3) and (4) which will give the same result at very small distances for arbitrary $\boldsymbol{M}(t)$ is

$$\boldsymbol{Z}_m(p) = \frac{\mu}{4\pi}(2vT)^{-3}\boldsymbol{m}(p)\times\nabla_a\left[a^{-1}\exp\left(-a\sqrt{p(p+2)}\right)\right] \tag{7}$$

where $\boldsymbol{m}(p)$ is the Laplace transform of $\boldsymbol{M}(t)$. Substituting (7) into (4), considerable manipulation gives

$$\boldsymbol{E} = (\mu/8\pi Tr^2)\boldsymbol{r}_0 \times \boldsymbol{M}_0 F(t) \tag{8}$$

$$\boldsymbol{B} = (\mu/4\pi r^3)\boldsymbol{r}_0 \times (\boldsymbol{r}_0 \times \boldsymbol{M}_0)G_1(t) + (\mu/4\pi r^3)[3(\boldsymbol{r}_0\cdot\boldsymbol{M}_0)\boldsymbol{r}_0 - \boldsymbol{m}_0]G_2(t) \tag{9}$$

where subscript 0 denotes a unit vector and where, in terms of the normalized variables defined in (2), the Laplace transforms of G_1, G_2, and F are

$$g_1(p) = a^2p(p+2)\exp\left\{-a[p(p+2)]^{1/2}\right\}m(p)$$

$$g_2(p) = \left\{1 + a[p(p+2)]^{1/2}\right\}\cdot\exp\left\{-a[p(p+2)]^{1/2}\right\}m(p)$$

$$f(p) = pg_2(p). \tag{10}$$

The Laplace inversion of $g_1(p)$ is readily obtained from standard references.[3] The other two functions, g_2 and f, were essentially inverted by Wait,[1] whose results can be stated as the following Laplace Transform pair

$$\mathfrak{L}\left\{b^3(t^2-b^2)^{-1}e^{-t}I_2[(t^2-b^2)^{1/2}]U(t-b)\right\} = \left\{1 + b[p(p+2)]^{1/2}\right\}\exp\left\{-b[p(p+2)]^{1/2}\right\} - \left\{1 + b(p+1) + \tfrac{1}{2}b^2\right\}\exp\left[-b(p+1)\right] \tag{11}$$

which may also be checked directly by evaluating the double integral of the pair (14) (with $\nu=2$).[4] In (11), $U(x)$ is the unit jump function defined by

$$U(x) = \begin{cases} 0, & \text{if } x < 0 \\ 1, & \text{if } x \geqq 0 \end{cases}$$

and the now standard notation, $I_n(Z) = i^{-n}J_n(iZ)$, denotes a Bessel function of imaginary argument. We shall have frequent use for the following "kernal" functions.

$$K_n(a,\tau) = a^3e^{-\tau}(\tau^2-a^2)^{-n/2}I_n[(\tau^2-a^2)^{1/2}]. \tag{12}$$

With the relation (11) all of the functions in (10) may be inverted:

$$G_1(\tau) = U(\tau-a)a^2e^{-a}[M''(\tau-a) + 2M'(\tau-a)] + U(\tau-a)\int_a^\tau K_1(a,u)[M''(\tau-u) + 2M'(\tau-u)]du \tag{13}$$

$$G_2(\tau) = U(\tau-a)[ae^{-a}M'(\tau-a) + (1+a+\tfrac{1}{2}a^2)e^{-a}M(\tau-a)] + U(\tau-a)\int_a^\tau K_2(a,u)M(\tau-u)du \tag{14}$$

$$F(\tau) = U(\tau-a)[ae^{-a}M''(\tau-a) + (1+a+\tfrac{1}{2}a^2)M'(\tau-a)] + U(\tau-a)\int_a^\tau K_2(a,u)M'(\tau-u)du \tag{15}$$

where primes denote differentiation with respect to the argument.

Eqs. (8), (9) and (13)–(15) constitute a complete solution (in our normalized units) for the magnetic dipole source. If we set $M'(t)=\delta(t)$, (8) and (15) become Wait's solution[1] for the electric field (as simplified by recurrence relations for the modified Bessel functions), while (9), (13), and (14) constitute an explicit expression

[2] See, for example, J. A. Stratton, "Electromagnetic Theory," McGraw-Hill Book Co., Inc., New York, N. Y., 1st ed., p. 237; 1941.

[3] For example, Erdélyi, Magnus, Oberhettinger, and Tricomi, "Tables of Integral Transforms," McGraw-Hill Book Co., Inc., New York, N. Y.; 1954.

[4] *Ibid.*, p. 201.

for the magnetic field. As will be seen below, $G_1(\tau)$ represents most of the transient magnetic field while G_2 contains the dc component if there is any. The latter fact is evident from the character of the vector factors in (9) and may also be proved (using $\lim_{p\to 0} pf(p) = \lim_{\tau\to\infty} F(\tau)$, if the latter exists) directly from (10), which shows that

$$\left.\begin{aligned} G_1(\tau) &\sim 2a^2M'(\tau) \\ G_2(\tau) &\sim M(\tau) \\ F(\tau) &\sim M'(\tau) \end{aligned}\right\} \text{ as } \tau = \infty.$$

The practical aspects of these various results will be discussed below.

Electric Dipole

With a small charge distribution for a source, the dipole moment may be defined as

$$\boldsymbol{P}(t) = \iiint r\rho dV. \tag{16}$$

For a static electric dipole, the scalar potential[5] is $(-1/4\pi\epsilon)\boldsymbol{P}\cdot\nabla(1/r)$ and the electric field (in the midplane) is proportional to $P/4\pi\epsilon r^3$; except for the factor $(1/\epsilon\mu)$ this field is the same as the magnetic field from a magnetic dipole. Comparing (4) with (5), we see that the correct fields will be obtained by using (5) instead of (4) and the following modification of (7)

$$\boldsymbol{Z}_e = \frac{1}{4\pi\epsilon}(2vT)^{-3}\boldsymbol{q}(p)\times\nabla_a[a^{-1}\exp(-a\sqrt{p(p+2)})] \tag{17}$$

where $\boldsymbol{q}(p)$ is the Laplace transform of $\boldsymbol{P}(t)$. Substituting (17) into (5), considerable manipulation gives the results,

$$\boldsymbol{B} = (\mu/8\pi Tr^2)\boldsymbol{P}_0\times\boldsymbol{r}_0R(t) \tag{18}$$

$$\boldsymbol{E} = (1/4\pi\epsilon r^3)\boldsymbol{r}_0\times(\boldsymbol{r}_0\times\boldsymbol{P}_0)S_1(t) + (1/4\pi\epsilon r^3)[3\boldsymbol{r}_0(\boldsymbol{r}_0\cdot\boldsymbol{P}_0) - \boldsymbol{P}_0]S_2(t) \tag{19}$$

where as before subscript, 0, denotes a unit vector and the time functions have the Laplace Transforms,

$$s_1(p) = a^2p^2q(p)\exp\{-a[p(p+2)]^{1/2}\}$$

$$s_2(p) = p(p+2)^{-1}q(p)\{1+a[p(p+2)]^{1/2}\}\cdot\exp\{-a[p(p+2)]^{1/2}\}$$

$$r(p) = (p+2)s_2(p).$$

If we define

$$\Pi(\tau) = e^{-2\tau}\int_0^\tau e^{2u}P'(u)du = P(\tau) - 2e^{-2\tau}\int_0^\tau e^{2u}P(u)du \tag{20}$$

then the functions s_1, s_2, and r may be inverted as before, and the following results are obtained.

$$S_1(\tau) = U(\tau-a)a^2e^{-a}P''(\tau-a) + U(\tau-a)\int_a^\tau K_1(a,u)P''(\tau-u)du \tag{21}$$

$$S_2(\tau) = U(\tau-a)[(1+a+\tfrac{1}{2}a^2)e^{-a}\Pi(\tau-a) + ae^{-a}\Pi'(\tau-a)] + U(\tau-a)\int_a^\tau K_2(a,u)\Pi(\tau-u)du \tag{22}$$

$$R(\tau) = U(\tau-a)[(1+a+\tfrac{1}{2}a^2)e^{-a}P'(\tau-a) + ae^{-a}P''(\tau-a)] + U(\tau-a)\int_a^\tau K_2(a,u)P'(\tau-u)du. \tag{23}$$

With regard to the function $\Pi(\tau)$, note that it is essentially a "smeared out" version of $P(\tau)$. The main effects of this smearing may be estimated by differentiating (20) which gives $\Pi' = P' - 2\Pi$. Thus $\Pi' = 0$ when $2\Pi = P'$, and it follows that (in normalized units),

$$\Pi_{\max} \leq \tfrac{1}{2}(P')_{\max}. \tag{24}$$

If $P(t)$ does not change appreciably in times of the order of $2T$, the equality in (24) will be a good approximation.

In this case, of course, there are no asymptotic dc fields unless $P(\tau)$ increases like τ indefinitely. As before, we can derive the asymptotic relations for $\tau\to\infty$,

$$S_1(\tau) \sim a^2P''(\tau)$$

$$S_2(\tau) \sim \tfrac{1}{2}P'(\tau)$$

$$R(\tau) = P'(\tau).$$

Attenuation and Signal Velocity

In considering the practical implications of the above results, it must be recalled that distances and times have been expressed in units of $2vT$ and $2T$, respectively. For sea water $2T = 3\times10^{-10}$ sec and $2vT \doteq 1$ cm. Thus the numerical values of a in the above equations are essentially equal to the range in centimeters, and at 1 km range, for example, $a = 10^5$. These large values of the variables have an essential effect on the general behavior of the functions $K_n(a,\tau)$ defined in (12), and it is necessary to examine their properties in some detail. We shall show that the integral terms in (13)–(19) and (21)–(23) determine the peak values of the fields.

When $\tau = a$, the fields first start to rise, and the values of the K functions are $K_1 = (a^3/2)e^{-a}$ and $K_2 = (a^3/8)e^{-a}$, but because the modified Bessel functions grow exponentially, the K functions gradually rise far above these very low initial values. When τ is very large, we may use the asymptotic expression,[6]

$$I_n(Z) \sim (a\pi Z)^{-1/2}e^Z \tag{25}$$

which is valid (for real Z) when

$$Z \gg (4n^2-1)/8. \tag{26}$$

[5] J. A. Stratton, *op. cit.*, p. 175.

[6] G. N. Watson, "Bessel Functions," Cambridge University Press, New York, N. Y., p. 203; 1952.

Substituting in (12), the asymptotic form of K_n (for fixed a and large $\tau - a$) is expressible in the form

$$K_n(a, \tau) \sim \frac{a^3 e^{-a^2/2\tau}}{(2\pi\tau)^{1/2}\tau^n}. \tag{27}$$

(In fact, this is even a fair approximation when $\tau = a$; it then contains a factor $e^{-a/2}$ and is, therefore, exceedingly small at ranges of interest in most practical problems.) Note that the final decay of K_n is not exponential but rather of the form τ^{-a}.

To locate the intermediate maximum in K_n, it is most convenient to assume at first that it coincides with the maximum of (27), which occurs at

$$\tau_m = a^2/(2n + 1). \tag{28}$$

For $a > 30$ (range > 30 cm approximately), $Z \equiv (\tau_m^2 - a^2)^{1/2}$ satisfies (26) more than adequately, thus justifying the procedure. By (27) and (28), the maximum values of the K_n are then

$$(K_1)_{\max} \doteq 0.462, \qquad (K_2)_{\max} \doteq 1.83/a^3 \tag{29}$$

occurring at $\tau = a^2/3$ and $a^2/5$, respectively.

To illustrate the peculiar behavior of these functions, consider a range of about 1 km in sea water, $a = 10^5$. Since $a^2/3 = 10^{10}/3$ and $2T$ is about 3×10^{-10} sec for sea water, we see that, while K_1 and K_2 start to rise (the signal "precursor" arrives) at about 30 μsec, the peak does not occur until about $t = 1$ second! The initial, "precursor" jump in K_1 is virtually zero, namely $(a^3/2)e^{-a} \doteq 10^{-43,000}$ as compared to the maximum value, ~ 0.462; note also that the peak of K_2 is only about 10^{-10} times that of K_1. Even for a range of 1 meter ($a = 10^2$) in sea water, $(K_1)_{\max} = 2500\ (K_2)_{\max}$ and these peaks occur at 1 μsec even though the "precursor" (magnitude about 10^{-38}) arrives at 1/30 μsec. Detailed values for $a = 10^4$ (100 m range in sea water) are given in Fig. 1 and Table I.

It is clear from these examples that for ranges of practical interest, at least in sea water, K_2 is usually much smaller than K_1 and that, in any case, the integral terms in (13)–(15) and (21)–(23) will be much larger than the other terms, which involve factors of e^{-a}. In this sense, the K functions are essentially the "delta function response" of the conducting medium.

Thus consider a brief pulse (either electric or magnetic dipole) of width W and with a more or less triangular shape. By "more or less triangular shape" we mean that the maxima of the derivatives of M or P are approximately given by

$$M_m' \doteq M_m/W, \qquad M_m'' \doteq M_m/W^2 \tag{30}$$

where the subscript m denotes maximum value. If the pulse width W satisfies

$$W/T \ll a^2 \tag{31}$$

then the kernal functions K_n are essentially constant in regions of width W/T near their maxima, and the integral terms in (13)–(15) and (21)–(23) can be approximated by taking the K functions outside the integral. In this way, for example, it follows from (13) and (29) that the peak value of $G_1(t)$ is approximately $\frac{1}{2}(M_m' + 2M_m) = M_m(1 + 1/2W)$ in normalized units or $M_m(1 + T/W)$ in arbitrary units. In this way the remaining functions can be approximately evaluated and the peak fields found. The results are (in ordinary mks units):

Magnetic dipole:

$$\boldsymbol{E}_{\max} \doteq (M_m/\pi\sigma r^4)\boldsymbol{r}_0 \times \boldsymbol{M}_0 \tag{32}$$

$$\boldsymbol{B}_{\max} \doteq (\mu M_m/4\pi r^3)\left(1 + \frac{T}{W}\right)\boldsymbol{r}_0 \times (\boldsymbol{r}_0 \times \boldsymbol{M}_0) + (\mu M_m W/\pi\sigma r^5)[3\boldsymbol{r}_0(\boldsymbol{r}_0 \cdot \boldsymbol{M}_0) - \boldsymbol{M}_0]. \tag{33}$$

Electric dipole:

$$\boldsymbol{E}_{\max} \doteq (P_m/4\pi\sigma W r^3)\boldsymbol{r}_0 \times (\boldsymbol{r}_0 \times \boldsymbol{P}_0) + (P_m/2\pi\sigma W r^3)(2vT/r)^2[3\boldsymbol{r}_0(\boldsymbol{r}_0 \cdot \boldsymbol{P}_0) - \boldsymbol{P}_0] \tag{34}$$

$$\boldsymbol{B}_{\max} \doteq (P_m/\pi\sigma r^4)(\boldsymbol{P}_0 \times \boldsymbol{r}_0). \tag{35}$$

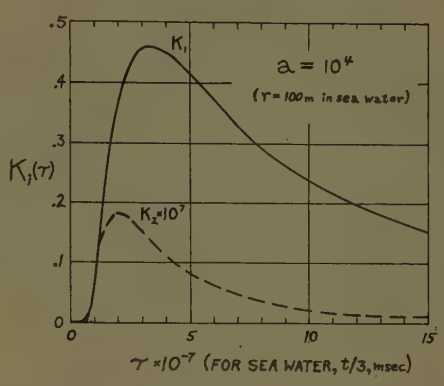

Fig. 1

TABLE 1

VALUES OF THE FUNCTIONS K_1, K_2 FOR $a = 10^4$ (100 METER RANGE IN SEA WATER)

τ	K_1	K_2	t, msec for Sea Water
10^4	5×10^{-4332}	1.25×10^{-4332}	0.003
10^6	7.6×10^{-20}	7.6×10^{-26}	0.3
3×10^6	4.5×10^{-6}	1.5×10^{-12}	0.9
6×10^6	0.00652	1.09×10^{-9}	1.8
10^7	0.0850	8.5×10^{-9}	3
1.5×10^7	0.245	1.63×10^{-8}	4.5
2×10^7	0.368	1.84×10^{-8}	6
2.5×10^7	0.432	1.73×10^{-8}	7.5
3×10^7	0.459	1.53×10^{-8}	9
3.33×10^7	0.462	1.39×10^{-8}	10
4×10^7	0.452	1.13×10^{-8}	12
5×10^7	0.415	8.03×10^{-9}	15
6×10^7	0.374	6.23×10^{-9}	18
8×10^7	0.298	3.72×10^{-9}	24
10^8	0.242	2.42×10^{-9}	30
2×10^8	0.110	5.50×10^{-10}	60
5×10^8	0.0323	6.46×10^{-11}	150
10^9	0.0120	1.20×10^{-11}	300
3×10^9	0.00239	7.98×10^{-13}	900
10^{10}	0.000398	3.98×10^{-14}	3000

These approximate values are valid for a pulse width, $W \ll T(r/2vT)^2 = \mu\sigma r^2/2$ and for a range, $r > 30(2vT) = (60/\sigma)\ (\epsilon/\mu)^{1/2}$. The second terms in (33) and (34) are usually much smaller than the first terms.

The results of (32)–(35) show that even the peak fields from a short pulse are attenuated algebraically rather than exponentially, in contrast to cw signals. Moreover, as already anticipated, the arrival times are surprisingly late. According to (28), the peak values (32)–(35) occur approximately when

$$t = t_m = (T/2)(r/2vT)^2 = \mu\sigma r^2/4.$$

This arrival time is perhaps more strikingly represented in terms of an average "practical" signal velocity,

$$\langle v \rangle_{\text{eff}} = r/t_m = 8v^2(T/r) = 8/r\sigma\mu. \tag{36}$$

For $r = 1$ km in sea water, this is 1.3×10^3 m/sec or about sonic velocity.

Conclusion

Exact expressions have been derived for the fields excited in an infinite conducting medium by magnetic or electric dipoles with arbitrary time variations. These rather unwieldy results are then studied for the special case of brief pulses in media such as sea water. Simple estimates for the peak transient fields at moderate to very large ranges are presented, which show that the attenuation with distance behaves like r^{-3} or r^{-4} instead of the very strong exponential cutoff characteristic of cw signals. The time of arrival of these peak fields is expressed as a mean effective "practical" signal velocity which varies with range and can be as low as sonic velocities.

By regarding a more general time—and space—variable source as a superposition of pulsed dipoles, these simple results can be used to obtain rapid approximate estimates of the important practical features of the resulting signals.

Determination of a Current Distribution over a Cone Surface Which Will Produce a Prescribed Radiation Pattern*

H. UNZ†

Summary—**The problem of determination of the current distribution over a cone surface, which will produce a prescribed radiation pattern, is formulated. *F* pattern and *G* pattern are defined and expressed in terms of a "potential" function Φ, in case of currents polarized in the direction of the generating lines of the cone.**

A matrix relationship is found between coefficients of a series expansion of Φ and coefficients of a series expansion of the currents. The relationship becomes a direct one to one correspondence in case of an infinite biconical system.

Introduction

THE problem of finding a current distribution along the surface of a cone in order to produce a prescribed far zone radiation pattern has become very important lately. While the mathematical formulation of the problem is not difficult and is based on already existing ideas, the method of solution in this paper is rather new.

The method of excitation of the required current distributions over the surface of the cone is not discussed herein. It is assumed that once the required current distribution has been found, it can be excited over the surface. The boundary value problem, which is quite difficult, also is not considered in this paper. We are interested here in the relationship between the far zone radiation field and the current distribution.

It is known that a problem of this kind is not unique, namely there are infinite numbers of current distributions which will produce, within a certain approximation, the same far zone pattern. By expanding the current and the far zone field in two double series, matrix relationships between the coefficients of the expansions can be found. Any two sets of coefficients, which obey those relationships, will be a solution of the problem of finding the far zone field which corresponds to the current dustribution or vice versa. In the case of an infinite biconical system, we have a one to one correspondence between the coefficients of the expansion of the far zone pattern and the coefficients of the expansion of the current distributions. It is similar to the result derived in the much simpler case of continuous line current distribution and its far zone pattern.[1]

* Manuscript received by the PGAP, September 30, 1957; revised manuscript received January 27, 1958. This work was supported by the U. S. Navy at the University of California, Berkeley, Calif., under Contract No. N7onr-29529.

† Elec. Eng. Dept., University of Kansas, Lawrence, Kan.

[1] H. Unz, "Linear Arrays with Arbitrarily Distributed Elements," University of California, Berkeley, E. R. L. Rep. Ser., No. 60, Issue No. 168, Navy Contract No. N7onr-29529, pp. 54–56; November 2, 1956.

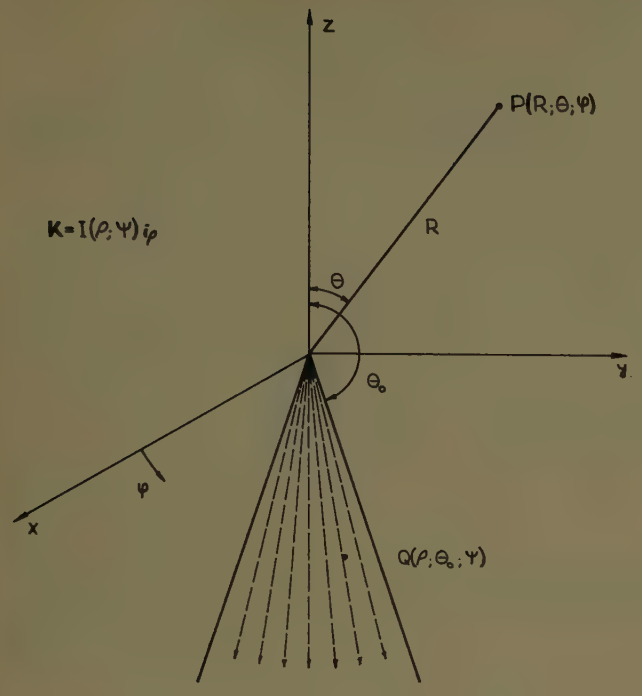

Fig. 1.

Formulation of the Problem

Spherical coordinates, with the origin at the apex of the cone (Fig. 1), are used. The surface of the cone is given by $\theta=\theta_0$. The coordinates of the observation point P are $P(R;\theta;\phi)$. The coordinates of the source point Q are $Q(\rho;\theta_0;\psi)$.

The far zone field is found by using the general formulas given by Silver[2]

$$E_\theta = -\frac{i\omega\mu}{4\pi R}e^{-ikR}\int_V\left[(\bar{J}_e\cdot\bar{i}_\theta) + \sqrt{\frac{\epsilon}{\mu}}(\bar{J}_m\cdot\bar{i}_\phi)\right]e^{ik\bar{a}\cdot\bar{i}_R}dV \quad (1a)$$

$$E_\phi = -\frac{i\omega\mu}{4\pi R}e^{-ikR}\int_V\left[(\bar{J}_e\cdot\bar{i}_\phi) - \sqrt{\frac{\epsilon}{\mu}}(\bar{J}_m\cdot\bar{i}_\theta)\right]e^{ik\bar{a}\cdot\bar{i}_R}dV \quad (1b)$$

where

$\bar{a}$ = radius vector from the origin to source point Q,
$\bar{J}_e$ = electric current density vector,
$\bar{J}_m$ = magnetic current density vector,
$\bar{i}_R$; $\bar{i}_\theta$; $\bar{i}_\phi$ = spherical coordinates unit vectors at $P(R;\theta;\phi)$,
$k=2\pi/\lambda=\omega/c$ $\quad i=\sqrt{-1}$,

with harmonic time variation $e^{+j\omega t}$.

From (1) it is seen that there is a complete similarity between the far zone fields received from electric currents ($\bar{J}_e$) and the far zone fields received from magnetic currents ($\bar{J}_m$). In order to discuss both of them in general, and since we discuss currents distributed over the surface of a cone; *i.e.*, surface currents $\bar{K}$, rather than volume currents $\bar{J}$, let us define the radiation pattern functions as

$$F(\theta;\phi) = \int\int_S(\bar{K}\cdot\bar{i}_\theta)e^{ik\bar{a}\cdot\bar{i}_R}dS \quad (2a)$$

$$G(\theta;\phi) = \int\int_S(\bar{K}\cdot\bar{i}_\phi)e^{ik\bar{a}\cdot\bar{i}_R}dS. \quad (2b)$$

$F(\theta;\phi)$ is called the F pattern and $G(\theta;\phi)$ is called the G pattern. In case of electric surface currents, the F pattern will be the radiation pattern of E_θ and the G pattern will be the radiation of E_ϕ. In case of magnetic surface currents (or slots), it will be the other way around.

The radius vector $\bar{a}$ from the origin to the source point on the surface of the cone $Q(\rho;\theta_0;\psi)$ is a straight line along a generating line of the cone and may be written

$$\bar{a} = \rho\bar{i}_\rho. \quad (3a)$$

The surface current density $\bar{K}$ is polarized in the direction of the generating lines

$$\bar{K} = I(\rho;\psi)\bar{i}_\rho \quad (3b)$$

where $I(\rho;\psi)$ is the current distribution over the surface of the cone $\theta=\theta_0$.

Substituting (3) in (2) and integrating over the cone surface we get

$$F(\theta;\phi) = \sin\theta_0\int_0^{2\pi}I(\rho;\psi)d\psi\int^{\rho_1}\rho d\rho(\bar{i}_\rho\cdot\bar{i}_\theta)e^{jk\rho\bar{i}_\rho\cdot\bar{i}_R} \quad (4a)$$

$$G(\theta,\phi) = \sin\theta_0\int_0^{2\pi}I(\rho;\psi)d\psi\int_{\rho_0}^{\rho_1}\rho d\rho(\bar{i}_\rho\cdot\bar{i}_\phi)e^{ik\rho\bar{i}_\rho\cdot\bar{i}_R}. \quad (4b)$$

Relation between F Pattern and G Pattern

From the vector analysis identities it may be easily shown[3] that

$$\frac{\partial}{\partial\theta}\bar{i}_R = \bar{i}_\theta \quad (5a)$$

$$\frac{\partial}{\partial\phi}\bar{i}_R = \bar{i}_\phi\sin\theta. \quad (5b)$$

Since ρ and $\bar{i}_\rho$ do not depend on θ and ϕ, we can write

$$\frac{\partial}{\partial\theta}e^{ik\rho(\bar{i}_\rho\cdot\bar{i}_R)} = e^{ik\rho(\bar{i}_\rho\cdot\bar{i}_R)}ik\rho\left(\bar{i}_\rho\cdot\frac{\partial\bar{i}_R}{\partial\theta}\right) \quad (6a)$$

$$\frac{\partial}{\partial\phi}e^{ik\rho(\bar{i}_\rho\cdot\bar{i}_R)} = e^{ik\rho(\bar{i}_\rho\cdot\bar{i}_R)}ik\rho\left(\bar{i}_\rho\cdot\frac{\partial\bar{i}_R}{\partial\phi}\right). \quad (6b)$$

[2] S. Silver, "Microwave Antenna, Theory and Design," McGraw-Hill Book Co., Inc., New York, N. Y., M.I.T., Rad. Lab. Ser. No. 12, p. 89, (134); 1949.

[3] H. B. Phillips, "Vector Analysis," John Wiley and Sons, Inc., New York, N. Y., p. 98, problem 14; 1933.

Substituting (5) in (6) and comparing with (4), we can write

$$F(\theta;\phi) = \frac{\partial}{\partial\theta}\frac{\sin\theta_0}{ik}\int_0^{2\pi} I(\rho;\psi)d\psi\int_{\rho_0}^{\rho_1} d\rho e^{ik\rho(\bar{\imath}_\rho\cdot\bar{\imath}_R)} \quad (7a)$$

$$G(\theta;\phi)\sin\theta = \frac{\partial}{\partial\phi}\frac{\sin\theta_0}{ik}\int_0^{2\pi} I(\rho;\psi)d\psi\int_{\rho_0}^{\rho_1} d\rho e^{ik\rho(\bar{\imath}_\rho\cdot\bar{\imath}_R)}. \quad (7b)$$

From (7) we see that we can write the far zone field in terms of a "potential" function $\Phi(\theta;\phi)$

$$F(\theta;\phi) = \frac{\partial}{\partial\theta}\Phi(\theta;\phi) \quad (8a)$$

$$G(\theta;\phi)\sin\theta = \frac{\partial}{\partial\phi}\Phi(\theta;\phi) \quad (8b)$$

where

$$\Phi(\theta;\phi) = \frac{\sin\theta_0}{ik}\int_0^{2\pi} I(\rho;\psi)d\psi\int_{\rho_0}^{\rho_1} d\rho e^{ik\rho(\bar{\imath}_\rho\cdot\bar{\imath}_R)}. \quad (9)$$

From (8) we get the identity

$$\frac{\partial}{\partial\phi}F(\theta;\phi) = \frac{\partial}{\partial\theta}[G(\theta;\phi)\sin\theta]. \quad (10)$$

Eq. (10) gives a direct relationship between the F pattern and the G pattern.

Determination of the Currents

From (8) we see that by giving the "potential" function $\Phi(\theta;\phi)$ we prescribe *both* the F pattern and the G pattern. In order to determine the current which will produce a prescribed radiation pattern, the integral (9) must be solved. [$\Phi(\theta;\phi)$ is a given function and $I(\rho;\psi)$ is the unknown current distribution function over the surface of the cone]. We solve this problem by transforming the integral (9) into infinite matrix relationships between the coefficients of the expansions of $\Phi(\theta;\phi)$ and $I(\rho;\psi)$. Since we are interested only in a radiation pattern which will approximate the required one, (9) could be solved by cutting off the infinite matrixes arbitrarily and inverting them.

It may be found that

$$\bar{\imath}_R = \sin\theta(\bar{\imath}_x\cos\phi + \bar{\imath}_y\sin\phi) + \bar{\imath}_z\cos\theta \quad (11a)$$

$$\bar{\imath}_\rho = \sin\theta_0(\bar{\imath}_x\cos\psi + \bar{\imath}_y\sin\psi) + \bar{\imath}_z\cos\theta_0. \quad (11b)$$

From (11) we get

$$\bar{\imath}_\rho\cdot\bar{\imath}_R = \sin\theta_0\sin\theta\cos(\psi-\phi) + \cos\theta_0\cos\theta. \quad (12)$$

Substituting (12) in (9) we get

$$\Phi(\theta;\phi) = \frac{\sin\theta_0}{ik}\int_0^{2\pi} I(\rho;\psi)d\psi\int_{\rho_0}^{\rho_1} d\rho \cdot\exp ik\rho[\sin\theta_0\sin\theta\cos(\psi-\phi) + \cos\theta_0\cos\theta]. \quad (13)$$

Expanding the current function and potential function in a complex Fourier series as follows

$$I(\rho;\psi) = \sum_{m=-\infty}^{+\infty} b_m(\rho)e^{im\psi} \quad (14a)$$

$$\Phi(\theta;\phi) = \sum_{m=-\infty}^{+\infty} B_m(\theta)e^{im\phi}. \quad (14b)$$

Substituting (14) in (13) and using the identity[4]

$$\int_0^{2\pi} e^{iz\cos\eta}e^{im\eta}d\eta = 2\pi i^{|m|}J_{|m|}(Z) \quad |m| = \text{integer} \quad (15)$$

we get, after comparing coefficients of the Fourier series on both sides,[5]

$$B_m(\theta) = \frac{2\pi\sin\theta_0}{ik}i^{|m|}\int_{\rho_0}^{\rho_1} b_m(\rho)d\rho e^{ik\rho\cos\theta_0\cos\theta} J_{|m|}(k\rho\sin\theta_0\sin\theta). \quad (16)$$

Expanding $B_m(\theta)$ in terms of associated Legendre polynomials

$$B_m(\theta) = \sum_{n=0}^{\infty} D_n^{(m)}P_n^{|m|}(\cos\theta). \quad (17)$$

Using the orthogonality properties[6]

$$\int_0^{\pi} P_n^{|m|}(\cos\theta)P_r^{|m|}(\cos\theta)\sin\theta d\theta = \frac{2}{2n+1}\frac{(n+|m|)!}{(n-|m|)!}\delta_{n,r}, \quad (18)$$

the coefficients in (17) become

$$D_n^{(m)} = \frac{2n+1}{2}\frac{(n-|m|)!}{(n+|m|)!}\cdot\int_0^{\pi} B_m(\theta)P_n^{|m|}(\cos\theta)\sin\theta d\theta. \quad (19)$$

Substituting (16) in (19) and using the identity[6]

$$\int_0^{\pi} e^{ikR\cos\alpha\cos\theta}J_m(kR\sin\alpha\sin\theta)P_n^m(\cos\theta)\sin\theta d\theta = 2i^n j_n(kR)P_n^m(\cos\alpha) \quad (20)$$

where $j_n(kR)$ = spherical Bessel function; we get

$$D_n^{(m)} = \frac{2\pi\sin\theta_0}{ik}i^{|m|}\frac{2n+1}{2}\frac{(n-|m|)!}{(n+|m|)!}2i^nP_n^{|m|}(\cos\theta_0)\cdot\int_{\rho_0}^{\rho_1} b_m(\rho)j_n(k\rho)d\rho. \quad (21)$$

Let us assume that $b_m(\rho)$ may be expanded as

[4] E. Jahnke and F. Emde, "Tables of Functions," Dover Publications, New York, N. Y., pp. 149, 131; 1945. The introduction of $|m|$ instead of m is a simple extension of the original identity.

[5] Similar relations have been developed by: K. M. Siegel, *et al.*, "Studies in Radar Cross Sections XXII—Elementary Slot Radiators," University of Michigan, Ann Arbor, Mich., E. R. I. Rep. 2472-13-T, p. 16; November, 1956; and G. Held, University of Washington, Seattle, Wash., private communication.

[6] J. A. Stratton, "Electromagnetic Theory," McGraw-Hill Book Co., Inc., New York, N. Y., p. 403, (16) and (17), p. 411, (69); 1951.

$$b_m(\rho) = \sum_{l=0}^{\infty} d_l^{(m)} j_l(k\rho) \tag{22}$$

and the series (22) converge for both large ρ and l. Let us denote the definite integral of spherical Bessel functions:

$$\int_{z_0}^{z_1} j_l(z) j_n(z) dz = \frac{\pi}{[(2l+1)(2n+1)]^{1/2}} I_{l,n}(z_0; z_1) \tag{23}$$

where $I_{l,n}(z_0; z_1)$ is a definite number.

Substituting (22) in (21) and using (23) we get

$$D_n^{(m)} = \frac{2\pi^2}{k^2} i^{n+|m|-1} [2n+1]^{1/2} \frac{(n-|m|)!}{(n+|m|)!} \sin\theta_0 P_n^{|m|}(\cos\theta_0) \cdot \sum_{l=0}^{\infty} \frac{I_{l,m}(\rho_0; \rho_1)}{[2l+1]^{1/2}} d_l^{(m)}. \tag{24}$$

Since $P_n^{|m|}(\cos\theta) = 0$ when $n < |m|$, we see from (24) that $D_n^{(m)} = 0$ when $n < |m|$. Taking this into account we have to rewrite (17) as follows

$$B_m(\theta) = \sum_{n=|m|}^{\infty} D_n^{(m)} P_n^{|m|}(\cos\theta). \tag{25}$$

Matrix Relations

The F pattern or the G pattern need not be exact. Therefore the "potential" function $\Phi(\theta; \phi)$ may be approximated, due to (14b) and (25), as follows

$$\Phi(\theta; \phi) = \sum_{m=-M}^{M} \sum_{n=|m|}^{N} D_n^{(m)} P_n^{|m|}(\cos\theta) e^{im\phi} \tag{26}$$

and the current distribution may be approximated, due to (14a) and (22), as

$$I(\rho; \psi) = \sum_{m=-M}^{M} \sum_{l=0}^{P} d_l^{(m)} j_l(k\rho) e^{im\psi}. \tag{27}$$

The relationship between the coefficients $D_n^{(m)}$ and $d_l^{(m)}$ is given by (24).

In Appendix I we prove that

$$I_{l,m}(-\infty; +\infty) = \delta_{l,m} \tag{28}$$

In case of infinite biconical system, (13) will have to be written twice, for θ_0 and $\pi - \theta_0$. If we assume that the current distribution in one cone is symmetric with respect to the apex of the biconical system to the other cone or

$$I^{(2)}(-\rho; \psi + \pi) = I^{(1)}(\rho; \psi), \tag{29}$$

we will have for the infinite biconical system the same type of relation as (13) with $\rho_0 = -\infty$ and $\rho_1 = +\infty$.

Substituting (28) in (24) we get

$$D_n^{(m)} = \frac{2\pi^2}{k^2} i^{n+|m|-1} \frac{(n-|m|)!}{(n+|m|)!} \sin\theta_0 P_n^{|m|}(\cos\theta_0) d_n^{(m)}. \tag{30}$$

Eq. (30) gives a one to one correspondence for the infinite biconical system between the pattern coefficients given by (26) and the current coefficients given by (27).

The result in (30) is rather interesting. In case of $n < |m|$ we see that since $P_n^{|m|}(\cos\theta) = 0$, we get $D_n^{(m)} = 0$ and $d_n^{(m)}$ for $n < |m|$ may be completely arbitrary. $d_l^{(m)}$ in (27) is determined for $l \geqq |m|$ but is completely arbitrary for $l < |m|$. This is a proof that the solution is not unique and there are different current distributions along the surface of the cone which will produce the same radiation pattern.

Eq. (24) is true for every n and every m, so it may be rewritten in a matrix form

$$D_n^{(m)}] = [M_{l,n}^{(m)}] \cdot d_l^{(m)}] \tag{31}$$

where (25) represents infinite matrices for every m. The terms of the matrix $[M_{l,n}^{(m)}]$ for every m become small very fast from a certain value l or n on, as may be seen from (24) and (23) and from the behavior of the spherical Bessel function $j_n(z)$. Therefore, the infinite matrix $[M_{l,n}^{(m)}]$ may be cut off to become a finite matrix for approximation purposes.

If we take in (31) $|m|$ = constant, we get a matrix relationship for each $|m|$. According to (24), $D_n^{(m)} = 0$ for $n < |m|$ regardless of $d_l^{(m)}$. In other words, if we use the relations in (26) and (27), we want to find $(P+1)$ unknown $d_l^{(m)}$ coefficients for each $|m|$, but we have only $(N-|m|+1)$ independent equations with given $D_n^{(m)}$. If we want to take the number of terms to be equal $N = P$, obviously we have arbitrariness, since we have $|m|$ more unknowns than equations. We might take $N = P + |m|$ and then we will have the same number of equations as the number of unknowns; the matrix in (31) will then become a square matrix and the formal solution of P equations with P unknowns may be written as

$$d_l^{(m)}] = [M_{l,n}^{(m)}]^{-1} D_n^{(m)}]. \tag{32}$$

The prescribed far-zone "potential" function $\Phi(\theta;\phi)$ should be such that it is possible to approximate it uniformly by the series given in (26), since the series is the most general expression in spherical coordinates. Otherwise the required current distribution over the surface of the cone cannot be found. In case of a finite cone system, we have assumed that there are no currents along the base of the cone.

The results found for the continuous current distribution may be transformed to the case of discrete array elements over the surface of a cone. We will have to approximate the results for continuous currents by sets of discrete elements.

Appendix I

Kapteyn[7] derived the following relation in Bessel functions

$$\int_0^{\infty} J_\mu(z) J_\nu(z) \frac{dz}{z} = \frac{2}{\pi} \frac{\sin(\mu - \nu)\pi/2}{\mu^2 - \nu^2} \tag{33}$$

[7] G. N. Watson, "A Treatise on the Theory of Bessel Functions," Cambridge University Press, Cambridge, Eng., p. 404(ff); 1952.

where μ; ν are real numbers. Substituting

$$\mu = m + \tfrac{1}{2} \qquad \nu = n + \tfrac{1}{2} \tag{34}$$

where m; n are positive integers or zero, in (33) and rearranging we get

$$\int_0^\infty \frac{\pi}{2z} J_{m+1/2}(z) J_{n+1/2}(z)\,dz = \frac{\sin (m-n)\pi/2}{(m+\tfrac{1}{2})^2 - (n+\tfrac{1}{2})^2}. \tag{35}$$

We have by definition

$$j_n(z) = \left[\frac{\pi}{2z}\right]^{1/2} J_{n+1/2}(z) \tag{36}$$

where $j_n(z)$ is the spherical Bessel function.

From (36) we can rewrite (35) as

$$\int_0^\infty j_m(z) j_n(z)\,dz = \frac{\sin (m-n)\pi/2}{(m-n)(m+n+1)}. \tag{37}$$

From the power series for $j_n(z)$ we can see that

$$j_n(-z) = (-)^n j_n(z). \tag{38}$$

Let us consider the integral

$$\frac{\pi}{[(2m+1)(2n+1)]^{1/2}} I_{m,n}(-\infty\,;+\infty) = \int_{-\infty}^{+\infty} j_m(z) j_n(z)\,dz \tag{39}$$

If both m, n are even or both m, n are odd integers, $I_{m,n}(-\infty, +\infty)$ will vanish according to (37) because $(m-n)$ are even integers. If m=odd and n=even or vice versa, $I_{m,n}(-\infty, +\infty)$ will vanish according to (38), because the integrand in (39) is an odd function. Finding the limit

$$\lim_{m\to n} 2\,\frac{\sin (m-n)\pi/2}{(m-n)(m+n+1)} = \frac{\pi}{2n+1}, \tag{40}$$

we see that

$$\frac{\pi}{[(2m+1)(2n+1)]^{1/2}} I_{m,n}(-\infty\,;+\infty) = \int_{-\infty}^{+\infty} j_m(z) j_n(z)\,dz = \frac{\pi}{2n+1}\,\delta_{m,n} \tag{41}$$

where m; $n \geq 0$. Eq. (41) may be rewritten as

$$I_{m,n}(-\infty\,;+\infty) = \delta_{m,n} \tag{42}$$

ACKNOWLEDGMENT

The author wishes to thank the staff of the Electronics Research Laboratory of the University of California for their help in preparing the original report and Miss H. McGregor and Mrs. E. Kruse of the School of Engineering, University of Kansas, for their help in preparing the manuscript.

The Effects of the Physical Parameters on the Bandwidth of a Folded Dipole*

J. P. GERMAN† AND F. E. BROOKS, JR.‡

Summary—**An expression is derived which yields the feedpoint admittance of a folded unipole or dipole at any desired frequency. This expression shows that the input admittance is composed of two parts—a radiation part and a transmission line part. The radiation part is analyzed as a vertical radiator while the transmission line part is analyzed by transmission line theory. The terms of this expression allow the input admittance of the antenna to be studied in terms of the physical parameters. By plotting the feedpoint admittance on a Smith chart it is possible to observe at what frequency the currents in the feeding transmission line exceed some desired standing wave ratio and thus obtain a measure of the bandwidth of the antenna.**

The findings show that the broad-band characteristics of the folded diple are obtained primarily through the increase in equivalent cross section caused by the folding of the two elements. The bandwidth is further aided by the reactive component of the transmission line part being opposite to the reactive component of the radiation part, even though the reactive component of the transmission line part is considerably smaller than desired. Experimental and calculated results show that for a given size conductor the bandwidth is improved as the spacing between conductors is increased. The spacing should be as wide as possible but still provide the desired field pattern and input admittance. The bandwidth of a folded dipole is improved if the conductor size is increased regardless of the spacing between elements. Maximum bandwidth is achieved by using large conductors with wide spacing.

INTRODUCTION

VARIATIONS in the conductor size and the spacing of a folded dipole will obviously influence the feedpoint impedance or admittance and, as a result, will influence the bandwidth of the antenna. It is the purpose of this paper to determine the best arrangement of the physical parameters in order to achieve a maximum bandwidth.

A measure of the bandwidth of any antenna may be had if the feedpoint impedance or admittance is plotted

* Manuscript received by the PGAP, May 14, 1956; revised manuscript received, May 13, 1957.

† School of Elec. Eng., Purdue University, Lafayette, Ind.
‡ Collins Radio Co., Dallas, Tex.

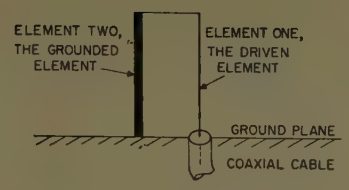

Fig. 1—A folded unipole.

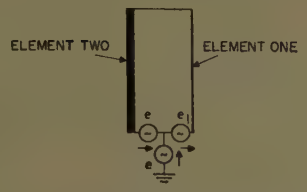

Fig. 2—A folded unipole with coaxial feed replaced by equivalent generators.

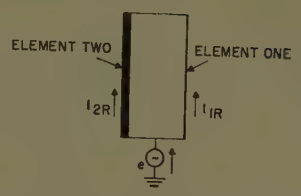

Fig. 3—The lower generator acting alone.

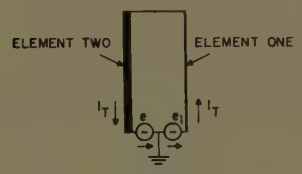

Fig. 4—The upper two generators acting alone.

on a Smith chart[1] so that it may be observed immediately at what frequency the currents in the feeding transmission line exceed some desired standing wave ratio. In order that the Smith chart plot may be made, it is necessary to have an expression which will provide the feedpoint impedance or admittance not only at resonance but at any frequency off resonance. The feedpoint impedance at resonance has been undertaken by Roberts[2] and Guertler,[3] but their findings do not provide sufficient information for plotting the feedpoint impedance at frequencies other than resonance. The first undertaking of this paper will be to derive an expression for the feedpoint admittance of the folded dipole as a function of frequency. Once this expression has been derived it will then be possible to examine what effect the conductor sizes and spacings will have on the feedpoint admittance and the bandwidth of the antenna.

The Feedpoint Admittance of a Folded Unipole

The treatment of the folded dipole will be analyzed from the standpoint of a folded unipole, *i.e.*, the antenna resulting when an ordinary folded dipole is cut in half and fed against ground as shown in Fig. 1. The operation and admittance characteristics are exactly the same as for the common folded dipole except that the admittance is doubled. Any admittance multiplying factor due to the folding will be the same for the folded unipole as it would be for the folded dipole.

In order to provide a suitable method of analysis it will be convenient to replace the coaxial feed on this folded unipole by three radio-frequency generators as suggested by Roberts.[2] Since these generators are purely imaginary, it can be stipulated that they have zero internal impedance. All generators are operated in phase, with polarities indicated by the arrows in Fig. 2, two with voltages e and one with voltage e_1. From Fig. 2 it can be seen that the generator on the left and the lower generator have opposite polarities, placing the lower end of element two, the grounded element, at ground potential as in Fig. 1. The generator on the right and the lower generator, operating in phase and with polarities adding, apply a voltage $(e+e_1)=e_T$ to the lower end of element one, the driven element. Thus, Fig. 2 is equivalent to Fig. 1.

The extra generators have been placed in the problem so that if the individual generator currents can be determined, they may be added, by means of the principle of superposition, to obtain the current entering the lower end of the driven element.

Assume for the moment there is only voltage on the lower generator (see Fig. 3). This radio-frequency generator is then feeding a radiator composed of two elements in parallel. If Y_R is the input radiation admittance of this composite radiator, then the lower generator will supply a total current of eY_R to this antenna. The current that is produced by the lower generator acting alone will divide inversely between element one and element two as the impedances it sees in the elements. The current flowing in element one, the fed element, will be designated as I_{1R} and the current flowing in element two, the grounded element, will be designated as I_{2R}. Note that both currents are instantaneously flowing in the same direction. From this it is possible to write

$$I_{1R} + I_{2R} = eY_R. \tag{1}$$

Now assume there is no voltage in the lower generator (see Fig. 4). Under this condition, the voltage $(e+e_1)$ is impressed upon a transmission line shorted at the far end. If the two conductors are unequal in size they will present unequal impedances to the two generators; therefore, the generators must be unbalanced in order to place the point between the generators at ground potential, and to make the currents in the two conductors equal and opposite. The current in this transmission line will be designated as I_T and this current has an

[1] P. H. Smith, "An improved transmission line calculator," *Electronics*, vol. 17, pp. 130–133; January, 1944.
[2] W. V. B. Roberts, "Input impedance of a folded dipole," *RCA Rev.*, vol. 8, pp. 289–300; June, 1947.
[3] R. Guertler, "Impedance transformation in folded dipoles," Proc. IRE, vol. 38, pp. 1042–1047; September, 1950.

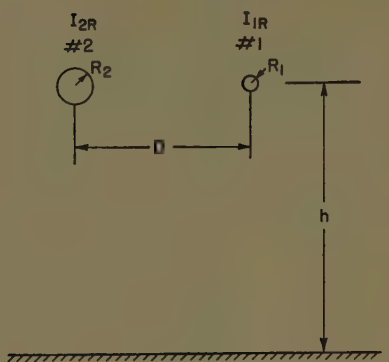

$$n = \frac{I_{2R}}{I_{1R}} = \frac{\log_{10}\frac{D}{R_1}}{\log_{10}\frac{D}{R_2}} \text{ as } h \to \infty$$

Fig. 5—Ratio of currents in the two conductors of a folded dipole.

instantaneous direction outward on one conductor and inward on the other. From transmission-line theory it is possible to write:

$$I_T = (e_1 + e) Y_c \coth \gamma l, \tag{2}$$

where Y_c is the characteristic admittance of the transmission line formed by elements one and two, l is the distance from the shorted end and γ is the propagation constant, generally denoted as $\gamma = \alpha + j\beta$ where α is the attenuation constant and β the phase-shift constant of the line.

The coaxial feedpoint admittance may be found by taking the ratio of the total current entering the lower end of the driven element to the total voltage applied to the lower end of this same element.

The feedpoint admittance may then be written as

$$Y = \frac{I_{1R} + I_T}{e + e_1}, \tag{3}$$

and defining the current ratio as

$$n = \frac{I_{2R}}{I_{1R}},$$

(1) becomes

$$I_{1R} = \frac{Y_R e}{1 + n}. \tag{4}$$

It will be assumed that since both elements are in parallel, in close proximity to each other, and generally under similar conditions, I_{1R} and I_{2R} are in phase, and hence n is a real number. The ratio of the currents in two parallel conductors of unequal size can be solved using logarithmic potential theory. Fig. 5 shows the results of this analysis with dimensions of the conductors as shown.

Now substituting (2) and (4) in (3) the feedpoint admittance becomes:

$$Y = Y_R\left(\frac{1}{1+n}\right)\left(\frac{e}{e+e_1}\right) + Y_c \coth \gamma l. \tag{5}$$

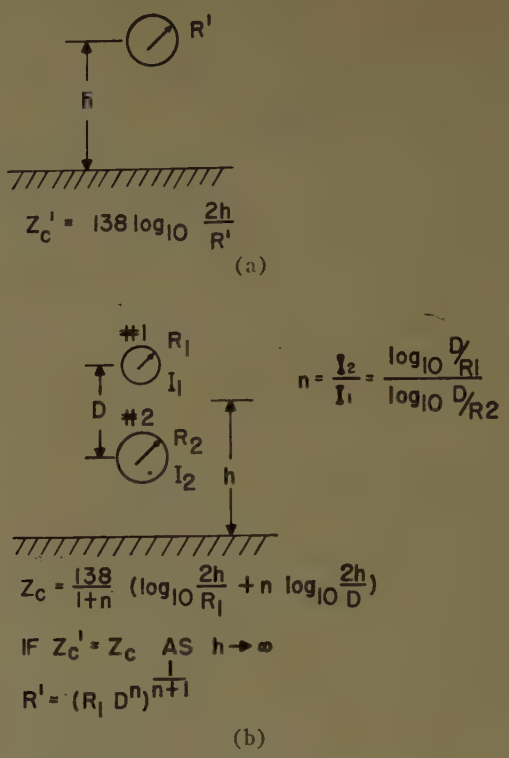

Fig. 6—Radius of equivalent cylindrical antenna.

It will be noticed that the first portion of this admittance expression, the radiation portion, has three parts. The term Y_R is simply the admittance that a radio-frequency generator would see when connected to a vertical radiator which is fed against ground. The equivalent cross section of the two elements in parallel may be solved for by assuming the conductors are parts of one-wire transmission lines far from the earth, and having equal characteristic impedances. Fig. 6 shows the results of this analysis. The input impedance of a simple vertical radiator fed against ground will not be reviewed in this paper, but the results of previous findings[4] will be used later.

Following the Y_R part of the feedpoint admittance expression there are two factors which, when multiplied into the term, modify this admittance. This modification is, of course, introduced by the two elements of the folded unipole, the conductor size and the spacing between them. The voltage ratio factor $[e/(e+e_1)]$, is dependent upon finding the neutral plane between the elements of the antenna, as shown in Fig. 7. The solution for the voltage ratio $[(e/e+e_1)]$, may be shown to be proportional to the characteristic impedances of the individual conductors against the neutral plane. The results of this analysis are shown in Fig. 7.

As a final portion of the feedpoint admittance there is an added term due to the transmission line component. If the transmission line is considered lossless the term

[4] E. Hallen, "Admittance Diagrams for Antennas and the Relation Between Antenna Theories," Cruft Laboratory, Harvard University, Cambridge, Mass., Tech. Rep. No. 46; June 1, 1948 (Office of Naval Res., N5ORI-76 Contract, Task Order No. 1, NR-078-011).

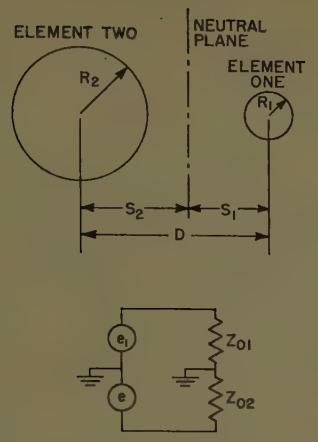

Spacing from conductor central to neutral plane

$$S_1 = D^2 + \frac{(R_1^2 - R_2^2)}{2D}, \qquad S_2 = D^2 + \frac{(R_2^2 - R_1^2)}{2D}$$

Characteristic impedance between conductor and neutral plane

$$Z_{01} = 60 \cosh^{-1} \frac{S_1}{R_1}, \qquad Z_{02} = 60 \cosh^{-1} \frac{S_2}{R_2}$$

Characteristic admittance of conductor pair

$$Y_C = \frac{1}{Z_{01} + Z_{02}}$$

Voltage division

$$\frac{e}{e + e_1} = \frac{Z_{02}}{Z_{02} + Z_{01}}$$

Fig. 7—Cross section of the transmission line.

$Y_c \coth \gamma l$ may be replaced by $-jY_c \cot 2\pi l/\lambda$ where λ is the wavelength on the line. The reactive component of this term has a sign opposite to the reactive component of the first part and this is one factor which aids in making the folded dipole more broadband than a simple dipole.

The Final Feedpoint Admittance Expression

It is now possible to write the feedpoint admittance of a folded unipole at any desired frequency.

$$Y_{FU} = Y_R \left(\frac{1}{1+n}\right)\left(\frac{Z_{02}}{Z_{02} + Z_{01}}\right) - jY_C \cot \frac{2\pi l}{\lambda}, \qquad (6)$$

where:

$$n = \frac{\log_{10} \frac{D}{R_1}}{\log_{10} \frac{D}{R_2}}; \quad Z_{01} = 60 \cosh^{-1} \frac{S_1}{R_1};$$

$$S_1 = \frac{D^2 + (R_1^2 - R_2^2)}{2D};$$

$$Z_{02} = 60 \cosh^{-1} \frac{S_2}{R_2}; \quad S_2 = \frac{D^2 - (R_1^2 - R_2^2)}{2D};$$

$$Y_C = \frac{1}{Z_{01} + Z_{02}}.$$

Y_{FU} = feedpoint admittance of the folded unipole.
Y_R = feedpoint admittance of a composite radiator made up of the two elements in parallel.
n = ratio of the currents in the two elements.
D = distance between centerlines of the two elements.
R_1 = radius of element one, the driven element.
R_2 = radius of element two, the grounded element.
Z_{01} = characteristic impedance of element one and a zero potential plane between elements one and two.
Z_{02} = characteristic impedance of the element two and a zero potential plane between elements one and two.
Y_C = characteristic admittance of the transmission line formed by the two elements.
l = distance from the shorted end of the transmission line.
λ = wavelength.

To determine Y_R from published literature,[4] it is necessary to calculate the equivalent radius of the two elements in parallel. This equivalent radius is given by

$$R' = (R_1 D^n)^{1/(n+1)},$$

where: R' = equivalent radius of the two elements in parallel. Other symbols are as defined above.

Accuracy of the Admittance Expression

The feedpoint admittance expression now allows the normalized input admittance of a folded unipole to be plotted on a Smith Chart so that a measure of the bandwidth can be obtained. This allows an immediate observation to be made of the frequency at which the feeding transmission line currents exceed some desired standing-wave ratio.

The results of measured admittances vs calculated admittances will be presented so that some idea of the accuracy of the feedpoint admittance expression may be obtained. Many examples have been calculated and measured, however only two curves will be shown since comparable results were obtained from all examples checked. Fig. 8 shows the calculated and measured (normalized to 6.66 millimho characteristic admittance) feedpoint admittance of a folded unipole made of two equal size conductors, and also the dimensions.

In order to apply the final feedpoint admittance expression it was necessary to calculate the equivalent cross section of the composite antenna composed of the two conductors in parallel. With this new cross section it was possible to go to available literature[4] and obtain Y_R, the input admittance of a simple cylindrical vertical radiator having the calculated cross section. The other parts of (6) were then calculated which in turn modified Y_R to fit the physical dimensions of the example under consideration. The results of these calculations were then checked by actual input admittance measurements. The measured and calculated data agree reasonably well.

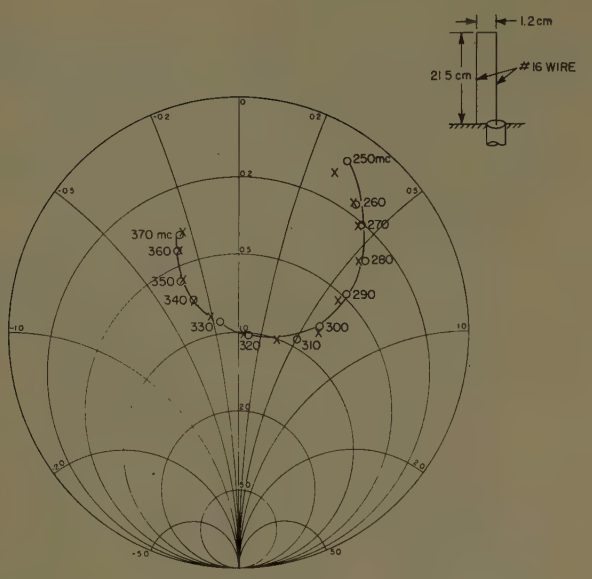

Fig. 8—Calculated (X) and measured (0) feed point admittance of a folded unipole, normalized to 6.66 millimhos.

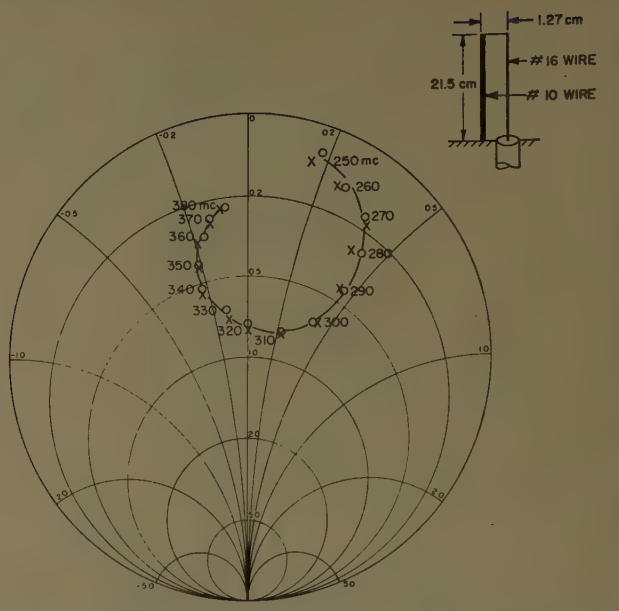

Fig. 9—Calculated (X) and measured (0) feed point admittance of a folded unipole with unequal size conductors normalized to 6.66 millimhos.

Fig. 9 shows the calculated and measured normalized feedpoint admittance of a folded unipole made from two unequal size conductors. As may be seen from the dimensions on Fig. 9 one conductor has a diameter twice that of the other. Again the calculated and measured data agree very well.

The Bandwidth Consideration

A sample calculation of the input admittance of a folded unipole will show that the susceptance of the radiation portion [the first term of (6)] is generally much larger than the susceptance of the transmission line component [the second term of (6)]. It would appear that maximum effectiveness would be obtained by making the characteristic admittance of the transmission line, Y_c, as high as possible.

If the characteristic admittance is made larger by decreasing the spacing D of the transmission line, the equivalent cross section of the composite radiator is reduced thus resulting in a reduced bandwidth. This unfortunate situation leaves only one method of increasing the characteristic admittance—that of increasing the size of the conductors. Calculation of a few examples soon shows that once the conductors have been increased in size, the bandwidth can still be increased by increasing the space between the conductors even though this might appear to be an ineffective technique.

It should be pointed out that neither conductor size vs bandwidth nor spacing vs bandwidth follow a linear or simple mathematical relation. The conclusion which must be drawn is that the increased bandwidth of a folded unipole comes about primarily through the increased equivalent cross section caused by the two elements rather than the cancelling of the reactive component by means of the transmission line term. The cancelling of the reactive component certainly contributes to the increase in bandwidth, but this term is not sufficiently large to become the controlling factor. The equivalent cross section is increased most easily by increasing the spacing between elements. The limit on the spacing between elements will in general be determined by other factors. The field pattern is altered as the spacing is increased and the input admittance becomes larger as the spacing increases and may reach a value too large for the transmission line feeding the antenna.

Conclusion

The analysis of the broad-band characteristics of the folded unipole and thus the corresponding folded dipole have led to the following conclusions:

1) The broad-band characteristics of the folded unipole come about primarily through the increase in equivalent cross section caused by the folding of the elements.
2) The broad-band characteristics are aided by the reactive component of the transmission line part being opposite to the reactive component of the radiation part; however, the reactive component of the transmission line part is considerably smaller than required for complete compensation.
3) Experimental and calculated results show that for a given size conductor the bandwidth is improved as the spacing between conductors is increased. The spacing should be as wide as possible but still provide the desired field pattern and input admittance.
4) The bandwidth of a folded unipole is improved if the conductor size is increased regardless of the spacing between elements. Maximum bandwidth is achieved by using large conductors with wide spacing.

The Radiation Characteristics of a Zig-Zag Antenna*

DIPAK L. SENGUPTA†

Summary—**The radiation properties of a single zig-zag antenna are reported. This is a special type of broad-band traveling-wave antenna which, when properly designed, produces a strong axial beam of radiation. The radiation pattern has a half-power beamwidth of 22° in the *E* plane and 28° in the *H* plane; the corresponding sidelobe ratios are 10.5 db and 17.5 db down, respectively, in the two planes. Approximate expressions for the radiation fields are also given and compared with the experimental values. The broad-band property of the antenna is studied by measuring the radiation patterns over a range of frequencies. The performance of the antenna is compared with the Yagi antenna. The high directivity of the antenna can be utilized advantageously in the vhf and uhf ranges. The results of impedance measurement also are reported.**

Introduction

THE purpose of this paper is to report some theoretical and experimental investigations about the radiation properties of a single zig-zag antenna, first reported by Cumming.[1] This is a special type of traveling-wave antenna which, when properly designed, produces a strong axial beam of radiation with a very low sidelobe.

In his paper Cumming studied the radiation properties of such an antenna at a single frequency; he made more elaborate experimental investigations about the properties of a balanced type of double zig-zag antenna. A more thorough investigation of the single zig-zag antenna has been necessary in connection with the building up of a radio telescope whose antenna assembly consists of a rectangular array of six zig-zag antennas. For the satisfactory design of the telescope, a better understanding of the radiation properties, especially the half-power beamwidth, sidelobe ratio, and the bandwidth of operation, has been necessary. The following investigations were made with this end in view.

This antenna may be considered as a special case of the well-known helical antenna. Theoretical expressions have been given for the radiation field by assuming a current distribution similar to that used in the helical case. The design condition for the axial mode of operation has been derived directly from this expression. Although, from the nature of the assumptions made, the expressions seem to be very approximate, the agreement between the calculated pattern and the experimentally determined patterns, especially in the *H* plane, is quite reasonable and can be worked with for practical purposes.

* Manuscript received by the PGAP, October 29, 1957; revised manuscript received, January 16, 1958. The work reported here was made possible by the financial assistance offered by the National Research Council of Canada under Radioastronomy Project, Grant No. G 587. Paper presented at the 1957 Canadian IRE Convention, Toronto, Can.

† Dept. of Elec. Eng., University of Toronto, Toronto, Can.

[1] W. A. Cumming, "A nonresonant endfire array for vhf and uhf," IRE TRANS. ON ANTENNAS AND PROPAGATION, vol. AP-3, pp. 52–58; April, 1955.

In the last part of this paper a comparative study is made between the properties of the zig-zag and the Yagi antennas. The better directivity and reasonably broad-band property of the former make this antenna a better choice than the Yagi in directional reception. Finally, the results of the impedance measurements are given.

Approximate Expressions for the Radiation Pattern

The single zig-zag is shown diagrammatically in Fig. 1. The coordinate system is chosen in such a way that the antenna lies entirely in the $Y-Z$ plane, the axis of the antenna being along the Z axis. The antenna is fed by a coaxial line whose inner conductor is connected to the antenna and the outer conductor is directly connected to the ground plane. Although the ground plane effects the performance of the antenna to some extent, especially regarding the back radiation, its main function is to offer a proper ground for the feed and, as is shown later, the size of the ground plane is not critical for the required performance of the antenna. The theoretical analysis becomes very complicated if the effect of the ground plane is taken into account. The expressions for the radiation field, given later, have been derived with the assumption that there is no ground plane.

To get the field expressions, a single current wave of constant amplitude is assumed to travel along the antenna as is done in the case of the helix.[2] Theoretically such a current wave fails to satisfy the boundary conditions at the open end and also fails to take care of any possible reflection at the corners. However, if the antenna is long, compared to wavelength, the amplitude of the reflected wave will be very small and hence may be neglected for practical purposes. The current distribution is assumed to be of the following form

$$I = I_0 e^{i\beta s} \qquad (1)$$

where, $\beta = 2\pi/\lambda$ and s is the distance measured along the antenna. The time dependence is of the form $e^{-i\omega t}$.

Physically we can think of the antenna as a number of V's connected in series. The length of each arm of the V and its angle should be chosen such that the radiation fron all the V's add in phase along $\theta = 0°$ direction. The relation to be satisfied by the armlength ($2L$) and the pitch angle (2α) (Fig. 1) is given later.

Once the field due to single V is known, the field due to the zig-zag can be found by the principle of multiplication of pattern.[1] The field also can be found by direct integration along the length of the antenna using the fundamental principles of antenna theory. The results obtained by both methods are same.

[2] J. D. Kraus, "Antennas," McGraw-Hill Book Co., Inc., New York, N. Y., p. 184; 1950.

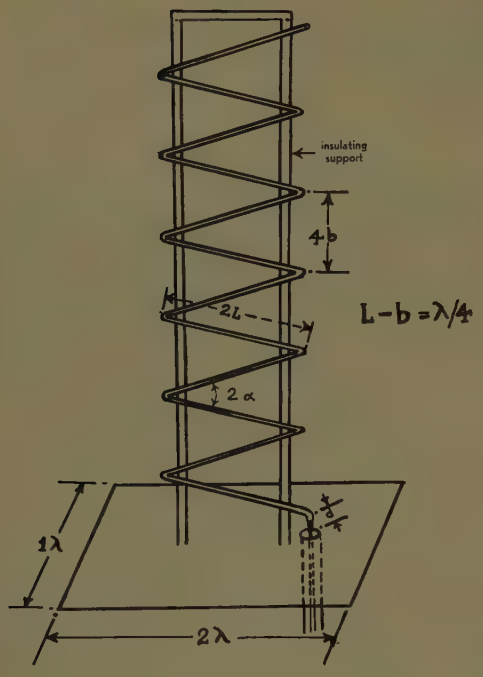

Fig. 1—The schematic diagram showing the zig-zag antenna with the feeding arrangement.

With these ideas in mind, if we carry out the analysis, it can be shown that the electric field in the $Y-Z$ plane (E-plane) due to the zig-zag is given by

$$E(\theta) = j\frac{120\pi I_0}{\beta\lambda}\cdot\frac{e^{i\beta r}}{r}\cdot\left[e^{-j2\beta(L-b\cos\theta)}\cdot\frac{\sin\beta L\{1+\sin(\theta-\alpha)\}}{\{1+\sin(\theta-\alpha)\}}\cos(\theta-\alpha) - \frac{\sin\beta L\{1+\sin(\alpha+\theta)\}}{\{1+\sin(\alpha+\theta)\}}\cos(\alpha+\theta)\right]\times F \quad (2)$$

where L, b, and α are as defined in Fig. 1 and $b=L\sin\alpha$. The factor F is given by,

$$F = \frac{1}{n}\cdot\frac{\sin n\psi/2}{\sin\psi/2} \quad (3)$$

where, n is the number of V's,
and

$$\psi = \left(\frac{8\pi L}{\lambda} - \frac{8\pi b}{\lambda}\cos\theta\right). \quad (4)$$

From (2) it is found that in order to have maximum radiation along $\theta=0°$ direction, the following equation

$$\left.\begin{aligned} L - b &= \lambda/4 \\ \text{i.e. } L(1-\sin\alpha) &= \lambda/4 \end{aligned}\right\}, \quad (5)$$

must be satisfied. This is the fundamental design relation for the zig-zag antenna.

Proceeding in exactly the same way it can be shown that the electric field in the $X-Z$ plane (H plane) is given by

$$E(\theta) = j\frac{120\pi I_0}{\beta\lambda}\cdot\frac{e^{j\beta r}}{r}\left[e^{-j2\beta(L-b\cos\theta)}\cdot\frac{\sin(\beta b\cos\theta)}{\cos\theta}\cdot\tan\alpha - \frac{\sin\beta L(1+\sin\alpha\cos\theta)}{(1+\sin\alpha\cos\theta)}\cdot\cos\alpha\right]F \quad (6)$$

the factor F is the same as in (3).

Experimental Results and Discussions

A number of zig-zags (for pitch angles 2α equal to 15°, 20°, 25°, 30°) each with six V's are designed according to (5). For the 20° zig-zag, the length of each arm ($2L$) is chosen to be equal to 1 63/64″ so that (5) is satisfied at 3600 mc; $4b$ is then found to be $\frac{3}{4}$″. For the other zig-zags the armlength $2L$ is taken to be equal to the proper value required by the corresponding angle. The ground plane in each case is of the dimension 2λ by $I\lambda$ at the frequency 3600 mc.

The radio telescope made up with the zig-zags operates at 300 mc. But at 300 mc, the physical dimensions of the antenna become unwieldy for elaborate pattern studies. From the principle of model measurement[3] it is known that the radiation pattern of the antenna at 300 mc will be the same as that at 3600 mc, provided that the physical dimensions of the antenna are scaled up by a factor of 12. The choice of 3600 mc as the frequency of measurement is found to be advantageous both electrically and mechanically. All the patterns are measured using an automatic antenna pattern plotter, where the required field is produced by a standard optimum horn and the antenna under test is used to receive that field. The receiving antenna is then rotated about the desired axis (choice of axis depends on the polarization of the field) and the received signal is then used to plot the directional pattern with the help of an automatic device.

The E- and H-plane radiation patterns at 3600 mc for the 20° antenna are shown in Fig 2 and Fig. 3. The theoretical patterns are superposed on these for comparison. The agreement between the two in the H plane is reasonable. The observed E-plane pattern shows a big sidelobe at an angle of 30°. The possible reason for this asymmetry is the feeding arrangement which causes an inherent asymmetry of the antenna in the E plane.

It is found experimentally that the length d of the feed (see Fig. 1) has some noticeable effect on the pattern if it is greater than $\lambda/4$. With the increase of d beyond $\lambda/4$ the sidelobe at 30° (in the E plane) increases and the direction of maximum shifts away from $\theta=0°$ direction towards the feed side. This is due to the fact that when d is large, it starts to radiate appreciably thereby effecting the end fire property of the antenna. The effect of d when it is less than $\lambda/4$ is not observable experimentally.

[3] G. Sinclair, "Theory of models of electromagnetic systems," Proc. IRE, vol. 36, pp. 1364–1370; November, 1948.

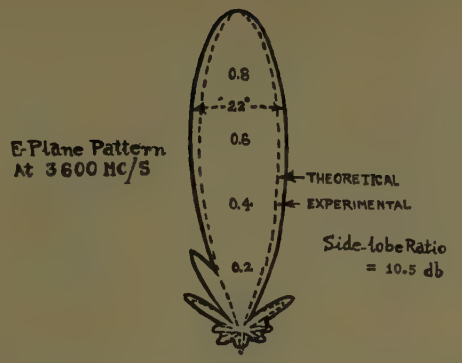

Fig. 2—The radiation pattern of the 20° zig-zag antenna in the E plane.
———— measured, – – – – – calculated

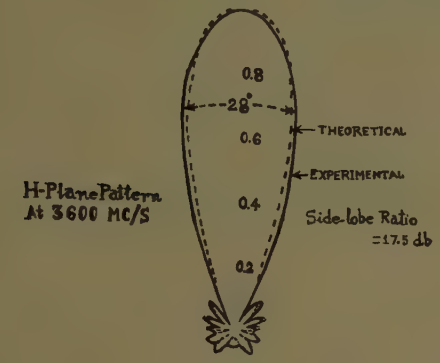

Fig. 3—The radiation pattern of the 20° zig-zag antenna in the H plane.
———— measured, – – – – – calculated.

From Fig. 2 and Fig. 3 it is found that considering the electrical length of the antenna (1.37λ) it has a very good directivity. The directive gain of the antenna is found to be equal to 13.5 db. The cross-polarization component of the antenna in the H plane is found to be 25 db down. From this it appears that the antenna may be used very advantageously for directional purposes; it seems to be better than the commonly used antennas for this purpose at the vhf and uhf ranges.

The measured half-power beamwidths of the patterns and the corresponding sidelobe ratios for the different antennas at 3600 mc are shown in Table I.

TABLE I

Pitch Angle	Half-Power Beamwidth		Sidelobe Ratio (db down)	
2α	E plane	H plane	E plane	H plane
15°	31°	36°	9.5	11.5
20°	22°	28°	10.5	17.5
25°	26°	34°	7.0	8.0
30°	26°	34°	4.4	6.0

Effect of Frequency on Pattern

The radiation patterns of the 20° zig-zag antenna are measured throughout a range of frequencies approximately 20 per cent above and below the center frequency 3600 mc, in both the E and H planes. These are reproduced in Fig. 4 and Fig. 5. It is found that about 5

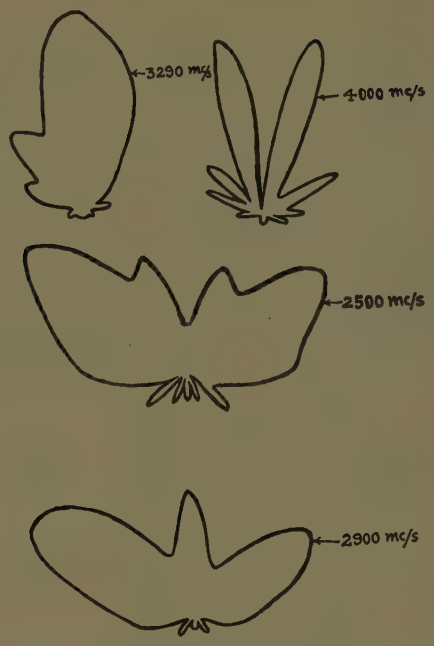

Fig. 4—Measured E-plane patterns of the 20° zig-zag antenna at different frequencies.

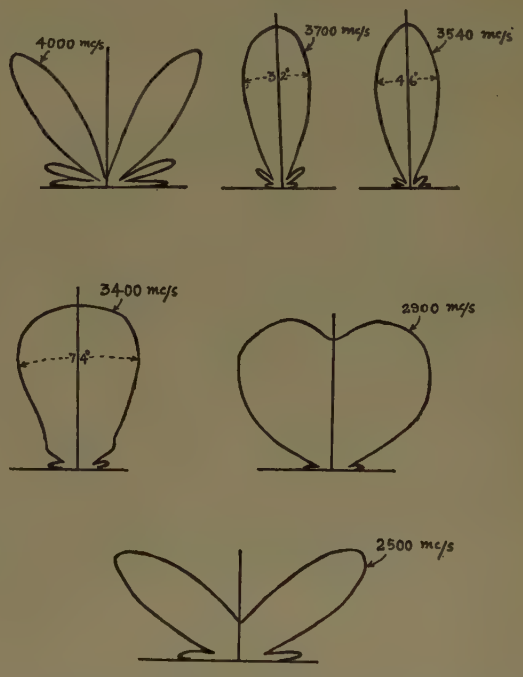

Fig. 5—Measured H-plane patterns of the 20° zig-zag antenna at different frequencies.

per cent above and below the center frequency the radiation pattern stays stable maintaining the maximum in the end-fire direction. As the frequency is changed further, the main beam gradually broadens and the sidelobe increases. When the frequency is about 10 per cent off from 3600 mc, the main beam splits up creating a minimum at the $\theta = 0°$ direction and two maxima on either side of it. This phenomenon is similar to the case of the helical antenna.[4] From the terminology used in

[4] Kraus, *op. cit.*, p. 211.

the helical case, we can say that the bandwidth of axial mode operation of the zig-zag, designed for 3600 mc, is 400 mc or about ± 5 per cent of the center frequency.

Comparison Between the Zig-Zag and the Yagi

It is worthwhile to make a comparative study of the Yagi and the zig-zag, because the former is an antenna very commonly used in the vhf range where the zig-zag can be used with great advantage. One conspicuous advantage of the zig-zag is its less frequency sensitiveness which makes it a very promising antenna for television reception.

The directivity of the zig-zag antenna is better than the Yagi. Alfred[5] reported that a Yagi at 300 mc with 8 elements and a cylindrical reflector has a half-power beamwidth of 39 in the E plane and 40 in the H plane. From the results reported above the properly designed 20° zig-zag has much better directivity in both the principal planes.

Alfred also found that the Yagi has a back to front ratio of 30 per cent, whereas the zig-zag has a 6 per cent back radiation even with a very small ground plane. However, the back radiation from the Yagi may be reduced considerably by slightly detuning the elements, but this causes a reduction in gain.

Impedance Characteristics of the Zig-Zag Antenna

The impedance of the full scale zig-zag (20°) is measured in the 300-mc band using the standard technique. The results of the measurements are shown in Table II.

TABLE II

Frequency (mc)	Input Impedance (ohms)
290	150—j40
295	135—j80
300	160—j80
305	110—j85
310	125—j85
315	152—j0
320	170—j80
325	135—j120
330	70—j95

Conclusion

From the above report it is evident that the zig-zag is a good directive antenna with low sidelobe and can be used in the vhf and uhf ranges. We have taken the length of the antenna as 1.37λ so that the antenna may not be large physically. By taking more V's the directivity of the antenna may be increased further. Although this is a special case of the helical antenna, it differs from the latter in being sensitive to linearly polarized waves.

Acknowledgment

The author wishes to express his thanks to Prof. G. Sinclair, who always has kindly given of his time whenever necessary, and to Dr. J. L. Yen, for very helpful suggestions. Thanks are also due to the Sinclair Radio Laboratories for use of their automatic antenna pattern recorder, and to the Radioastronomy Group of the University of Toronto, for help during the time of taking the readings.

[5] R. V. Alfred, "Experiments with Yagi aerials at 600 mc/s," *J. IEE*, vol. 93, pt. IIIa, p. 1490; 1946.

A Note on the Effective Aperture of Electrically Scanned Arrays*

R. W. BICKMORE†

***Summary*—Since the size of current radar antennas must be increased in order to detect aircraft and missiles flying at supersonic speeds, it is no longer possible to use rapid mechanical scanning. Therefore this type of scanning is being gradually replaced by electrical scanning.**

The popular approximation which states that the effective aperture length is proportional to cos θ_0, where θ_0 is the scan angle from broadside, is examined and shown to be adequate in many cases where the end-fire effect is negligible. An exact effective aperture based on half-power beamwidth is derived and compared with the approximate solution for various aperture lengths as a function of scan angle.

* Original manuscript received by the PGAP, July 31, 1957; revised manuscript received, December 19, 1957.

† Res. Labs., Hughes Aircraft Co., Culver City, Calif.

THE popular approximation which states that the effective aperture length is proportional to cos θ_0, where θ_0 is the scan angle from broadside, has come to be regarded by many as an exact relation. For many arrays, this approximation can be shown to be completely adequate. However, the increased use of electrical scanning as a replacement for mechanical scanning makes a re-evaluation of the effective aperture particularly important.

For the purposes of this paper, consideration of a plane square aperture carrying a uniform, linearly polarized, continuous current will be most convenient. As shown in Fig. 1, the aperture lies in the xy-plane with

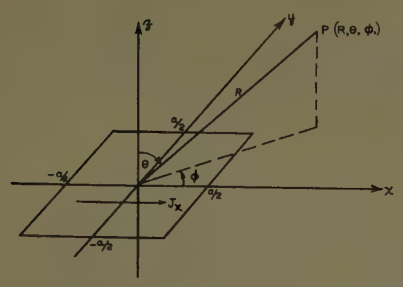

Fig. 1—Far zone geometry for a square array.

current J_x flowing from $-a/2$ to $a/2$. The phase distribution is assumed to be separable and linear.

Upon evaluation of the far-field components in the usual manner,[1] the following expressions are obtained in the three principal planes:

$$E_\phi(\theta)\Big|_{\phi=\pi/2} \sim \frac{\sin u_1}{u_1}, \tag{1}$$

where $u_1 = ka/2\ (\sin\theta - \sin\theta_{01})$, θ_{01} = direction of main beam in the yz-plane.

$$E_\theta(\theta)\Big|_{\phi=0} \sim \frac{\sin u_2}{u_2}\cos\theta \tag{2}$$

where $u_2 = ka/2\ (\sin\theta - \sin\theta_{02})$, θ_{02} = direction of main beam in the xz-plane.

$$E_\phi(\phi)\Big|_{\theta=\pi/2} \sim \frac{\sin v_1}{v_1}\,\frac{\sin v_2}{v_2}\sin\phi \tag{3}$$

where $v_1 = ka/2\ (\cos\phi - \cos\phi_0)$, ϕ_0 = direction of main beam in the xy-plane, $v_2 = ka/2\ (\sin\phi - \sin\phi_0)$.

The element factor is immediately seen to be unity in (1), $\cos\theta$ in (2), and $\sin\phi$ in (3).

The array factor is seen to be the same function of u regardless of scan angle in the two elevation planes. However, neither u nor $\sin^{-1} u$ are linearly related to physical space except when $\theta_0 = 0$ (*i.e.*, broadside radiation). In order that the pattern remain unchanged with scan angle θ_0, the quantity $(\sin\theta - \sin\theta_0)$ would have to be identical to the quantity $\sin(\theta - \theta_0)$. However, it is easily shown that

$$\sin\theta - \sin\theta_0 = \sin(\theta-\theta_0)\cos\theta_0 - [1-\cos(\theta-\theta_0)]\sin\theta_0. \tag{4}$$

The quantity $\cos\theta_0$ is thus factorable when the second term of (4) is negligible. This would appear to be true only when θ_0 is small, which corresponds to radiation near broadside.

It can be noted that the approximation completely fails to predict the end-fire phenomenon of the array factor. That is, the approximation indicates an omnidirectional pattern when $\theta_0 = \pi/2$, whereas the more exact expression gives

$$E \sim \frac{\sin\left[\frac{ka}{2}(1-\sin\theta)\right]}{\frac{ka}{2}(1-\sin\theta)} \tag{5}$$

which is far from omnidirectional.

The approximate solution also fails to predict the lack of symmetry of the radiation pattern. The angular distances of each half-power point from the peak of the main beam are unequal.

If these angles are designated Δ and δ, then the total half-power width is

$$\Theta = \Delta + \delta = \arcsin\left[0.443\frac{\lambda}{a} + \sin\theta_0\right] + \arcsin\left[0.443\frac{\lambda}{a} - \sin\theta_0\right] \tag{6}$$

where Δ is the semi-half-power width for $\theta > \theta_0$. δ is the semi half-power width for $\theta < \theta_0$.

This expression for Θ may now be used to determine an "effective aperture" by equating it to the half-power width of a broadside array and solving for the required broadside aperture length. This procedure circumvents the mathematical difficulty of equating the expressions for gain, and still allows for obtaining an "effective gain" by using the expression $G_1/G_2 = [\Theta_2/\Theta_1]^2$, which is a good approximation for arrays larger than about 10λ in length.

If a' is the effective aperture length,

$$\frac{a'}{\lambda} = \frac{0.443}{\sin\left\{1/2\left[\arcsin\left(0.443\frac{\lambda}{a}+\sin\theta_0\right)+\arcsin\left(0.443\frac{\lambda}{a}-\sin\theta_0\right)\right]\right\}} \tag{7}$$

or

$$\frac{a'}{\lambda} = \frac{a}{2\lambda}\left\{\left[\left(1+0.443\frac{\lambda}{a}\right)^2 - \sin^2\theta_0\right]^{1/2} + \left[\left(1-0.443\frac{\lambda}{a}\right)^2 - \sin^2\theta_0\right]^{1/2}\right\}. \tag{8}$$

The approximation, of course, states that

$$\frac{a'}{\lambda} \approx \frac{a''}{\lambda} = \frac{a}{\lambda}\cos\theta_0. \tag{9}$$

Figs. 2(a) and 2(b) show the ratio of these two values of effective aperture plotted against the scan angle θ_0

[1] S. Silver, "Microwave Antenna Theory and Design," McGraw-Hill Co., Inc., New York, N. Y.; 1949.

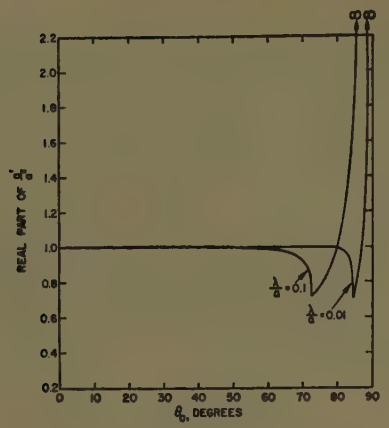

(a)

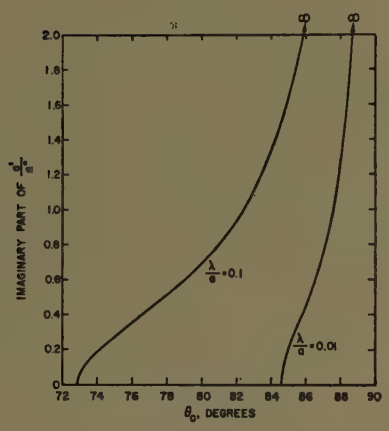

(b)

Fig. 2—Ratio of exact to approximate effective aperture.

for $a/\lambda = 10$ and $a/\lambda = 100$. A unidirectional array is assumed, in these computations, and when the Δ semi-half-power point passes into the region $\theta > \pi/2$, it becomes a point in imaginary space. The curves in Fig. 2(a) and Fig. 2(b) then give an exact solution to the problem of an array above an infinite ground plane. The portion of the beam in imaginary space gives rise to an imaginary component of effective aperture, and the associated energy appears as stored energy in the case of an infinite ground plane or becomes available to be diffracted or absorbed in the case of a finite ground plane.

Returning to the array factor (3), it can be seen to differ from (1) and (2) in that it is the product of two complementary array factors. The general effect is that of sharpening the pattern in the plane perpendicular to the plane of scan. However, for fairly large arrays, the sharpening is quite small. This can be seen by observing the pattern in the vicinity of $\phi_0 = 0$ or $\phi_0 = \pi/2$, where one factor will be found to almost completely dominate the other. Thus, except for short arrays, the pattern on a surface orthogonal to the scan plane remains essentially unaffected.

However, the broadening in the plane of scan is not negligible and becomes more pronounced as the array length increases. This can be illustrated by comparing the half-power beamwidths of the array factors for $\theta_0 = 0$ and $\theta_0 = \pi/2$. The quantity $\sin u/u$ has a maximum value of unity for $u = 0$ and becomes 0.707 for $u = 1.39$. Therefore,

$$\Theta\Big|_{\theta_0 = 0} = 2 \sin^{-1}\left[0.443 \frac{\lambda}{a}\right] \approx 0.88 \frac{\lambda}{a} \quad \text{for } a \gg \lambda, \tag{10}$$

and

$$\Theta\Big|_{\theta_0 = \pi/2} = 2 \cos^{-1}\left[1 - 0.443 \frac{\lambda}{a}\right] \approx 1.88 \sqrt{\frac{\lambda}{a}} \quad \text{for } a \gg \lambda. \tag{11}$$

Thus the ratio of the *full* end-fire beamwidth to broadside beamwidth becomes $2.14\sqrt{a/\lambda}$ in the plane of scan. As Jordan[2] points out, however, a comparison of first-null widths reveals that the end-fire pattern is only $\sqrt{2a/\lambda}$ times as broad.

It is readily seen that in order to avoid this beam deterioration, the individual elements comprising a unidirectional square aperture that is a wavelengths on a side must be progressively rearranged, as the scan angle is increased, to form a rectangle of increasingly greater aspect ratio until, at end-fire, the elements form a line source $4.57\ (a/\lambda)^2$ wavelengths long.[3] The physical undesirability of such an arrangement illustrates the major disadvantage suffered by an electrically scanned planar array compared with a cylindrical surface array for one-dimensional scanning or a spherical surface array for two-dimensional scanning.

Acknowledgment

The author is indebted to R. J. Spellmire for the derivation of (8) and for computation of the curves in Figs. 2(a) and 2(b).

[2] E. C. Jordan, "Electromagnetic Waves and Radiating Systems," Prentice-Hall, Inc., New York, N. Y.; 1950.

[3] Assuming no supergaining in the purely end-fire direction.

The Characteristic Impedance of Two Infinite Cones of Arbitrary Cross Section*

ROBERT L. CARREL†

Summary—**A theoretical method of finding the characteristic impedance of two infinite cones of arbitrary cross section is presented. In this problem, the spherical geometry can be mapped on a plane, thus reducing the problem to finding the solution of Laplace's equation by using conformal mapping techniques. This method is applied to the inclined biconical antenna and several types of fin antennas. The solution for the biconical antenna is $Z_0=\eta/2\pi \cosh^{-1}F$, where F is a function of the geometry of the antenna. For the fin, the solution takes the form $Z_0=\eta K(k)/K'(k)$ where K and K' are complete elliptic integrals of the first kind and k depends on the geometry.**

Introduction

THE problem is to find the characteristic impedance, Z_0 of an antenna consisting of two infinitely long conical conductors which have a common apex. The following method is applicable to all cone-shaped surfaces of arbitrary cross section, *i.e.*, surfaces which can be defined by the two spherical angles θ and ϕ. Basically, the problem consists of solving Maxwell's equations subject to the condition that tangential E vanishes on the surface of the conductors. For the TEM spherical wave it can be shown that Maxwell's equations reduce to Laplace's equation in two dimensions. Conjugate function theory is then applied in solving this two-dimensional potential problem.

Formulation of the Problem

A TEM spherical wave is defined as having no radial components of electric and magnetic field $\overline{E}$ and $\overline{H}$. With the usual $e^{i\omega t}$ time convention, it follows from Maxwell's equations $\nabla\times\overline{H}=i\omega\epsilon\overline{E}$ and $\nabla\times\overline{E}=-i\omega\mu\overline{H}$ that a TEM spherical wave is represented by $\overline{H}=\nabla\times\hat{r}g$ and $\overline{E}=\nabla\times H/i\omega\epsilon$ where $\hat{r}=$unit vector in the radial direction and $g=e^{-i\beta r}T(\theta,\phi)$ is a scalar function of the spherical coordinates r, θ, and ϕ such that $\beta^2=\omega^2\mu\epsilon$ and $\nabla^2T=0$. Such a wave can be propagated along two inclined conical surfaces if the function T is constant on the surfaces of the conductors and if $\nabla^2T=0$ in the surrounding space.

We seek a change of variables that will transform the spherical coordinates θ and ϕ into a plane in such a way that the identity of the conical boundaries is preserved and that Laplace's equation remains unchanged.
Let

$$\begin{aligned}\rho &= f(\theta)\\ \phi_c &= \phi\\ V(\rho,\phi_c) &= T(\theta,\phi).\end{aligned}\tag{1}$$

(In this and the following development ρ, ϕ_c, and z are cylindrical coordinates; r, θ, and ϕ are spherical coordinates). If $\partial V/\partial z=\partial T/\partial r=0$ (the initial premise of the theory), Laplace's equation in the two coordinate systems is

$$\frac{\partial}{\partial\rho}\left(\rho\frac{\partial V}{\partial\rho}\right)+\frac{1}{\rho}\frac{\partial^2V}{\partial\phi_c^2}=0,\tag{2}$$

and

$$\frac{\partial}{\partial\theta}\left(\sin\theta\frac{\partial T}{\partial\theta}\right)+\frac{1}{\sin\theta}\frac{\partial^2T}{\partial\phi^2}=0.\tag{3}$$

After transforming the variables as dictated by (1), (2) becomes

$$\frac{\partial}{\partial\theta}\left[\frac{f(\theta)}{f'(\theta)}\frac{\partial T}{\partial\theta}\right]+\frac{f'(\theta)}{f(\theta)}\frac{\partial^2T}{\partial\phi^2}=0,\tag{4}$$

where

$$f'(\theta)=\frac{d[f(\theta)]}{d\theta}.$$

(3) and (4) will be identical if

$$f'(\theta)/f(\theta)=\csc\theta.\tag{5}$$

After integration we find that $f(\theta)=c\tan\theta/2$, where c is an arbitrary constant of integration which we may set equal to unity. The required mapping relation is then

$$\left.\begin{aligned}\rho &= \tan\theta/2\\ \phi_c &= \phi\end{aligned}\right\}.^{1}\tag{6}$$

The transformation maps the surface of any sphere $r=$constant into the (ρ,ϕ_c) plane. Further, the upper hemispherical surface maps onto the interior of the unit circle; the lower hemispherical surface maps onto the exterior of the unit circle. Fig. 1 shows the mapping of a cone of arbitrary cross section. It can be seen that the radial lines $\phi_c=$constant describe the spherical coordinate ϕ, and the concentric circles $\rho=\tan\theta/2$ correspond to the spherical coordinate θ. Since the transformation (6) also preserves Laplace's equation, all that remains is to find a solution for the cylindrical problem in the (ρ,ϕ_c) plane. Thus the dynamic field problem has been reduced to a static field problem, the solution of which yields the capacity per unit length. However, we are primarily interested in the characteristic impedance, a dynamic field quantity, which is related to the capacity for the case of a two conductor

* Manuscript received by the PGAP, September 3, 1957. This work was performed under the sponsorship of the U. S. Air Force, Wright Air Dev. Center, Wright-Patterson Air Force Base, Ohio.
† Antenna Lab., University of Illinois, Urbana, Ill.

[1] For a similar result see W. R. Smythe, "Static and Dynamic Electricity," McGraw-Hill Book Co., Inc., New York, N. Y., pp. 243–245; 1950.

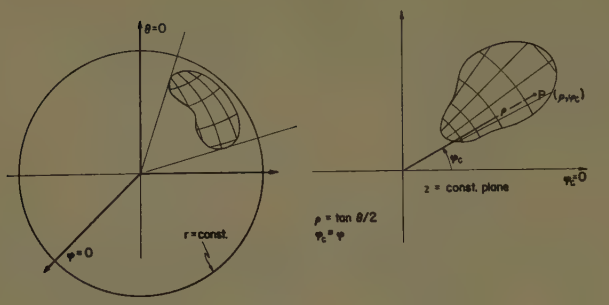

(a) (b)

Fig. 1—The transformation of a general conical section onto a plane. (a) Sperical coordinates, (b) Cylindrical coordinates.

system operating in the principal mode. Specifically, $Z_0=\epsilon\eta/C$, where ϵ is the capacitivity, η is the intrinsic impedance of the medium, and C is the capacity per unit length.

Let us consider some examples involving different geometrical shapes and orientations.

The Coaxial Biconical Antenna

The coaxial biconical antenna affords a straightforward illustration of the technique. The structure is positioned in the spherical geometry as shown in Fig. 2(a), and yields two concentric circles in the (ρ, ϕ_c) plane. This is the familiar coaxial line problem for which the solution is known.

$$Z_0 = \eta/2\pi \log b/a, \tag{7}$$

where η is the intrinsic impedance of the medium between the conductors. Substituting for b and a gives

$$Z_0 = \eta/2\pi \log \cot \psi_1/2 \cot \psi_2/2. \tag{8}$$

This is the exact solution given by Schelkunoff.[2]

The Noncoaxial Biconical Antenna[3]

This structure is positioned in the spherical coordinate system so that the singular point $\theta=\pi$ is exterior to both cones. The plane of the axes of the cones is the $\phi=\pi/2, 3\pi/2$ plane, as shown in Fig. 3(a).

The equation of a cone in the spherical coordinate system is

$$\sin\theta' \cos\phi' \sin\theta \cos\phi + \sin\theta' \sin\phi' \sin\theta \sin\phi + \cos\theta' \cos\theta = \cos\psi, \tag{9}$$

where ψ is the cone half angle, and θ' and ϕ' describe the axis of the cone. Transforming variables is dictated by (6), we find that

$$2\rho \sin\theta' \cos(\phi_c - \phi') + (1-\rho^2)\cos\theta' = (1+\rho^2)\cos\psi. \tag{10}$$

If we make another change of variables from cylindrical coordinates (ρ, ϕ_c) to cartesian coordinates (u, v) such

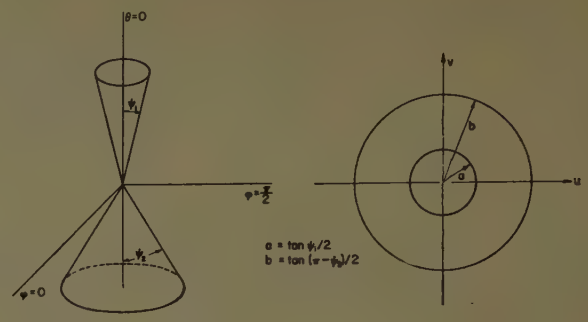

(a) (b)

Fig. 2—The transformation of two coaxial cones onto the w plane. (a) Spherical coordinates, (b) $w=u+iv$ planes.

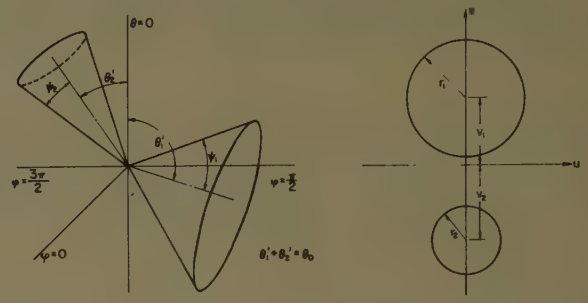

(a) (b)

Fig. 3—The transformation of two noncoaxial cones onto the w plane. (a) Spherical coordinates, (b) w plane.

that $\rho^2=u^2+v^2$ and $\phi_c=\tan^{-1}v/u$, we find that (10) is the equation of a circle. After some algebraic manipulation we obtain

$$\left(u - \frac{\sin\theta' \cos\phi'}{\cos\theta' + \cos\psi}\right)^2 + \left(v - \frac{\sin\theta' \sin\phi'}{\cos\theta' + \cos\psi}\right)^2 = \left(\frac{\sin\psi}{\cos\theta' + \cos\psi}\right)^2. \tag{11}$$

Thus the two cones in Fig. 3(a) map into the two circles in the $w=u+iv$ plane, as shown in Fig. 3(b).

This problem corresponds to finding the characteristic impedance of a uniform two-wire transmission line. Its well-known solution is[4]

$$Z_0 = \eta/2\pi \cosh^{-1}\left[\frac{(v_1+v_2)^2 - r_1^2 - r_2^2}{2r_1r_2}\right]. \tag{12}$$

Upon substituting

$$v_1 = \frac{\sin\theta_1'}{\cos\theta_1' + \cos\psi_1} \qquad v_2 = \frac{\sin\theta_2'}{\cos\theta_2' + \cos\psi_2}$$

$$r_1 = \frac{\sin\psi_1}{\cos\theta_1' + \cos\psi_1} \qquad r_2 = \frac{\sin\psi_2}{\cos\phi_2' + \cos\psi_2}$$

and noting that $\theta_1'+\theta_2'=\theta_0$ where θ_0 is the angle between the axes of the cones, we find that

$$Z_0 = \eta/2\pi \cosh^{-1}\left[\frac{\cos\psi_1 \cos\psi_2 - \cos\theta_0}{\sin\psi_1 \sin\psi_2}\right]. \tag{13}$$

[2] S. A. Schelkunoff, "Electromagnetic Waves," D. Van Nostrand Co., Inc., New York, N. Y., p. 287; 1943.

[3] S. A. Schelkunoff, "Advanced Antenna Theory," John Wiley and Sons, Inc., New York, N. Y., p. 27; 1952.

[4] W. R. Smythe, "Static and Dynamic Electricity," McGraw-Hill Book Co., Inc., New York, N. Y., pp. 80–82; 1950.

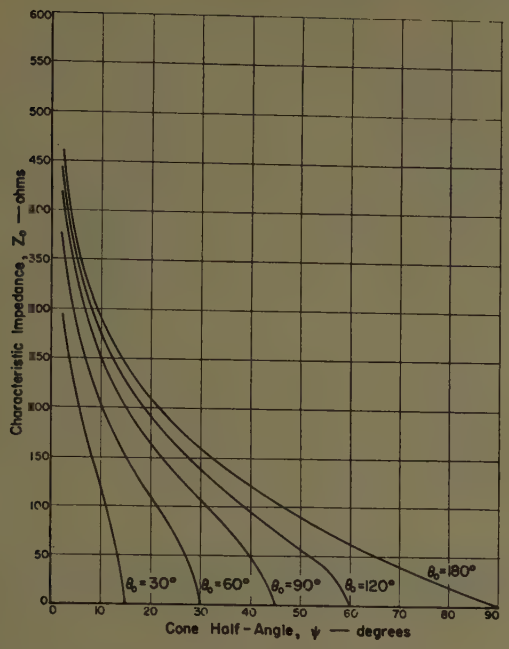

Fig. 4—The characteristic impedance of a biconical antenna with equal cone angles. θ_0 is the angle between the axes of the cones, ψ is the cone half angle.

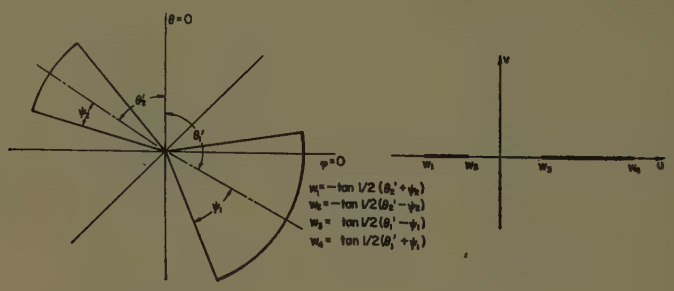

Fig. 5—The transformation of two coplanar fins onto two slits in the w plane. (a) Spherical coordinates, (b) w plane.

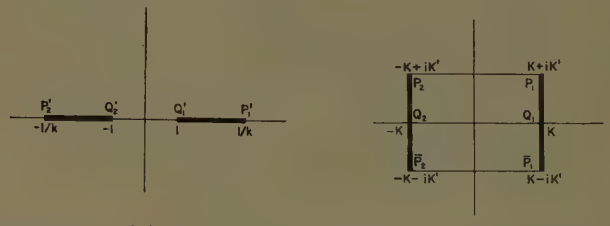

Fig. 6—Mapping the slit σ plane onto a period rectangle in the ζ plane. (a) Complex σ plane, (b) Complex ζ plane.

It can be shown that (13) reduces to (8) when $\theta_0=\pi$. Fig. 4 is a graph of the characteristic impedance of a biconical antenna with equal cones showing the dependence on θ_0.

The Coplanar Fin Antenna

The coplanar fin antenna is shown in Fig. 5(a). It consists of two infinitesimally thin conductors which have a common apex and lie in a plane. The fins are oriented to exclude the singular point $\theta=\pi$, and lie in the $\phi=0$, π plane.

It is instructive to consider first the special case of two equal fins,[5] *i.e.*, $\psi_1=\psi_2=\psi$. Let $\theta_1'=\theta_2'=\theta_0/2$ where θ_0 is the angle between the axes of the fins. The extension to the more general case involves several intermediate steps and will be presented later. It is seen that under the transformation of variables dictated by (6) the two fins map onto two equal slits in the $w=u+iv$ plane. The mapping of the w plane onto the σ plane by the function

$$\sigma = \cot\left[\frac{1}{2}\left(\frac{\theta_0}{2}-\psi\right)\right]w \tag{14}$$

is shown in Fig. 6(a).

The Schwarz-Christoffel transformation,

$$\zeta = \int_0^{\sigma} \frac{d\sigma}{\sqrt{(1-\sigma^2)(1-k^2\sigma^2)}} \tag{15}$$

maps the σ plane onto the interior of the rectangle $P_1\bar{P}_1\bar{P}_2P_2$ in the ζ plane as shown in Fig. 6(b). With the help of (15), both K and K', as defined in Fig. 6(b) can be expressed in terms of k. We have

$$K = \int_0^1 \frac{dt}{\sqrt{(1-t^2)(1-k^2t^2)}} \tag{16}$$

and

$$iK' = \int_1^{1/k} \frac{ds}{\sqrt{(1-s^2)(1-k^2s^2)}}.$$

The latter integral can be brought into a more elegant form if we make the substitution $s=(1-k'^2t^2)^{-1/2}$ where

$$k'^2 + k^2 = 1. \tag{17}$$

Thus

$$K' = \int_0^1 \frac{dt}{\sqrt{(1-t^2)(1-k'^2t^2)}}. \tag{18}$$

Notice that (16) and (18) are complete elliptic integrals of the first kind of modulus k and k', respectively. The configuration in the ζ plane can be considered as a parallel plate transmission line, which has a characteristic impedance given by

$$Z_0 = \eta d/b, \tag{19}$$

where η is the intrinsic impedance of the medium between the two conductors, d is the distance between plates, and b is the width of the plates. Note that this is the exact solution; there are no fringing effects, because the total electric field in the σ plane is mapped into the interior of the period rectangle in the ζ plane. Thus the characteristic impedance of the fin is given by

$$Z_0 = \eta K/K', \tag{20}$$

where

$$k = \sqrt{1-k'^2} = \frac{\sin\theta_0/2 - \sin\psi}{\sin\theta_0/2 + \sin\psi}. \tag{21}$$

[5] This topic is the subject of a University of Illinois Antenna Lab. Rep. by R. L. Carrel, "The Characteristic Impedance of the Fin Antenna of Infinite Length," Tech. Rep. No. 16, Contract AF33(616)-3220, January 15, 1957, and is included here for completeness.

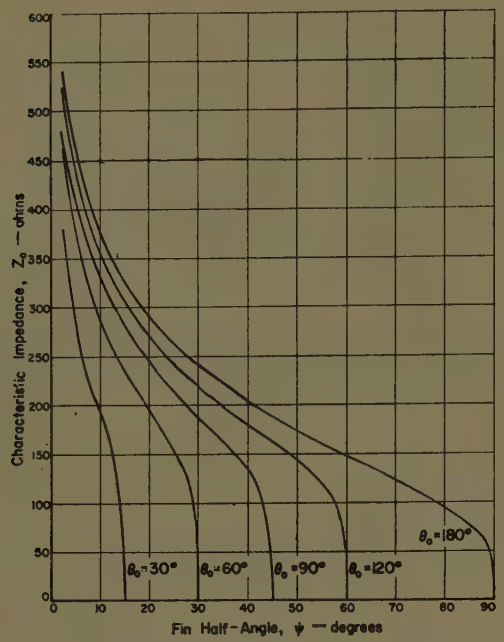

Fig. 7—The characteristic impedance of the coplanar fin antenna with equal fin angles. ψ is the fin half angle, θ_0 is the angle between the axes of the fins.

A graph of Z_0 vs ψ for various values of the parameter θ_0 is shown in Fig. 7.

In the case of arbitrary fin angles, as shown in Fig. 5(a), a slightly more complicated mapping function is needed to obtain the symmetrical configuration in the σ plane. As shown in Fig. 5(b), the configuration in the $w=u+iv$ plane exhibits no symmetry about the v axis. The general bilinear transformation may be employed to obtain the desired mapping. This transformation has the well-known property of mapping any three points in the w plane into any three arbitrarily chosen points in the σ plane. Let us choose this correspondence between points as follows:

$$\begin{aligned} w_1 &\Rightarrow \sigma_1 = -1/k \\ w_2 &\Rightarrow \sigma_2 = -1 \\ w_3 &\Rightarrow \sigma_3 = +1. \end{aligned} \tag{22}$$

This transformation takes the form:

$$\frac{w_2 - w_3}{w - w_3}\cdot\frac{w_2 - w_3}{w_2 - w_1} = \frac{\sigma + 1/k}{\sigma - 1}\cdot\frac{2}{1 - 1/k}. \tag{23}$$

Note that k is as yet undetermined. To fix its value we can require $w=w_4$ when $\sigma=\sigma_4=1/k$. Making this substitution in (23) along with the values of w_1, w_2, w_3, and w_4 from Fig. 5(b), and solving for k, we find

$$k = 1 - \frac{2}{c} + \frac{2}{c}\sqrt{1-c}, \tag{24}$$

where

$$c = \frac{w_4 - w_1}{w_4 - w_3}\cdot\frac{w_2 - w_3}{w_2 - w_1} = \frac{1}{2}\cdot\frac{\cos\theta_0 - \cos(\psi_1 + \psi_2)}{\sin\psi_1 \sin\psi_2}, \tag{25}$$

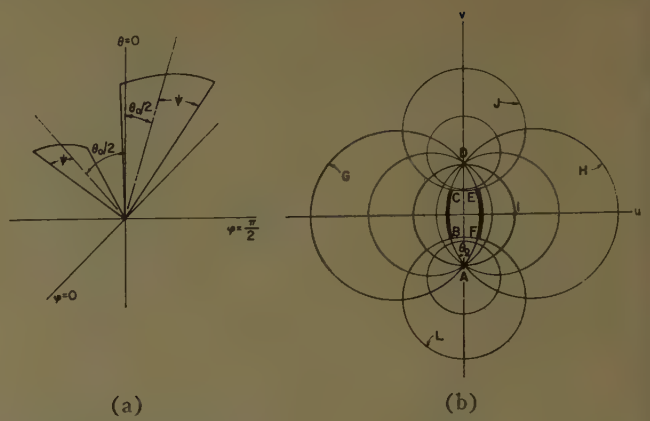

Fig. 8—The transformation of equal noncoplanar fins into arcs of circles in the w plane. (a) Spherical coordinates, (b) Complex w plane.

and $\theta_0=\theta_1'+\theta_2'$ is the angle subtended by the axes of the fins. Thus (23) maps the w plane of Fig. 5(b) into the σ plane of Fig. 6(a). From this configuration, we can proceed directly to the solution by the method outlined for the case of two identical fins described earlier, with the exception that the modulus k is given by (24) and (25). Therefore,

$$Z_0 = \eta K/K', \tag{26}$$

where K and K' are the complete elliptic integrals of the first kind.

The Noncoplanar Fin Antenna

This section considers an antenna consisting of two equal fins, which are not in the same plane, and have a common apex such that the fins are normal to the plane passing through the center line of each fin, as shown in Fig. 8(a). To resolve this problem, it is necessary to determine how (6) transforms planes through the $\theta=\pi/2$, $\phi=\pi/2$ axis. For any value of θ_0 ($\theta_0/2$ is the inclination of the plane to $\theta=0$) such that $0<\theta_0<\pi$, there are two possible planes passing through the $\theta=\pi/2$, $\phi=\pi/2$ axis. The equation of these planes in spherical coordinates is

$$\pm\cot\frac{\theta_0}{2}\tan\theta\cos\phi + 1 = 0. \tag{27}$$

If the transformation (6) is followed by a transformation to cartesian coordinates in the w plane, we find that (27) becomes

$$\left(u \pm \cot\frac{\theta_0}{2}\right)^2 + v^2 = \csc^2\frac{\theta_0}{2} \tag{28}$$

which is the equation of a family of circles centered on the u axis passing through the points $v=\pm 1$.

It is also necessary to find the locus of the edges of a fin of constant half angle ψ as the θ_0 angle is varied. It can be seen that this locus describes two cones whose axes are the lines

$$\theta = \frac{\pi}{2}, \quad \phi = \frac{\pi}{2} \quad \text{and} \quad \theta = \frac{\pi}{2}, \quad \phi = \frac{3\pi}{2}.$$

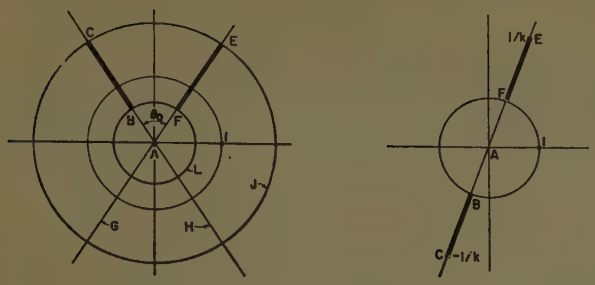

(a) (b)

Fig. 9—Maps of the fins in the complex ξ and σ planes. (a) Complex ξ plane, (b) Complex σ plane.

The equation of these cones in spherical coordinates is

$$\pm \sin\theta \sin\phi = \sin\psi. \tag{29}$$

By using transformation (6) followed by a transformation to cartesian coordinates in the w plane, (29) becomes

$$u^2 = (v \mp \csc\psi)^2 = \cot^2\psi, \tag{30}$$

which is the equation of a family of circles centered on the v axis. The representation of a typical set of fins, along with the above family of circles, is shown in Fig. 8(b).

In order to map the fins BC and EF of Fig. 8(b) into a more amenable geometry, we apply a bilinear transformation followed by a power transformation.

$$\xi = \frac{i + w}{1 + iw} \tag{31}$$

$$\sigma = (R\xi)^{\pi/\theta_0} \tag{32}$$

where

$$R = \left(\frac{1 + \sin\psi}{1 - \sin\psi}\right)^{1/2}.$$

The bilinear transformation (31) maps the circles centered on the u axis in the w plane in Fig. 8(b) into the radial lines in the ξ plane; it also maps the circles centered on the v axis onto concentric circles, as shown in Fig. 9(a). Thus the fins BC and EF map into the inclined slits as shown. The power transformation (32), containing the normalizing factor R, yields the colinear slits, as in Fig. 9(b). This corresponds to Fig. 6(a), aside from a rotation. The coordinates of point E in Fig. 8(b) are determined by the intersection of the two circles G and J. The value of k can be found by substituting the coordinates of point E into the transformations (31) and (32). Thus,

$$k = \left(\frac{1 - \sin\psi}{1 + \sin\psi}\right)^{\pi/\theta_0} \qquad 0 < \theta_0 \leqq \pi. \tag{33}$$

The solution for the geometry of Fig. 9(b) has been obtained in a previous problem. It is given by

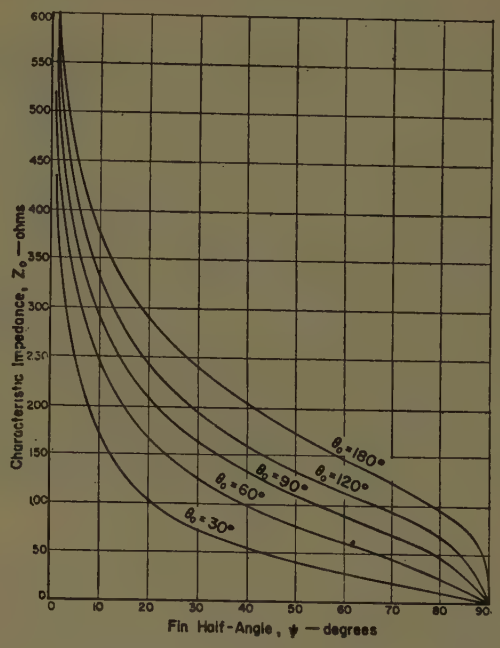

Fig. 10—The characteristic impedance of the noncoplanar fin antenna with equal fin angles. ψ is the fin half angle, θ_0 is the angle between the fins.

$$Z_0 = \eta K/K'$$

where k, the modulus of the complete elliptic function K, is given by (33), Fig. 10 is a graph of Z_0 vs ψ for various values of θ_0.

The extension of these results to arbitrary fin orientations is straightforward; however, the results appear in a cumbersome form, so no attempt will be made to present them here.

Acknowledgment

The author gratefully acknowledges the assistance and directive guidance of Profs. V. H. Rumsey and P. E. Mayes, of the University of Illinois.

Bibliography

[1] Schelkunoff, S. A., and Friis, H. T., *Antennas: Theory and Practice*, New York, N. Y.: John Wiley and Sons, Inc., 1952.
[2] Schelkunoff, S. A., *Advanced Antenna Theory*, John Wiley and Sons, Inc., New York, N. Y., 1952.
[3] Schelkunoff, S. A., *Electromagnetic Waves*, D. Van Nostrand Co., Inc., New York, N. Y., 1943.
[4] Smythe, W. R., *Static and Dynamic Electricity*, McGraw-Hill Book Co., Inc., New York, N. Y., 1950.
[5] Ramo, S. and Whinnery, J. R. *Fields and Waves in Modern Radio*, New York, N. Y.: John Wiley and Sons, Inc., 1953.
[6] Thomson, J. J. *Recent Researches in Electricity and Magnetism*, London, England: Oxford University Press, 1893.
[7] Oberhettinger, F., and Magnus, W. *Anwendung der Elliptischen Funktionen in Physik und Technik*, Berlin, Germany: Springer-Verlag, 1949.
[8] Nehari, Z. *Conformal Mapping*, New York, N. Y.: McGraw-Hill Book Company, Inc., 1952.
[9] Bowman, F. *Elliptic Functions*, New York, N. Y.: John Wiley and Sons, Inc., 1953.
[10] Whittaker, E. J. and Watson, G. N. *Modern Analysis*, London, England: Cambridge University Press, 1952.
[11] Rumsey, V. H. *The Resistance between Two Circular Electrodes on a Spherical Shell or the Characteristic Impedance of Two Inclined Cones*, WADC Technical Note 56–36, ASTIA Document No. AD 130880, June, 1957.

Microwave Stepped-Index Luneberg Lenses*

G. D. M. PEELER† AND H. P. COLEMAN‡

Summary—**Since materials with a continuous variation of index of refraction were unavailable for the construction of spherical Luneberg lenses, an investigation was made of stepped-index lenses in which the desired continuous variation of index with radius was approximated by a number of constant-index spherical shells. Experimental data on two-dimensional, TE_{10} mode, stepped-index Luneberg lenses indicated that 10 shells were sufficient for 18-inch diameter lenses for use at *X* band. Expanded polystyrene materials, developed with dielectric constants ranging from 1.1 to 2.0 in increments of 0.1, were used to construct 10-step, 18-inch diameter, spherical Luneberg lenses. Performance data for these lenses are given at wavelengths of 3.2, 1.8, and 0.8 centimeters.**

Introduction

IN RECENT YEARS, the Luneberg lens has come to be considered by many workers in microwave optics an ideal wide-angle objective due to its complete symmetry. The lack of suitable materials has, however, made the construction of spherical lenses difficult. As a result, most Luneberg lenses constructed have been two-dimensional models[1] which utilize waveguide or geodesic analog techniques to achieve the well-known variation of index of refraction n with radius r

$$n = \sqrt{2 - r^2}.$$

These techniques are not adaptable to the construction of spherical lenses; the construction of these lenses is consequently dependent upon the development of materials with a suitable range of refractive indices. This paper describes the development of a lens, utilizing expanded plastic materials. The variation in n is obtained by varying the density of the materials.

It would be desirable, of course, to obtain dielectric materials which could produce a continuous variation of n with position and to construct a lens from these. The limitation of available techniques, however, prohibits this, and consequently it was decided that a stepped variation approximating the continuous variation of n should be investigated as a means of lens construction. The first part of the paper discusses the choice of stepped positions and index increments, and considers certain stepped-n, two-dimensional lenses constructed for the purpose of determining the effects of stepping. The latter portions of the paper are devoted to the performance of an 18-inch stepped-spherical lens.

* Manuscript received by the PGAP, February 8, 1957.

† Missile Systems Div., Raytheon Mfg. Co., Bedford, Mass. Formerly with the U. S. Naval Res. Lab.

‡ Microwave Antennas & Components Branch, U. S. Naval Res. Lab., Washington, D. C.

[1] G. D. M. Peeler, and D. H. Archer, "A two-dimensional microwave luneberg lens," IRE TRANS. ON ANTENNAS AND PROPAGATION, vol. AP-1, pp. 12–23, July, 1953, and references therein.

Stepping Techniques

Some conclusions about stepped-index lenses may be reached through general considerations. For example, if a lens were constructed with a large number of steps and with small index increments, it would be expected that ray paths through the lens would be only slightly perturbed from those in the ideal continuous lens and, as a consequence, little deterioration in performance would result. On the other hand, for a lens with few steps, especially if the distance between steps were large compared to a wavelength, ray paths would pass through only a few large constant-index regions and only slight focusing could be expected. Thus, there probably exists a minimum number of steps for a lens to provide some specified performance. A choice may be made among several distinct methods for determining the radii of step positions, and the constant index values between steps so as to approximate the desired continuous index vs radius variation. One method is to choose equal index increments,

$$n_m - n_{m+1} = \Delta n = \text{constant},$$

and to choose the step positions at the radii of mean index, $(n_m + n_{m+1})/2$, in the ideal lens. Here m is an integer denoting the particular shell. Another method is to choose equal dielectric constant steps

$$\epsilon_m - \epsilon_{m+1} = \Delta\epsilon = \text{constant},$$

where $\epsilon = n^2$ and to choose step positions at the radii of mean ϵ in the ideal lens. Still another method is to choose increments in either n or ϵ so that the ratio of successive step values is constant

$$\frac{n_m}{n_{m+1}} = \text{constant or} \frac{\epsilon_m}{\epsilon_{m+1}} = \text{constant}$$

and then to choose step positions accordingly.

Originally it was hoped that phase fronts could be calculated for stepped-index lenses, with a range of steps for each of the stepping methods, in order to provide a basis for determining the minimum necessary number of steps and the optimum stepping method for designing a lens with specified performance. However, attempts to set up valid phase-front calculations were unsuccessful. Calculations were performed by introducing the approximation that ray paths are straight lines between lens steps and that Snell's law is satisfied at the steps. It was evident from these calculations, however, that this approximation was too gross to provide any useful information.

Two-Dimensional Stepped-Index Luneberg Lenses

The construction and measurement of two-dimensional stepped-index lenses was chosen as the most advantageous method of obtaining guides for a stepped-index spherical lens design. The equal ϵ increment method of stepping was chosen since ϵ is usually more directly measured than n. In a continuously variable Luneberg lens ϵ varies with radius r according to the formula $\epsilon = n^2 = 2 - r^2$, where $0 \leq r \leq 1$. Thus, assuming equal ϵ increments for a lens with p steps, $\Delta\epsilon = 1/p$, and the dielectric constant ϵ_m for the mth region is

$$\epsilon_m = 2 - \frac{m}{p}, \tag{1}$$

where $m = 0$ for the center region. The step positions were chosen at radii for which $\epsilon = 2 - (m + 1/2)\Delta\epsilon$ in the continuously variable lens, where $m = 0, 1, \cdots, p-1$. In this arrangement ϵ deviations from $2 - r^2$ are maximum at the steps and equal in magnitude on each side of the step. The boundary radii for the mth region are

$$r = \sqrt{\frac{m \pm \frac{1}{2}}{p}}. \tag{2}$$

Two lenses were constructed, one with $p = 10$ and the other with $p = 20$. The polystyrene-filled-waveguide technique, previously used for constructing a two-dimensional, continuously variable index lens,[2] was chosen for constructing the stepped-index lenses. The desired equivalent dielectric constants were obtained by varying the plate spacing stepwise, with constant plate spacing between steps. For a waveguide filled with a material of dielectric constant ϵ' propagating the TE_{10} mode, the equivalent dielectric constant is

$$\epsilon = \epsilon' - \left(\frac{\lambda}{2a}\right)^2, \tag{3}$$

where λ is the wavelength and a is the H-plane waveguide dimension. The plate spacing for the mth region is obtained by combining (1) and (3) to give

$$a = \frac{\lambda}{2\sqrt{\epsilon' - 2 + (m/p)}}, \tag{4}$$

where $m = 0, 1, \cdots, p$. (There are $p+1$ regions.)

Fig. 1 is a diagram of the construction of the two-dimensional lenses designed to operate at $\lambda = 3.2$ cm. Polystyrene ($\epsilon' = 2.503$) was used in their manufacture. The tolerance on thickness of the dielectric slab and on depth of steps in the aluminum coverplates was within ± 0.002 inch. The actual plate-spacing tolerance could not be determined; however, both the polystyrene slab and the aluminum cover plates were stress-relieved before machining in an attempt to minimize warpage and to maintain plate-spacing tolerances near the machining tolerances. If a plate-spacing tolerance of ± 0.004 inch is assumed, the error in desired equivalent ϵ is ± 0.005 at the lens center and ± 0.023 at the lens edge. Each lens was illuminated with the polystyrene-loaded-waveguide horn utilized for the continuously variable lens.[3]

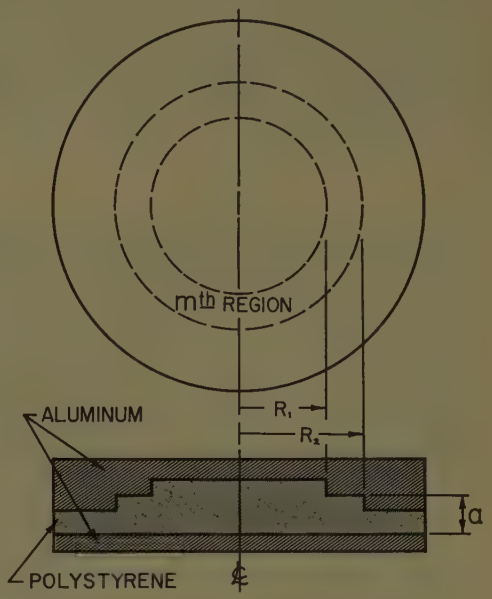

Fig. 1—Diagram for two-dimensional lens construction.

The phase front of each lens in the plane of the lens and along a tangential aperture, was measured using standard techniques.[4] Typical sets of phase front data for these two 18-inch-diameter lenses are shown in Fig. 2. For the 10-step lens, deviations of the phase front from a linear phase front are approximately twice the deviations for the 20-step lens, although the deviations in each case are less than $\lambda/10$.

Typical E-plane radiation patterns (in the lens plane) for the two lenses are shown in Fig. 3. The half-power beamwidths of both patterns are 4.5°; the beamwidth factor, defined as beamwidth × lens diameter/wavelength, is 64°. Side lobes are down from peak power 20 db for the 10-step lens and down 18 db for the 20-step lens. These compare favorably with the calculated sidelobe level of 17.5 db from a continuously variable index lens. Although the phase front data indicate that the sidelobe level should be slightly larger for the 10-step lens than for the 20-step lens, the phase errors are small enough that such comparison has little meaning.

[2] *Ibid.*

[3] Peeler and Archer, *op. cit.*, Fig. 2.

[4] S. Silver, Ed., "Microwave Antenna Theory and Design," Rad. Lab. Ser., Vol. 12, sec. 15:11; 1949.

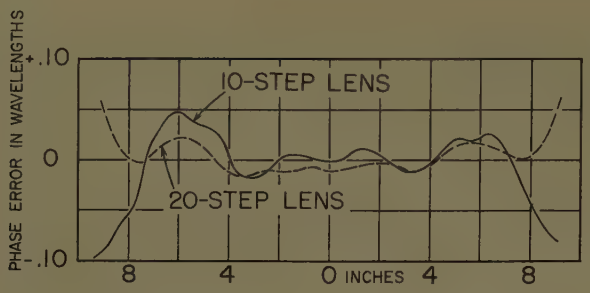

Fig. 2—Typical phase fronts for two-dimensional lenses.

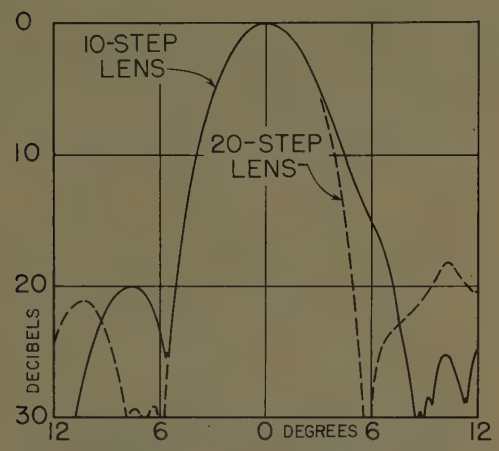

Fig. 3—Typical *E*-plane radiation patterns for two-dimensional lenses.

The above data indicate that for this aperture-to-wavelength ratio, ten steps are sufficient and that the method of stepping is adequate. The data also show that if continuously variable index materials are unobtainable, stepped spherical Lunebergs can be constructed. For other aperture-to-wavelength ratios, the phase-front data may be scaled to provide some indication of lens performance for this method of stepping. For 1° beams which require an aperture-to-wavelength ratio 4.5 times as large as for these lenses, a 20-step lens is indicated if phase errors are to be kept below $\lambda/10$. For beamwidths of one degree or less, the method of stepping may be optimized to decrease the number of steps necessary for a given maximum phase error.

Spherical Stepped-Index Lenses

It was decided to attempt construction of a stepped-index spherical Luneberg lens utilizing the technique of nesting together molded hemispherical shells of isotropic, homogeneous materials in which the index variation from shell to shell is obtained by a density variation. Since this lens should have no bandwidth limitations other than those imposed by the steps and aperture-to-wavelength ratio, it was desirable to choose an aperture size and a number of steps such that data at *X* band and higher frequencies would indicate limitations imposed by steps better than did the two-dimensional lens data. Based on the two-dimensional lens data, 10-equal-ϵ steps and an 18-inch diameter were chosen.

Since materials with the required dielectric constants were not available, it was necessary to develop suitable materials. It was not expected that the materials developed for the first lens would meet all the requirements for use in general weather conditions and over an extreme range of temperatures; the goal was to obtain materials suitable for a laboratory lens with as many desirable properties as possible incorporated without undue expenditure of time or funds. The specifications on materials were as follows: specified dielectric constants maintained within ± 0.02; loss tangent 0.001 or less; water absorption less than 0.1 lb per square foot of exposed skin surface; stable both mechanically and electrically over the temperature range $-20°$ to $+150°$ F; permit moderate handling without cracking or denting. The specified tolerance on dielectric constant is that obtained with the two-dimensional lenses. The loss tangent specification provides for total lens losses less than 0.5 db at $\lambda = 3.2$ cm or less than 2.0 db at 8 mm. The water absorption and temperature specifications insure against variations in dielectric constant and loss tangent under ambient weather conditions.

Material Development and Lens Manufacture

It was recognized at the beginning of this project that many expanded plastic materials would meet most of the specifications, but most of these materials have loss tangents greater than 0.001 at densities which provide a dielectric constant of 2.0. Foam-in-place materials, in general, have density variations from point to point too large to satisfy the tolerance on dielectric constant. It was decided to use polystyrene as the base material since it meets the loss tangent specification even in solid form and its mechanical properties are reasonably good even at low densities. However, polystyrene materials of adjusted density had to be developed which were amenable to molding into spherical shells with accurate radii. A contract was consequently let to Emerson and Cuming, Inc., Canton, Mass. for appropriate material development and lens construction[5] which was jointly sponsored by Air Force Cambridge Research Center and Naval Research Laboratory.

Several methods for producing polystyrene foams were considered and preliminary experiments were run. The method which appeared to be most promising was to prepare a free-flowing polystyrene powder which upon compacting would have a predetermined bulk density. When heated above the softening point of polystyrene (about 85°C), the discrete particles of powder weld together into a rigid material. By carefully select-

[5] G. D. M. Peeler, *et al.*, "Microwave Stepped-Index Luneberg Lenses," NRL Rep. No. 4843; October, 1956.

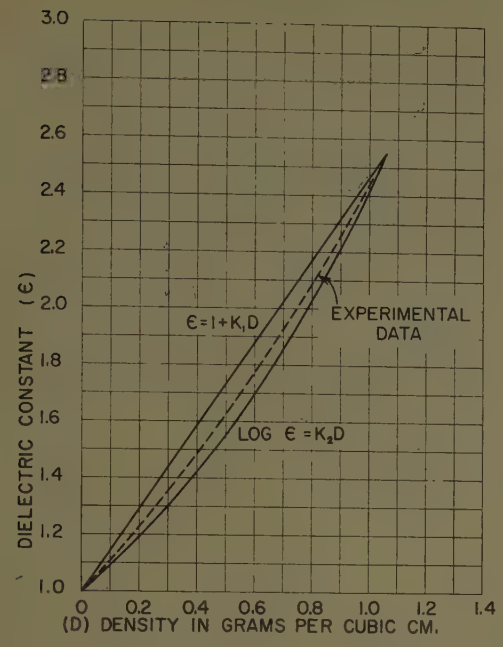

Fig. 4—Dielectric constant vs density for expanded polystyrene.

ing particle size and shape, a wide range of densities is possible. It was found advantageous to perform the welding operation in a closed mold, and to incorporate in the polystyrene a blowing agent which would decompose or vaporize during the welding operation and thus create positive pressure in the mold.

A polystyrene material, termed expandable beads, was made available commercially just prior to the start of this program. These are discrete spheroids of polystyrene which contain a blowing agent. When heated above about 85°C, the spheroids expand and the degree of expansion can be controlled.

A series of experiments was performed to develop formulations and processing techniques for the desired range of dielectric materials. Materials were molded in small rectangular aluminum molds. When the work had progressed to the point that good mechanical quality polystyrene-based dielectrics were consistently obtained, measurements were made to determine the required density for the material in each shell. The loss tangent of all these materials was less than 0.001. Fig. 4 shows the experimentally determined variation of ϵ with density; for comparison, Fig. 4 includes curves for both a linear and a logarithmic variation of ϵ with density. Using these experimental data, the formulations and densities for each shell were determined. The hemispherial shells were then cast and trimmed for assembly. A set of such shells, comprising one half of a lens, is shown in Fig. 5. The lens was then assembled, staggering the seams between adjacent shells and cementing only the outside layer together. The completed lens is shown, mounted for test, in Fig. 6. The completed lens is of 17.54-inch diameter, where the outer layer

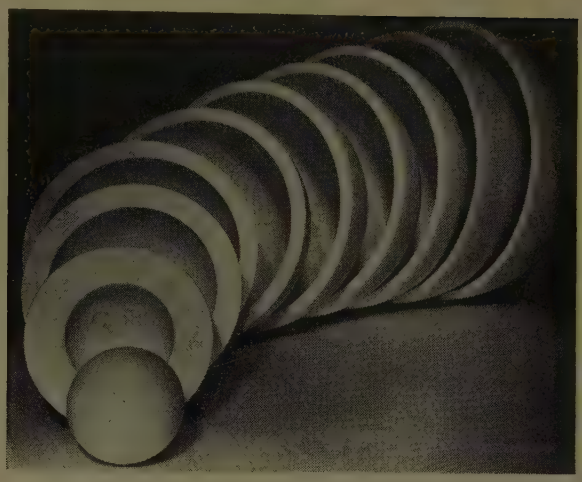

Fig. 5—Exploded view of lens shells.

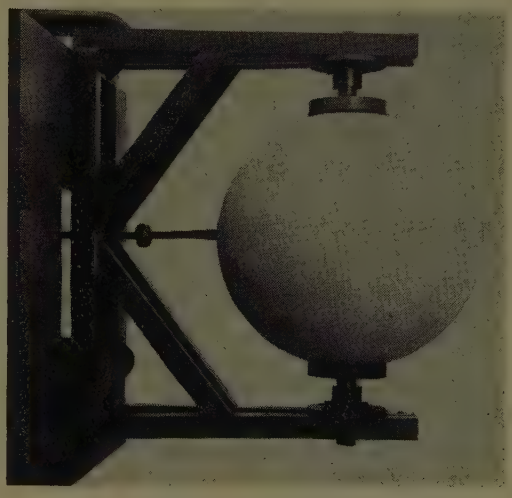

Fig. 6—Completed spherical luneberg lens.

($\epsilon=1$, 18-inch diameter) may be thought of as being comprised of air.

Microwave Data: Three 18-inch diameter spherical Luneberg lenses were constructed. Materials for the first lens were formulated on the basis of the linear curve in Fig. 4 and therefore the dielectric constants of its shells are too high. Materials for the second and third lenses were formulated on the basis of the experimental curve in Fig. 4. The third lens was delivered directly to Air Force Cambridge Research Center.

H-plane radiation pattern measurements were made at three wavelengths: 3.2 cm, 1.8 cm, and 0.8 cm. A typical radiation pattern of the second lens at $\lambda=3.2$ cm is shown in Fig. 7. Summary data for a number of patterns for the first and second lenses are given in Table I. Patterns were taken for 18 equally spaced feed positions on a circumference of the lens; in some cases, patterns were taken for feed positions on three orthogonal planes. Illumination taper refers to the free space, primary radiation pattern taper of the flared waveguide at $\pm 90°$, the taper being the same in the *E* and *H* planes.

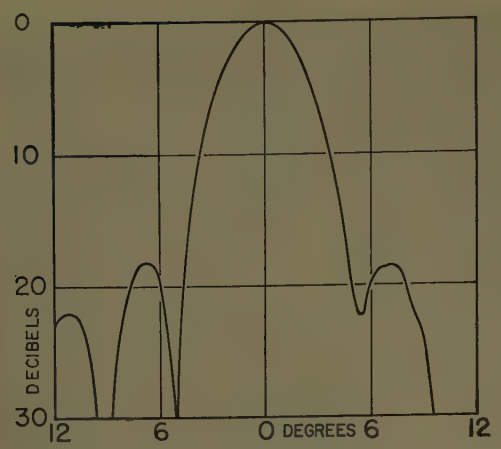

Fig. 7—Typical radiation pattern for spherical Luneberg lens.

TABLE I

RADIATION PATTERN DATA ON SPHERICAL LUNEBERG LENSES

Lens No.	λ (cm)	Illumination Taper (db)	Beamwidth (deg)	Beamwidth Factor (deg)	Side Lobe Level (db)	No. of Patterns
1	3.2	10	4.3	61	17.2	54
2	3.2	10	4.0	57	14.1	18
2	3.2	20	4.4	63	17.1	54
2	3.2	30	4.8	68	19.4	18
2	1.8	20	2.6	66	14.9	18

Beamwidths and sidelobe levels are presented as average values in Table I. The beamwidth factor, defined as beamwidth×diameter/wavelength, was computed in each case on the basis of the average beamwidth and an 18-inch diameter, although the diameter of shell No. 9 is 17.55 inches. Only the second lens was measured at $\lambda = 0.8$ cm; it did not focus for any feed position at this wavelength. The design radial feed position was 0.228 inch from the outer edge of shell No. 9 (the outer edge of shell No. 10). For the first lens, the radial feed position should have been slightly inside shell No. 9; in order not to destroy the lens, measurements were taken with the feed at the outer edge of shell No. 9 with the radiation patterns slightly defocused. For the second lens, measurements were taken at the feed position for best focused patterns, displaced $\frac{1}{4}$ inch from the outer edge of shell No. 9, which corresponds quite well to the design focal position.

The measured gain for the second lens with 20 db illuminated taper at $\lambda = 3.2$ cm is 31.0 db. The gain computed from $27{,}000/\theta_E\theta_H$, where θ_E and θ_H are the E-and H-plane beamwidths respectively, assuming beamwidths of 4.4°, is 31.5 db. The gain computed from $4\pi A/\lambda^2$ is 33.0 db. If the measured gain is equated to $k4\pi A/\lambda^2$, $k = 0.63$, where k is the aperture efficiency.

Phase fronts from the second lens were measured, along a tangential aperture, by standard techniques at

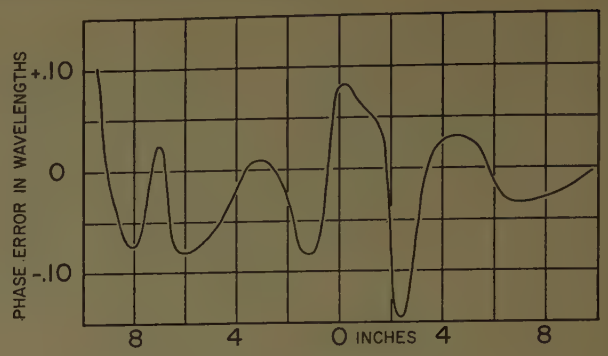

Fig. 8—Typical phase front from second spherical lens. $\lambda = 3.2$, 20 db illumination taper.

TABLE II

DIELECTRIC CONSTANTS OF SHELLS IN SECOND SPHERICAL LENS

Shell No.	ϵ	Specified ϵ
0	$1.85^{+0.18}_{-0.20}$	2.0
1	$1.90^{+0.06}_{-0.03}$	1.9
2	$1.89^{+0.02}_{-0.03}$	1.8
3	$1.70^{+0.03}_{-0.11}$	1.7
4	1.61 ± 0.01	1.6
5	1.51 ± 0.02	1.5
6	$1.41^{+0.06}_{-0.09}$	1.4
7	$1.31^{+0.07}_{-0.03}$	1.3
8	$1.22^{+0.03}_{-0.02}$	1.2
9	$1.25^{+0.07}_{-0.14}$	1.1

$\lambda = 3.2$ cm for a number of feed positions. A typical phase front is shown in Fig. 8. The deviations from a linear phase front are approximately three times as large as those for the two-dimensional lenses shown in Fig. 2. Assuming the same phase front deviations at 1.8 and 0.8 cm, the deviations at these wavelengths are approximately 0.4λ and 0.9λ, respectively. These data correlate quite well with the radiation pattern deterioration at the shorter wavelengths.

It was desirable to obtain some idea of the point-to-point dielectric constant variations in the second lens shells. Only one-half of each shell was used for sampling. From each hemisphere used, four samples were cut from positions on a great circle: two samples were taken almost diametrically opposite each other, one sample at the center of the hemispherical shell, and one at an intermediate position. Average dielectric constants and the total deviations are given in Table II.

Since the number of samples was small, these deviations do not necessarily represent the total deviation in each shell.

It is apparent from the above data that the randomness of the dielectric constant variations throughout the lens would permit relaxation of the dielectric constant tolerance ± 0.02 for an 18-inch-diameter lens at $\lambda = 3.2$ cm. However, it is also apparent that dielectric constant deviations as large as those found in the second lens are noticeable at 1.8 and 0.8 cm. In the absence of a rigorous theoretical study of stepped-index Luneberg lenses for comparison, it is difficult to determine what amount of performance deterioration is due to the stepping technique itself and what amount is due to dielectric constant variations.

Conclusion

In the absence of materials to use for constructing continuous variation-of-index Luneberg lenses, the technique of using a stepped variation of index was investigated. Data on two-dimensional, TE_{10} mode, Luneberg lenses show that with a reasonable number of steps good lens performance can be obtained, although as expected the performance is not as good as from continuous index lenses. Expanded polystyrene materials were developed with dielectric constants from 1.1 to 2.0 in increments of 0.1. 10-step spherical Luneberg lenses were constructed by assembling molded hemispherical shells of these materials.

The quality control on the expanded polystyrene materials at present appears adequate for small lenses but needs improvement for extension to larger lenses. It is felt that the technique of using molded hemispherical shells lends itself to accurate quality control in large quantity production where much of the hand labor would be eliminated.

The expanded polystyrene materials appear reasonably weatherproof and may be satisfactory for limited outdoor use. However, a thin, weatherproof cover which will absorb ultraviolet radiation is probably desirable for prolonged outdoor applications. These materials are dimensionally stable although resilient, and seem capable of surviving normal mechanical abuse. They do not show a tendency to crack and craze as does solid polystyrene. For high-temperature applications, expanded materials, such as silicones, teflon, or ceramics, should be developed. For applications requiring lightweight lenses (an 18-inch diameter Luneberg lens of expanded polystyrene weighs 35 pounds) the use of loaded, lightweight foams is indicated.

Acknowledgment

The authors appreciate the diligence of M. C. Volk and W. R. Cuming, of Emerson and Cuming, Inc., in the materials development and spherical lens construction, and the cooperation of F. S. Holt, Air Force Cambridge Research Center, in helping finance and direct the contract with Emerson and Cuming, Inc.

communications

Measurements of 1250-MC Scatter Propagation as Function of Meteorology*

D. L. RINGWALT†, W. S. AMENT†, AND F. C. MACDONALD†

DURING the week of December 3–8, 1956, the Naval Research Laboratory and the University of Florida conducted a 1250-mc scatter propagation experiment on a 262-nautical-mile overwater path, with transmitter at Cape Canaveral, Fla., and receiver at Nassau, Bahamas. Airborne refractometer soundings were taken at four selected points along the path every six hours. Meteorological observers in the aircraft recorded cloud formation, haze-layer heights, etc. Six-hourly radiosonde and pilot balloon runs were made at Patrick AFB, Grand Bahama (near midpath), Eleuthera, and Mayaguana. The received signal was monitored and recorded continuously at the Florida Field Station and Nassau, and NRL's Flying Laboratory measured field strength in the air.

The purpose of the program was to ascertain whether there is a correlation between low-level refractometer soundings (500 to 15,000 feet) and the median signal power received on the ground-to-ground link. One hundred and five full-length refractometer soundings were taken during the week. Each profile showed a break of about 40 or 50 n units in a 1000-foot interval centered at altitudes from 4000 to 6000 feet, moist oceanic air of high refractive index being found below the break. This break corresponded with a visible haze layer, a temperature inversion, and the base of scattered cumulus clouds. The clouds, and probably the mixing of air at the inversion height, produced large random excursions of the refractometer outputs. The larger cumulus formation rose to over 13,000 feet and may be regarded as imposing a 10–40-mile horizontal meso-meteorological scale on the path meteorology. As a result, the 105 refractometer soundings may be regarded as roughly independent samples of a single meteorological situation having a dominant 40–50 n-unit break.

Supporting this view, the synoptic weather charts throughout the week showed a stationary high-pressure area off Cape Hatteras and a stationary, dissolving cold front eastward of Cuba.

Minor aspects of the soundings were: At altitudes 13,000–14,000 feet, a thin 4 or 5 n-unit layer was generally encountered. This layer is believed to represent the horizontal leakage of water vapor from the higher cumulus clouds. Apart from this layer and away from clouds, the air above the inversion was featureless, although there were occasional wedge-like intrusions, just above the inversion, of magnitude of 5–6 n-units. A diurnal trend (pointed out by Cullen Crain) occurred in the inversion height at midpath; the inversion height was maximum in the afternoon and minimum in the early morning. (No corresponding diurnal effect in signal was observed.)

[* Manuscript received by the PGAP, March 15, 1957.
† Wave Propagation Branch, Electronics Div., Naval Res. Lab., Washington 25, D. C.

The 1250-mc signal received at the Florida Field Station showed Rayleigh fading, characteristic of a scatter-propagated signal, at all times. Hourly medians of the signal were substantially constant throughout the week except for the first 18 hours of December 5. During this period the hourly medians averaged about 10-db higher (two medians were 24-db higher). Since no major feature in the refractometer soundings correlated with this signal enhancement, the wind shear across the inversion was investigated. Pibal data, available at 1000-foot height intervals, and radiosonde data gave wind vectors of considerable scatter at inversion height (possibly due to convective mixing there). Hence, wind shear across the inversion was estimated from the relatively stable wind data at heights roughly 1500 feet above and below the inversion. Midpath wind shear values were high during the high signal period. When medians of the hourly signal medians for each of fifteen six-hour periods and the corresponding wind shear value at midpath are compared by the rank-order method, odds three in four, that the correlation of wind shear with signal is not accidental, are obtained. However, wind shear data from Patrick AFB and Eleuthera, near the path's endpoints, show little correlation with signal level and confirmation of this wind shear signal correlation is needed.

According to original plans, the Flying Laboratory was to fly at 1000 feet from Nassau to Cape Canaveral, measuring the dependence of signal on range. The return flight to Nassau was to be devoted to refractometer soundings with spot signal observations. Those spot observations indicated a signal maximum at inversion height. This fact (and the failure of attempts to correlate the ground-to-ground signals with the refractometer soundings) caused a reassignment of the efforts of the Flying Laboratory in favor of more frequent measurement of signal vs height.

The inbound runs at 1000 feet showed a Rayleigh distributed signal, roughly a three-second interval between median crossings, and a range-attenuation rate of about 0.17 db per nautical mile. With height, the signal increased 5–15 db in the 1000 feet below the inversion height, diminished 5 to 15 db in the next 1000 feet, and then increased with altitude. Near and above the inversion, the Rayleigh fading was usually (four out of six times) superimposed on a slower fade having a period of about one minute with fades of about 10 db. These features occurred at ranges beyond 160 nautical miles. At closer ranges, a rapid increase of mean signal and shallow fading showed that the dominant propagation mechanism was diffraction and/or ducting.

The attenuation rate of 0.17 db/mile is in agreement with much other work. The height gain data (as well as the suggested shear correlation) suggest two alternative scatter mechanisms.

1) The consistent 40–50 n-unit break at inversion height could have acted as a curved partially reflecting ceiling, with the signal beneath arriving by multiple bounces. 2) This 40–50 n-unit break constituted an elevated duct about 1000 feet thick having about a 10 n-unit (maximum) n-deficit. This erratically defined, and hence randomly leaky, duct could have been coupled with both receiver and transmitter via scattering at either end of the path.

The slow underlying fade in the signals at inversion height suggests the duct mechanism, while the midpath shear correlation supports the leaky ceiling picture.

An additional effect of low-level meteorology was noted: A subsidiary haze layer and cloud deck occurred on December 7. This layer was at an altitude of 1500–2500 feet over Nassau and extended about 70 miles along the path, and appeared as an 8–12 n-unit "inversion" in the corresponding soundings. It served to enhance the ground-to-air signal over Nassau at the expense of the ground-to-ground signal.

Among the conclusions unlikely to be altered by continuing analysis of the data are: the prominent 18-hour, 10-db increase in ground-to-ground signal did not correlate with the refractometer soundings in the 500–10,000-foot height region. High signal periods correlate suggestively with periods of wind shear across the dominant 40–50 n-unit inversion at 4000–6000 feet. High signals with slow underlying fades, observed at inversion altitudes, indicate ducting or multiple scattering as the dominant mechanism for long-range microwave propagation in this meteorological regime. The refractometer profiles were varied in detail because of the mesometeorological scale imposed by cumulus clouds protruding through the inversion at scattered points.

The University of Florida work was performed under ONR contract Nonr 580(04). Communications, meteorological observations, and other valuable support was provided by the Air Force Missile Test Center, Patrick Air Force Base. The Naval Air Development Unit, South Weymouth, Mass., gave outstanding support in flying a portion of the refractometer schedule. Valuable advice and aid in data interpretation were given by volunteer participants from Lincoln Laboratory, Air Force Cambridge Research Center, and the Applied Physics Laboratory. Certain Lincoln Laboratory equipment was vital in obtaining the ground-to-air signals.

Design Data for Small Annular Slot Antennas*

W. A. CUMMING† AND M. CORMIER‡

Summary—**While several excellent papers have been published describing the theory of operation of the annular slot radiator, certain design parameters have not been too readily available. This note gives susceptance data for practical configurations having electrical diameters of from 0.2 to 0.6 wavelength.**

ANNULAR slot antennas have a number of airborne and vehicular applications in the vhf and uhf bands. From the theoretical viewpoint this type of radiator has been treated as an open-ended coaxial line with an infinite conducting flange attached to the outer conductor.[1–4] Various field configurations can be set up in the annular aperture thus formed, but since most applications require an omnidirectional *E*-plane pattern, dominant-mode excitation is most commonly used. Different methods of achieving this excitation have been proposed,[5,6] but all basically involved excitation from a radial transmission line, or a conical transmission line, or a combination of the two. Excitation by a radial transmission line appears to be the most promising method when space limitations are severe, and when the bandwidth requirement is not excessive. Slot susceptance data were therefore obtained with reference to this type of feed.

Following the method of Johnson and Rothe[6] the dielectric-covered annular slot is backed on the shadow side of the ground plane by a radial transmission line, short circuited at its inner radius. This system is tuned to resonate in the dominant mode, and matching to a coaxial line source is accomplished through a magnetic coupling loop, as shown in Fig. 1. The usual design procedure is to tune the cavity to resonance by matching the radial line susceptance to the slot susceptance at the inner slot boundary a. The series slot resistance R_s' is then matched to the characteristic impedance of the coaxial transmission line by suitably adjusting the mutual impedance X_m, and finally the loop reactance is tuned out by means of a series tuning capacitor C. An equivalent circuit of this configuration is shown in Fig. 2.

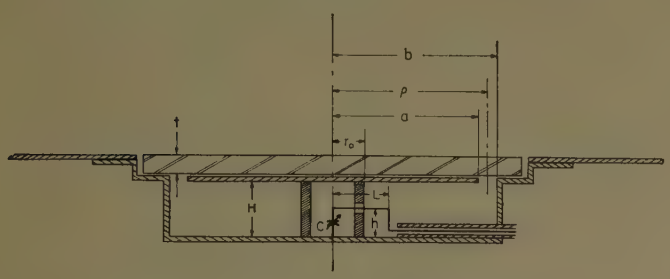

Fig. 1—Annular slot fed by radial transmission line.

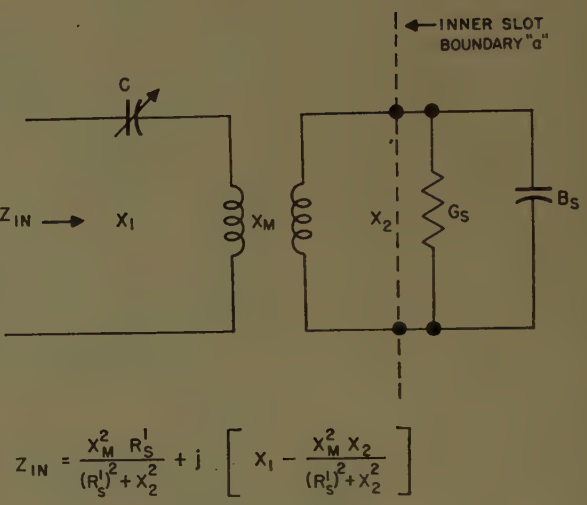

Fig. 2—Equivalent circuit.

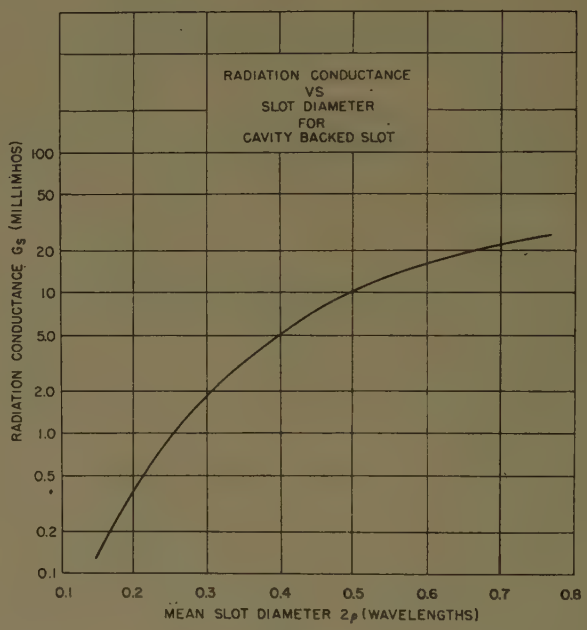

Fig. 3.

Slot conductance G_s can readily be calculated from the field configuration in the slot, and is given graphically in Fig. 3. The susceptance of the radial transmission line B_t can also be calculated, and design curves of this quantity are presented in Fig. 4. The mutual impedance

* Manuscript received by the PGAP, August 14, 1957; revised manuscript received, January 20, 1958.

† Radio and Elec. Eng. Div., Natl. Res. Council of Canada, Ottawa, Can.

‡ Dept. of Physics, University of Montreal, Montreal, P. Q., Can.

[1] R. W. Bickmore, "Circular Slot Antennas," Rep. No. 168, Antenna Lab., University of California, June, 1950.

[2] C. H. Papas, "Radiation from a Circular Diffraction Antenna," Rep. No. 76, Cruft Lab., Harvard Univ., Cambridge, Mass. April, 1949.

[3] A. A. Pistolkors, "Theory of the circular diffraction antenna," PROC. IRE, vol. 36, pp. 56–60; January, 1948.

[4] C. H. Papas and H. Levine, "Theory of the circular diffraction antenna," *J. Appl. Phys.*, vol. 22, pp. 29–43; January, 1951.

[5] A. Dorne, "The Design of a Flush-Mounted Annular Slot Antenna," Dorne and Margolin Rep., No. 702, March, 1952.

[6] W. A. Johnson and P. Rothe, "A Wide-Band Circular-Slot Radiator," R.A.E. Tech. Note RAD-453, June, 1949.

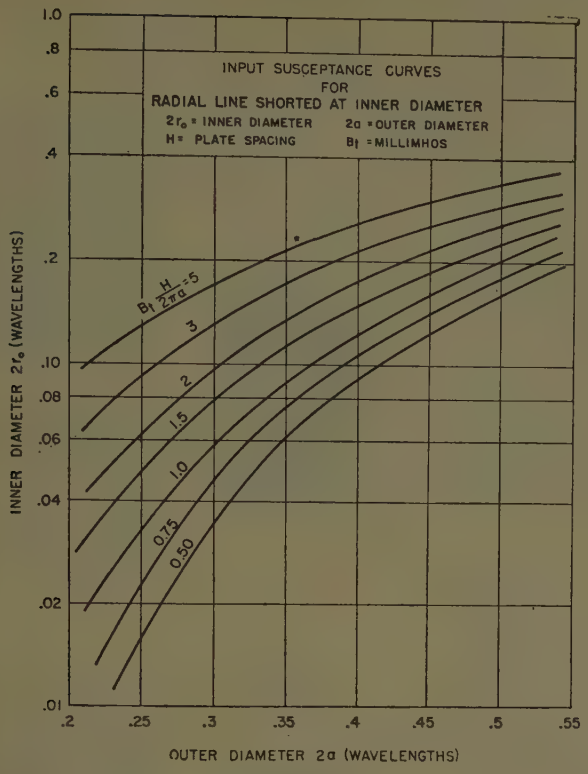

Fig. 4.

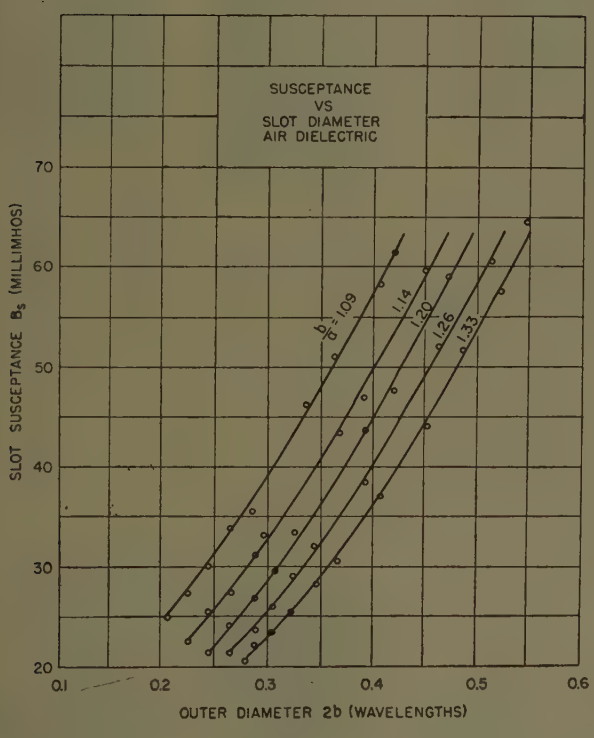

Fig. 5.

X_m of the coupling loop is given by

$$X_m = -\frac{j\omega\mu_0 h\lambda}{4\pi^2 r_0} \cdot \frac{N_0\left(\frac{2\pi a}{\lambda}\right) J_0\left(\frac{2\pi L}{\lambda}\right) - J_0\left(\frac{2\pi a}{\lambda}\right) N_0\left(\frac{2\pi L}{\lambda}\right)}{J_1\left(\frac{2\pi r_0}{\lambda}\right) N_0\left(\frac{2\pi a}{\lambda}\right) - N_1\left(\frac{2\pi r_0}{\lambda}\right) J_0\left(\frac{2\pi a}{\lambda}\right)}.$$

Finally, measured values of slot susceptance B_s, re-

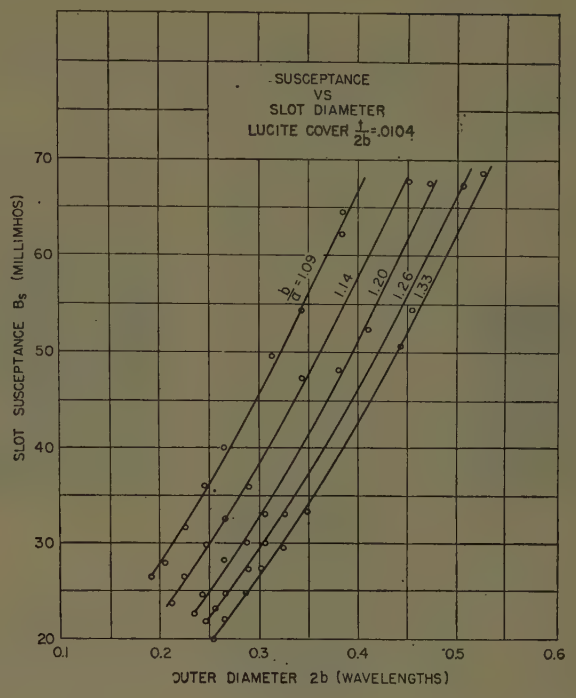

Fig. 6.

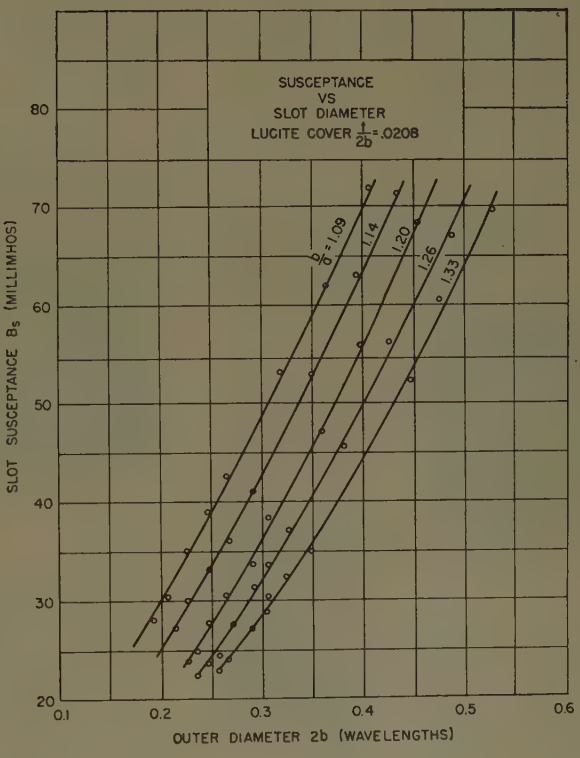

Fig. 7.

ferred to the inner radius of the slot are given in Figs. 5, 6, and 7, for slots of various widths and dielectric coverings. These data were obtained by placing both an input and output coupling loop in the radial transmission line, and using it as a lossy transmission device. At the resonant frequency of the system, the input susceptance of the radial transmission line was calculated and equated to the slot susceptance. This procedure was carried out for a number of slot widths and radial transmission line dimensions.

Contributors

Robert W. Bickmore was born in San Francisco, Calif. on November 8, 1923. From 1943 to 1946, he served as a communications chief with the U.S. Air Force in the Asiatic-Pacific theatre. He received the B.S. degree in 1948, the M.S. degree in 1950, and the Ph.D. degree in 1953, all in electrical engineering, from the University of California at Berkeley. From 1949 to 1953 he was a lecturer in electrical engineering and a research engineer at the University of California electronic research laboratory. He joined the Hughes Research Laboratories in 1953 and became, in succession, head of the slot antenna research group, head of the antenna research section, and currently senior staff engineer, microwave laboratory.

R. W. Bickmore

Dr. Bickmore is a member of Sigma Xi, RESA, American Physical Society, and Commission VI, URSI.

❖

Åke F. Blomquist was born in Västerås, Sweden, on December 10, 1924. He received his preparatory education in Västerås. From 1947 to 1951, he attended the Chalmers Institute of Technology, Gothenburg, where he received the Civilingenjör degree in electrical engineering.

Å. F. Blomquist

Since 1951 he has been employed at the Research Institute of National Defense, Stockholm, as a research engineer in the laboratory for antennas and propagation. He is engaged in propagation research especially concerning vhf- and uhf-ground wave problems.

Mr. Blomquist is a member of Svenska Teknologföreningen.

❖

Ralph Bolgiano, Jr. was born on April 1, 1922 in Baltimore, Md. He received the B.S.E.E. degree from Cornell University, Ithaca, N. Y., in 1944.

A member of the U. S. Army Signal Corps from 1943 through 1946, he was engaged in the training of radio teletype personnel. From 1947 to 1949, he was an instructor in electronics and did graduate work in communications at Cornell, where he received the M.E.E. degree.

For the next five years he was employed by the General Electric Company, first in its Electronics Laboratory, Syracuse, N. Y., and subsequently in its Advanced Electronics Center, Ithaca, N. Y., where he was supervisor in communication theory. During this time, he was primarily concerned with communication systems development, especially in the fields of data transmission and navigation. In 1954 he left General Electric to re-enroll at Cornell as a candidate for the Ph.D. degree. He has since devoted himself entirely to the study of radio propagation and atmospheric turbulence.

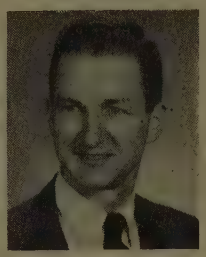

R. Bolgiano, Jr.

Mr. Bolgiano is a member of Eta Kappa Nu, Tau Beta Pi, and Sigma Xi.

❖

Frederick E. Brooks, Jr. (S'42–A'44–M'48–SM'54) was born in Mineola, N. Y. on October 14, 1916. He received the B.S. degree in electrical engineering in 1940 from the University of Kansas, Lawrence, Kan., and the Ph.D. degree in engineering from Yale University, New Haven, Conn., in 1944.

F. E. Brooks, Jr.

From November, 1943 until July, 1957, he was a member of the faculty of the University of Texas, Austin, Tex., the last three years as professor of electrical engineering. In addition, he assisted in the organization of the electrical engineering research laboratory of the University of Texas in 1946 and was assistant director of the laboratory from 1948. He has worked primarily in the fields of low angle tropospheric radio propagation, antenna systems, and analog computers for data reduction.

In July, 1957, he joined Collins Radio Company, Dallas, Tex. as assistant director of research and development.

Dr. Brooks is a member of Sigma Xi, Tau Beta Pi, and Eta Kappa Nu.

❖

E. Gösta R. Carlson was born on January 12, 1930, in Vadstena, Sweden. He entered the Royal Institute of Technology, Stockholm, Sweden in 1948, where he received the degree of Civil-ingenjörsexamin in electrical engineering in 1954.

E. G. R. Carlson

Since 1952 he has been with the Research Institute of National Defense, Stockholm, as a research engineer, where he participates in wave propagation research especially concerning beyond-the-horizon phenomena.

Mr. Carlson is a member of Svenska Teknologföreningen.

❖

Robert L. Carrel (S'54) was born in Fort Wayne, Ind., on February 8, 1933. He received the B.S. degree in electrical engineering in 1955 from Purdue University, Lafayette, Ind., and the M.S. degree in electrical engineering from the University of Illinois, Urbana, in 1957.

R. L. Carrel

He was employed by the Farnsworth Electronics Company from February to September, 1955, as an antenna engineer in the microwave section. He entered the University of Illinois in September, 1955, as a research assistant in the Antenna Laboratory, and is currently working toward the Ph.D. degree.

Mr. Carrel is a member of Eta Kappa Nu and Tau Beta Pi.

❖

H. P. Coleman was born in November, 1928, at Paeonian Springs, Va. He studied at the College of William and Mary, Williamsburg, Va., and at American University, Washington, D.C.

H. P. Coleman

In 1945, he joined the U. S. Naval Research Laboratory, Washington, D. C. as a summer employee, and was engaged in vacuum tube development and later in accelerator development. Mr. Coleman became a member of the Microwave Antennas and Components Branch, Electronics Division in 1952. Since then he has worked in the field of microwave antennas, principally with scanning systems.

K. Folke Eklund was born on July 17, 1924, in Västerås, Sweden. After preparatory education and military service he entered the Chalmers Institute of Technology, Gothenburg, in 1945 where, in 1949 he received the Civilingenjör degree in electrical engineering.

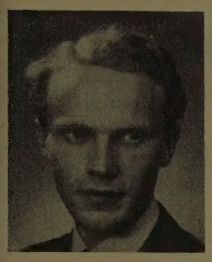

K. F. EKLUND

Since 1949 he has been with the Research Institute of National Defense, Stockholm, where he is a section leader in the laboratory for antennas and propagation.

He has been concerned mainly with microwave propagation problems.

Mr. Eklund is a member of Svenska Teknologföreningen.

❖

John P. German (A'51–SM'55) was born in Livingston, Tex., in 1917. He received the B.S.E.E. degree from The University of Texas, Austin, Tex., in 1940, and spent the next two years working in industry. He spent three and a half years in the U. S. Army, serving in the India-Burma theater of operations as a radar officer. After World War II he returned to The University of Texas for graduate work in electrical engineering. He received the M.S.E.E. degree in 1949 and the Ph.D. degree in 1955. During this time he also served as a teacher and as a radio engineer for the electrical engineering research laboratory at The University of Texas. In 1955 he accepted appointment as associate professor of electrical engineering at Purdue University, West Lafayette, Ind.

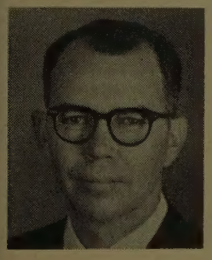

J. P. GERMAN

Dr. German is a member of Eta Kappa Nu, Sigma Pi Sigma, and Sigma Xi.

❖

Bengt A. S. Josephson (M'55) was born June 28, 1914, in Stockholm, Sweden. He received the Civilingenjörsexamen degree in electrical engineering in 1942 and the Teknologie Licentiatexamen degree in 1947 at the Royal Institute of Technology in Stockholm, where he also worked as laboratory and research assistant from 1940 to 1943.

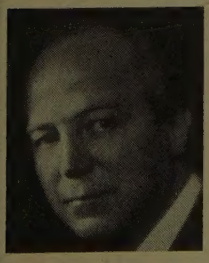

B. JOSEPHSON

During 1944 and 1945 he was employed with Telefonaktiebolaget L. M. Ericsson in Stockholm, and was mainly engaged there in development of uhf measuring instruments. He then joined the Research Institute of National Defence (FOA) in Stockholm, where he is in charge of the laboratories for transmission lines, antennas and propagation.

In 1946, he was granted a fellowship by the American Scandinavian Foundation and spent half a year with the RCA Laboratories in Princeton, N. J., and Long Island, N. Y. Since 1947 he has been part-time teaching uhf techniques at the Royal Institute of Technology and since July, 1957 he has been professor pro tempore in microwave engineering (during leave from FOA).

Mr. Josephson has been active in Swedish and International standardization work on rf transmission lines and is chairman of a working group on waveguides within the International Electrical Commission.

❖

George D. M. Peeler (M'52) was born in Rockwell, N. C. on January 10, 1923. He received the A.B. degree cum laude in physics in 1943 from Catawba College, Salisbury, N. C. and the M.A. degree in engineering science and applied physics in 1948 from Harvard University, Cambridge, Mass.

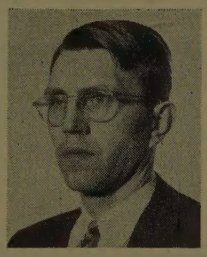

G. D. M. PEELER

He taught physics for one year at the University of North Carolina, Chapel Hill, and also attended the University of Maryland, College Park. He was employed by the Naval Research Laboratory in Washington, D. C. as a member of the Search Radar Branch from 1944 to 1950 and as a member of the Microwave Antenna and Components Branch from 1950 to 1956. Since February, 1956, he has been head of the Antenna Branch in the Missile Systems Division of Raytheon Manufacturing Co., Bedford, Mass.

Mr. Peeler is a member of the American Physical Society.

❖

Paul I. Richards (A'45) was born in Orono, Maine, on February 8, 1923. He received the M.A. degree in 1946 and the Ph.D. degree in physics in 1947 from Harvard University, Cambridge, Mass., with a thesis on the analytic theory of impedance-functions.

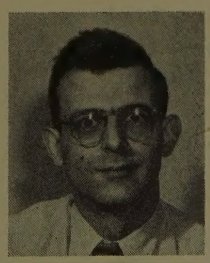

P. I. RICHARDS

From 1947 to 1952 he was a physicist at Brookhaven National Laboratory, where he worked on theoretical physics and on the experimental development of a time-of-flight mass spectrometer.

After spending a year at Transistor Products, Inc., in 1954 he joined Technical Operations, Inc., where he is presently employed in theoretical analysis of various problems in physics, engineering, and operations research, mainly under the sponsorship of various government agencies. His recent contributions have centered primarily in the transport theory of nuclear and optical radiation.

Dr. Richards is a member of the American Physical Society, Sigma Xi, and Phi Beta Kappa.

❖

Dipak L. Sengupta (S'55) was born in Bengal, India in 1931. He received the B.Sc. degree with honors in physics in 1950 and the M.Sc. degree in radiophysics and electronics in 1952 both from Calcutta University. He worked at that institution as a Government of India senior research scholar until September, 1954. During that time he designed and developed a special type of transmitter and receiver suitable for super-refraction studies at 300 mc.

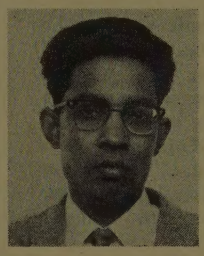

D. L. SENGUPTA

At the present time, Mr. Sengupta is in the last year of graduate study at the Electrical Engineering Department of the University of Toronto. He is also working as a part-time assistant on the radioastronomy project in the Electrical Department, where he is responsible for the development of the antenna assembly of the recently installed radio telescope. His main interests are in em theory, microwave antennas, and microwave theory.

❖

Hillel Unz (S'53–M'57) was born in Darmstadt, Germany, on August 15, 1929. He went to Israel in 1931 and served in the Israel Defense Forces during the war of independence in 1948–1949. He received the B.S. degree in electronics, summa cum laude, from Israel Institute of Technology, in 1953.

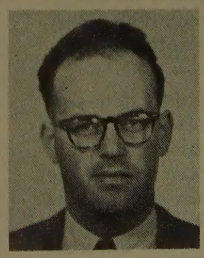

H. UNZ

From 1953 to 1956, he was a research assistant in the microwave antenna laboratory (Office of Naval Research Project) in the Electrical Engineering Department at the University of California, Berkeley, Calif., where he received the M.S. degree in 1954, and the Ph.D. degree in 1957.

Since January, 1957, he has been an assistant professor of electrical engineering at the University of Kansas, Lawrence, Kan. His main interest is in the fields of electromagnetic theory, boundary value problems, diffraction theory, and antennas.

Dr. Unz is a member of Sigma Xi.

AVAILABLE BACK ISSUES OF IRE TRANSACTIONS ON ANTENNAS AND PROPAGATION

Publication	*Prices*		
	Group Members	*IRE Members*	*Non-Members**
AP-1, No. 1, July, 1953	$1.20	$1.80	$3.60
AP-1, No. 2, October, 1953	$1.20	$1.80	$3.60
AP-2, No. 1, January, 1954	$1.35	$2.00	$4.05
AP-2, No. 2, April, 1954	$2.00	$3.00	$6.00
AP-2, No. 3, July, 1954	$1.50	$2.25	$4.50
AP-3, No. 4, October, 1954	$1.50	$2.25	$4.50
AP-3, No. 1, January, 1955	$1.60	$2.40	$4.80
AP-3, No. 2, April, 1955	$1.60	$2.40	$4.80
AP-4, No. 4, October, 1956	$2.10	$3.15	$6.30
AP-5, No. 1, January, 1957	$3.20	$4.80	$9.60
AP-5, No. 2, April, 1957	$1.75	$2.60	$5.25
AP-5, No. 3, July, 1957	$2.00	$3.00	$6.00
AP-5, No. 4, October, 1957	$1.70	$2.25	$5.10
AP-6, No. 1, January, 1958	$3.85	$5.80	$11.55

* *Colleges, Universities, Subscription Agencies, and all Libraries, may purchase at IRE Member rate.*

INSTITUTIONAL LISTINGS

The IRE Professional Group on Antennas and Propagation is grateful for the assistance given by the firms listed below, and invites application for Institutional Listing from other firms interested in the field of Antennas and Propagation.

ANDREW CORPORATION, 363 E. 75th St., Chicago 19, Ill.
Antennas, Antenna Systems, Transmission Lines, Development and Production.

ANTLAB, INC., 6330 Proprietors Rd., Worthington, Ohio
Antenna Pattern Range Systems—Recorders & Mounts.

BLAINE ELECTRONETICS, INC., 14757 Keswick St., Van Nuys, Calif.
Antennas, Paraboloids, Scale Models, Antenna Radiation Pattern Measurement Towers.

COLLINS RADIO COMPANY, Cedar Rapids, Iowa
Antenna Design and Propagation Research Related for Airborne and Ground Communication Systems.

DEVELOPMENTAL ENGINEERING CORP., 1001 Conn. Ave. N.W., Washington, D. C. and Leesburg, Va
Research, Development, Installation of Antennas and Antenna Equipment for Super Power Stations.

THE GABRIEL LABORATORIES, Div. of the Gabriel Co., 135 Crescent Road, Needham Heights 94, Mass.
Research and Development of Antenna Equipment for Government and Industry.

HUGHES AIRCRAFT COMPANY, Culver City, Calif.
Research, Development, Mfr.: Radar, Missiles, Antennas, Radomes, Tubes, Solid State Physics, Computers.

I-T-E CIRCUIT BREAKER CO., Special Products Div., 601 E. Erie Ave., Philadelphia 34, Pa.
Design, Development and Manufacture of Antennas, and Related Equipment.

JANSKY & BAILEY, INC., 1339 Wisconsin Ave. N.W., Washington 7, D. C.
Radio & Electronic Engineering; Antenna Research & Propagation Measurements; Systems Design & Evaluation.

MARK PRODUCTS CO., 6412 W. Lincoln Ave., Morton Grove, Ill.
Multi Element Grid Parabolas, Antennas for Two-Way Communications, R & D.

MARYLAND ELECTRONIC MANUFACTURING CORPORATION, College Park, Md.
Antenna and System Development and Production for Civil and Military Requirements.

THE RAMO-WOOLDRIDGE CORPORATION, Los Angeles 45, Calif.

TRANSCO PRODUCTS, INC., 12210 Nebraska Ave., Los Angeles 25, Calif.
Res., Design, Dev., & Mfr. of Antenna Systems & Components for Missile, Aircraft & Ground Installations.

WHEELER LABORATORIES, INC., 122 Cutter Mill Road, Great Neck, N. Y.
Consulting Services, Research and Development, Microwave Antennas and Waveguide Components.

The charge for an Institutional Listing is $25.00 per issue or $75.00 for four consecutive issues. Application may be made to the Technical Secretary, The Institute of Radio Engineers, 1 East 79th Street, New York 21, N.Y.